Catalysts for Enhanced CO_2 – CH_4 Exchange in Natural Gas Hydrates

-

An experimental feasibility study of exchange enhancement by use of chemical additives

A Master's Thesis in Reservoir Physics

By

Reza Hossainpour

Department of Physics and Technology
University of Bergen

June 2013

Summary

Gas hydrate is a solid state of gas and water at high pressure and low temperature conditions. Vast energy potential is associated with gas hydrates and extensive on-going research aims at addressing the technical viability of production from hydrate deposits. Two different approaches to produce natural gas from hydrate reservoir have been proposed. Either decompose the hydrate by altering thermodynamic conditions or expose the hydrate to a thermodynamically more stable hydrate former inducing a replacement process of the encaged CH_4 molecule in the lattice structure with the introduced new hydrate former. The latter has gained recent attention both in research and industrial communities. CO_2 is an attractive candidate for such process due to both offering a better hydrate stability and possibilities for sequestrating a climate gas as gas hydrates in the earth.

The work presented in this thesis is a series of experiments which studied processes involved during hydrate formation and hydrate dissociation within porous rocks. Methane hydrate was successfully and repeatedly formed within Bentheim sandstone core samples. The generated PVT-data were used to estimate the amount of methane stored in hydrate, the amount of free methane in the pores as well as the post hydrate formation water saturation. A comparison of data acquired in this study with in-house data demonstrated a trend towards higher post hydrate formation water saturation for increased initial water saturation and higher brine salinity. A number of experiments were conducted to study hydrate dissociation based production methods. Depressurization as a production method was investigated and production data acquired were compared with numerical simulation results acquired using TOUGH + HYDRATE. Thermal stimulation was investigated where temperature of the hydrate system was increased stepwise in order to find the dissociation threshold temperature at the experimental conditions. These data were later used to test the hydrate stability calculator CSMGem.

Production by *in situ* exchange with liquid CO_2 was studied during six experiments. These experiments were categorized by temperature during the exchange and presence of chemical additives during the exchange process. Two baseline exchange experiment was conducted at 83bar and 9.6 ºC using pure CO_2. Another exchange experiment was conducted at 83bar and 4ºC to study the impact of temperature on the exchange rate. Enhancement of the exchange rate would potentially benefit from both increased methane production as well as the larger amount of CO_2 stored in hydrate. Initial experiments of using Monoethanolamine (MEA) and Methyldiethanolamine (MDEA) to enhance the exchange rate were performed at 83bar and 4ºC. MEA and MDEA are respectively primary and tertiary alkanolamines that react with CO_2 in an exothermic reaction. The generated heat from the reaction has the potential of triggering hydrate dissociation. Two experiments were conducted where slugs of MDEA and MEA were added to the injected CO_2. Heat loss along the injection line resulted in low or no effect on the production. In order to minimize the heat loss, the chemical additive and CO_2 had to be injected separately and react within or at the inlet of the core. The experimental setup had to be modified in order to allow for the latter. The amount of heat generated from the reaction between the injected chemical additive and CO_2 resulted in dissociation of methane hydrate and high methane recovery.

As a part of this master thesis, a mass flow meter was implemented, tested, and used in the production line enabling more accurate production measurements. Data acquired by mass flow meter in conjunction with data from a gas chromatograph were used to quantify the production as a function of time. In addition, a new confinement system using confinement buffers were implemented offering better confinement stability during the experiments. A new experimental setup was designed and built during spring 2012 as a part of the work presented here.

Acknowledgements

First of all, it is with immense gratitude that I acknowledge the support and help of my supervisor Professor Arne Graue. He has been an inspiration and has provided me with the opportunity to work with the challenging and interesting subject of gas hydrates for my thesis. I am grateful for his guidance and patience.

Also, I would like to offer my special thanks to associate Professor Geir Ersland whom has been generous with knowledge, taught me how to be adaptive and for guiding me through this thesis and desperate times.

The assistance provided by Professor Bjørn Kvamme was greatly appreciated, for teaching me about the exciting world of gas hydrates and for his time.

To Phd. Student, Lars Petter Øren Hauge for his valuable and constructive suggestions during laboratory work and data analysis, and for providing us with an extensive and thorough in-house database.

I wish to acknowledge the collaboration with laboratory partner and dear friend, Truls Hamre Håheim. Thank you for your optimism and hard work. I would also like to thank my fellow reservoir physics students for a great study environment.

Also, I wish to sincerely thank my parents for their support and encouragement throughout my studies and for always believing in me. Without their support, I would not be where I am today. I would also like to thank my siblings.

Finally, I would like to express my great appreciation to my girlfriend Maiken, for always motivating me in my work, for your patience and encouragement, and for keeping me sane during chaotic times.

Bergen, May 31. 2013

Reza Hossainpour

Table of Contents

Introduction

Gas hydrates are solid crystalline compounds in which gas molecules, often referred to as guest molecules, occupy and stabilize water structures under high pressure and low temperature. Typical guest molecules are methane, ethane propane and carbon dioxide. Naturally occurring gas hydrates contain methane where methane is compressed by a factor of 164 when compared to standard conditions.

Gas hydrates were first discovered as a laboratory curiosity in 1800, but it was in 1965 that mankind recognized that they were common in nature (Sloan et al., 2008). The estimates of the amount *in situ* gas hydrates have varied since they were first discovered, but even the most conservative estimates indicate a vast energy resource with global distribution in permafrost and in submarine environments. Given the limited amount of conventional fossil fuel reserves, the increasing energy demand and the relative clean burn upon combustion gas hydrates represent, they are considered to a play a role in the future energy mix.

Production methods proposed for natural gas hydrates are commonly based on dissociation of gas hydrates. Lowering the pressure, raising the temperature or shifting the stability conditions for gas hydrates may result in dissociation of the gas hydrates, a process which releases the entrapped gas and produces large quantities of liquid water. The idea of producing methane from gas hydrates by exposing them to a thermodynamically more stable molecule has gained recent attention in research and industrial communities. CO_2 has been an attractive candidate for such process (Ebinuma, 1993) for two main reasons: 1) CO_2 offers a better hydrate stability and 2) Sequestration in hydrates may be one of many means in the effort to mitigate climate change resulting from anthropogenic CO_2 release to the atmosphere. In addition, natural gas production by $CH_4 – CO_2$ replacement benefits from that there is little or no water production during the process (Graue et al., 2006). Thermodynamic stability of natural gas hydrates is limited to local temperature and pressure. In addition, hydrate has to be in a state of equilibrium with its surroundings. Normally it is not even possible to reach equilibrium due to Gibbs phase rule and the picture is even more complicated (Kvamme, 2013). One serious issue regarding stability of natural gas hydrates, especially near the surface of the submarine or permafrost deposits is the possibility of hydrate dissociation. This can be result of a gradual increase in temperature of the sediment over geological time scales, but can also be related to changes in the sediments in the form of new or increased fractures that brings the hydrate in contact with undersaturated groundwater. Eventually, this could result in subsidence of the formation and huge methane release into the water column or atmosphere. $CH_4 – CO_2$ replacement benefits also from increased stability of the hydrate saturated sediment.

In recent years, several experimental studies have been conducted at the University of Bergen in collaboration with ConocoPhillips. In these studies MRI – visualizations confirmed replacement of $CH_4 – CO_2$ in the hydrate saturated core sample (Ersland, 2008; Graue et al., 2006; Graue et al., 2008; Husebø, 2008). The recovery was estimated to 50 – 80% in these experiments, based on the produced methane. After nearly a decade of research and based on promising laboratory results, the ConocoPhillips Ignik Sikumi #1 field trial was initiated on North Slope of the Alaska in winter 2011.
During $CH_4 – CO2$ experiments a decrease in exchange rate due to slow diffusion of CO_2 through an already formed CO_2 - hydrate has been observed (Graue et al., 2008; Yoon et al., 2005). The objective of the present study has been to investigate the possibility of enhancing the $CH_4 – CO_2$ exchange rate by injection of chemical additives. A second objective of this study has been to better estimate the

recovery from the system by measuring mass produced. In order to achieve the latter a mass flow meter was implemented in the production line. The acquired data from mass flow meter in conjunction with data from a gas chromatograph were used to quantify the production as function of time. In addition, the confinement system was modified and upgraded using confinement buffers. These offered much better confinement stability during the experiments. Moreover, several injection and production lines were changed due to maintenance. A new experimental setup was designed and built during spring 2012 as a major part of the work presented in this thesis.

This thesis is presented in two main parts. Part I (Chapter 1 and 2) will introduce a basic understanding of natural gas hydrates, considering how and at what conditions they are formed, proposed production methods and examples from field tests. Part II (Chapter 3, 4, 5 and 6) will present the experimental setup used during this master thesis, the results achieved and finally a discussion and concluding remarks on the achieved results.

Part I

Theory

1 Basic review of natural gas hydrates

The following chapter will focus on the question "what are gas-hydrates?" the conditions under which hydrates may form and the kinetic of hydrate formation. The chapter also concerns the naturally occurrence of gas hydrates as well as proposed production method for these.

1.1 Gas Hydrates

Gas hydrates are crystalline inclusion compounds in which gas molecules, from here referred to as guest molecules, are encapsulated inside a host water lattice. Gas hydrates can be found as methane hydrates in sediments in the permafrost regions and below the sea bottom around the world. The vast amount of energy stored in natural gas hydrates has drawn great attention towards potential of gas hydrates as a possible energy source for the future. Under proper conditions of pressure and temperature, the hydration reaction of a gas G (guest) is described by the general equation (Moridis et al., 2009):

$$G + N_H H_2O = G\ N_H H_2O \tag{1.1}$$

where the N_H the hydration number is the number of the water molecules surrounding and encapsulating each gas molecule. To better understand the gas hydrates and their properties a basic review of water molecule is presented below.

1.1.1 The water molecule

The structure of water molecule is made of two light atoms (H) and one relatively heavy atom (O). The oxygen atom has electronic configuration $1s^2 2s^2 2p^4$, the total number of electrons is eight and the atom is missing two electrons to fill up its second shell. The two hydrogen atoms provide the two missing electrons through a covalent bonding in such way the valence shell is filled up for all atoms. The hydrogen atoms are separated by an angle of 104.45°. The covalent binding between the oxygen and hydrogen has a polar character. This is due to the difference in the electronegativity between oxygen and hydrogen. The electronegativity is a parameter introduced by Linus Pauling as a measure of the power of an atom to attract electrons to itself when it is part of a compound (Atkins et al., 2006, p. 379). The oxygen atom has an electronegativity of 3.44, and the hydrogen atom has an electronegativity of 2.20 on the Pauling scale. This results in a dipole water molecule that has a negative charge close to the oxygen atom (δ-), while hydrogen side becomes slightly positively charged (δ+).

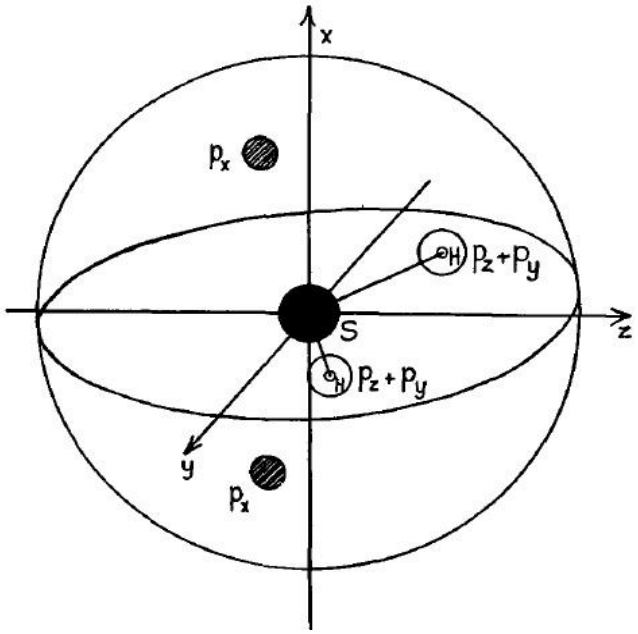

Figure 1-1 The electron distribution in the water molecule suggested by Bernal (Bernal et al., 1933)

1.1.2 Water properties

Water has several unique properties; these can be explained by the structure of the molecule and the consequences of this structure. It is the unique structure of the water molecule that leads to the possibility of hydrate formation (Carroll, 2009). The molecule has two positive and two negative charges. The two negatively charges are caused by the two "lone pair" electrons from the oxygen and the shared electrons with the protons give the molecule two positively charges (Sloan et al., 2008). The hydrogen bond in water occurs due to the attraction of the positive pole on one molecule to a negative pole on a neighboring water molecule. The result is a water molecule that is interconnected to four other water molecules. In ice and hydrates, only one hydrogen lies between two oxygen atoms with a distance between oxygen nuclei of 2,76 Å[1](Sloan et al., 2008).

Hydrogen bonds affect some important properties of water. The hydrogen bond separates water molecules rigidly and is the reason to why ice floats on water. One of the unusual properties of water is the density maximum as a function of temperature. Stillinger indicates a maximum density of (1.0000 g/cm^3) at 4 °C (Stillinger et al., 1974). The hydrogen bond is more than an order of magnitude stronger than a typical van der Waals bond. But the hydrogen bond is not nearly as strong as a covalent chemical bond. The energy required to break one hydrogen bond is 21kJ/mol, while the energy needed to break one van der Waals bond is 1,3kJ/mol and 427kJ/mol for one chemical bond.

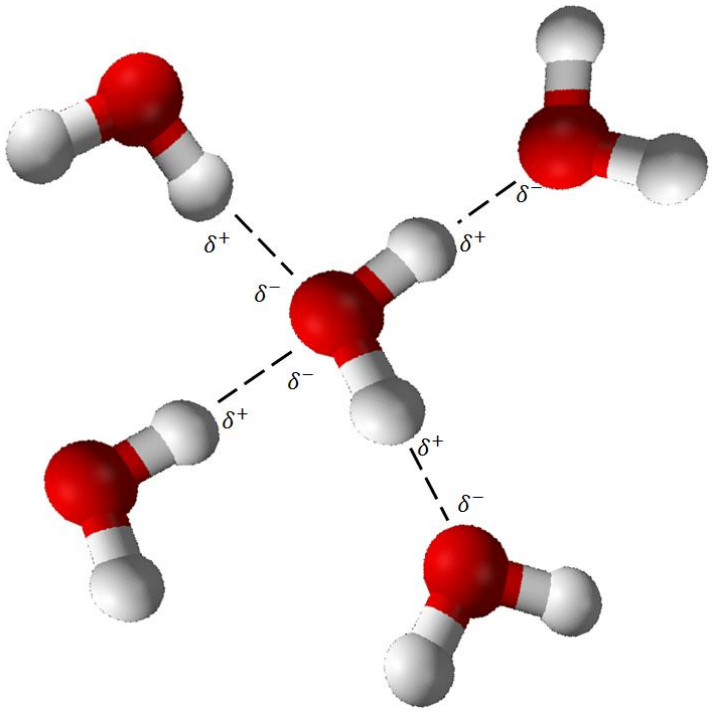

Figure 1-2 Water molecule interconnected with four other molecules through hydrogen bonds.

Hydrogen bonds between the water molecules are the cause to the waters relatively high boiling point in contrast to molecules with the same molecular weight. The boiling point of water at ambient pressure is 260K higher than methane which has a similar molecular weight (Sloan et al., 2008). In nature, water exists in liquid, ice and vapor states. Figure 1-3 shows the phase diagram for water under different ambient pressure and temperature. A phase diagram shows the preferred physical state of matter at different temperature and pressure. The material is uniform with respect to its chemical

[1] A unit of length equal to 10^{-10} meter. The unit is named after Anders Ångström.

composition and physical state within each phase. Each solid line on the figure shows a phase boundary. The line represents conditions under which two phases coexist. Small changes in temperature and pressure along the phase boundary result in change of state of the matter (Chaplin, 2008). The triple point in the figure is where all three phases coexist in equilibrium. At typical temperatures and pressures most water found on earth is liquid. But water becomes gaseous if the temperature is raised to over 373 K, and it becomes solid if temperature is lowered below 273 K. The solid phase of water, ice resembles hydrates in structure.

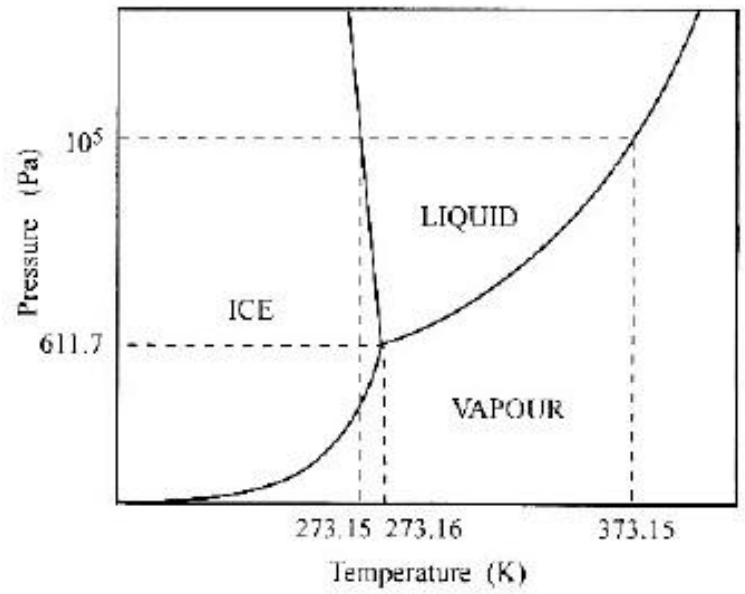

Figure 1-3 Phase diagram for ice Ih, water and vapor (Travesset, 2008).

1.1.3 Similarities between ice and hydrate

The commonly seen form of ice is known as ice I_h (hexagonal ice). But ice has at least thirteen other phases which exist under different pressure and temperature (Travesset, 2008). In ice, tetrahedrally hydrogen-bonded water molecules form hexagonal rings. Due to no geometrical distortion, the tetrahedral O—O—O angles, that is the oxygen atoms that are hydrogen-bonded, is 109.5°. In ice, the hydrogen protons that are covalently bonded lie in a distance of 1Å from the oxygen nucleus. The distance between the protons and the next oxygen nucleus through the hydrogen bond is 1.76 Å. This distance is 1% longer in hydrates (Sloan et al., 2008). Figure 1-4 shows the structure pattern of ice.

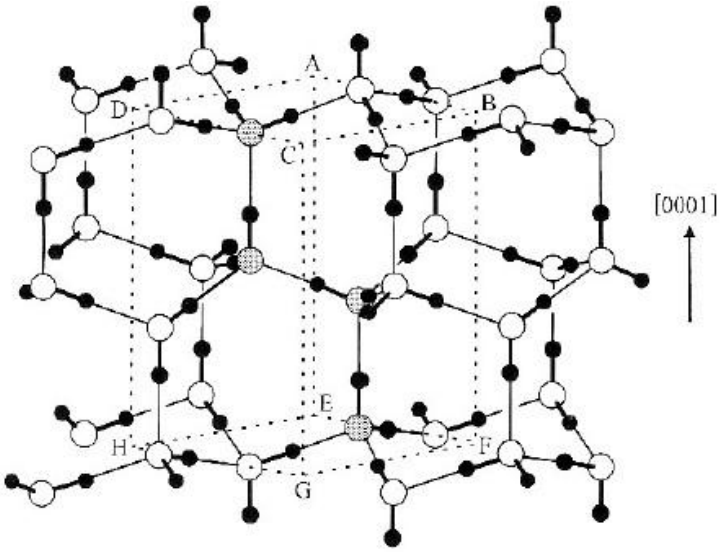

Figure 1-4 Crystal structure of ice Ih, the white circles represent oxygen atoms and the dark circles represent hydrogen atoms (Travesset, 2008).

Structurally, clathrate hydrates are dominated by five-membered rings. While in ice, tetrahedrally hydrogen-bonded water molecules form non-planar puckered hexagonal rings (Sloan et al., 2008). All common hydrate structures are formed of about 85% water on a molecular basis, and that is why many of mechanical properties of the hydrates resemble the mechanical properties of ice I_h. Among the exceptions, Sloan mentions yield strength, thermal expansivity and thermal conductivity.

Table 1-1 Comparison of different properties of ice and hydrates(Sloan et al., 2008).

Property	Ice	Structure I	Structure II
No. of H_2O molecules	4	46	136
Dielectric constant at 273 K	94	58	58
Thermal conductivity [$Wm^{-1}K^{-1}$]	2.23	0.49±0.02	0.51±0.02
Heat capacity [$Jkg^{-1}K^{-1}$]	1700±200	2080	2130±40
Density [g/cm^3]	0.91	0.94	1.291

1.1.4 Hydrates structures

Water molecules have the unique property that, in association with other water molecules, they can form four tetrahedrally-disposed hydrogen bonds, half of which are donors and half acceptors (Jeffrey, 1984). When water molecules are in vicinity of hydrophobic molecules (water fearing, insoluble in water), the thermodynamic and structural processes caused by the foreign molecule, (e.g. methane), lead to enhancement of the local structure of water. In hydrates, the water molecules interconnect in a specific manner structuring polyhedra[2] formed cavities. The polyhedral cavities are made of pentagonal and hexagonal faces. The characteristic water structure in clathrate gas hydrate is the *Pentagonal Dodecahedra*, $H_{40}O_{20}$, with its 12 pentagonal faces, (5^{12})[3], 20 vertices and 30 edges shown in Figure 1-5(a). When these polyhedra are linked together, each water molecule is interconnected to

[2] A solid bound by polygonal faces (Daintith et al., 2010)

[3] Nomenclature description (n_i^{mi}) has been suggested by Jeffrey for these polyhedra, where $n_i$is the number of edges in face type "i", and $m_i$is the number of faces with n_i edges (Jeffrey, 1984). The faces have equal edge length and angles.

four other water molecules in the same manner as in ice I_h with a geometry which is closed to tetrahedral, the angle deviation from tetrahedral geometry is 1.5°. In a pentagonal dodecahedra, there are 20 water molecules, with 30 bonds, 10 of these are pointing away from the structure, as potential connection points to other molecules or cavities (Sloan et al., 2008). *Structure I* is made by 46 water molecules structuring two pentagonal dodecahedra Figure 1-5(a), and 6 tetrakaidecahedron, Figure 1-5(b), leaving 8 cavities per crystal cell. *Structure II* is a result of 136 water molecules structuring 16 pentagonal dodecahedra and 8 hexakaidecahedron. The number of cavities per crystal cell for structure II is 24. Table 1-2 lists some of the main properties of the different hydrate structures. The *structure H* has an intermediate size cavity in addition to small and large. The structure is made of three dodecahedrons, Figure 1-5(a), two irregular dodecahedra, Figure 1-5(d), and one icosahedron shown in Figure 1-5(e).

.

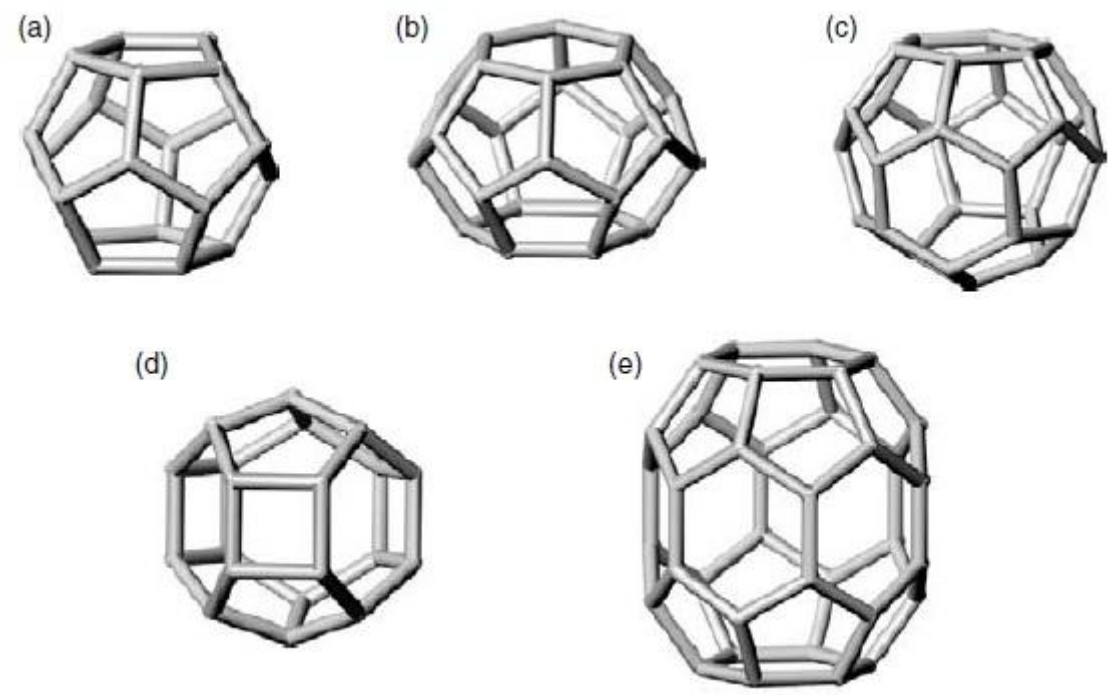

Figure 1-5 Five cavities in clathrate gas hydrates: (a) pentagonal dodecahedron (5^{12}), (b) tetrakaidecahedron ($5^{12}6^2$), (c) hexakaidecahedron ($5^{12}6^4$), (d) irregular dodecahedron ($4^3 5^6 6^3$, and (e) icosahedron ($5^{12}6^8$) (Sloan et al., 2008).

Table 1-2 Important properties of structure I, II and H

Hydrate Crystal Cell Structure	I		II		H		
Cavity	Small	Large	Small	Large	Small	Medium	Large
Description	5^{12}	$5^{12}6^2$	5^{12}	$5^{12}6^4$	5^{12}	$4^3 5^6 6^3$	$5^{12}6^8$
No. of cavities per unit cell	2	6	16	8	3	2	1
Average radius of the cavity (Å)	3.95	4.33	3.91	4.73	3.94	4.04	5.79
Variation in radius[4] (%)	3.4	14.4	5.5	1.73	4.0	8.5	15.1
No. of H_2O molecules	46		136		34		

[4] Variation in distance of oxygen atoms from the center of a cage. A smaller variation in radius indicates a more symmetric cage.

In order to stabilize the volume of the structures described over, a guest molecule is needed. For the guest molecule to be able to stabilize the cavities there are conditions to be fulfilled, these conditions are discussed in following section.

1.1.5 The guest molecule

In hydrate structures, the voids (cavities) are stabilized by non-polar or slightly polar guest molecules. For the guest molecule to be able to stabilize the cavities it must: 1) Fit volumetrically within the cavity, 2) Contain neither a single strong hydrogen-bonding group nor a number of moderately strong hydrogen-bonding groups. i.e. the guest molecule must not compete or interfere with the already existing hydrogen bonds (Jeffrey, 1984). For the guest molecule to be able to fit within the cavities and stabilize them, the ratio of guest diameter/cavity diameter is to be within the range of 0.76 – 1.0. A ratio below 0.76 leads to less stability of the cavity and collapsing of the structure. A ratio equal or above the upper bound indicates that the molecule will not fit within the cavity. This rule is not always obeyed by the hydrate formers. Nitrogen is the smallest natural gas hydrate former (guest molecule). It is able to stabilize the 5^{12} cavity of structure II with a ratio of 0.82, and nitrogen occupies the large cavity, $5^{12}6^4$, with a ratio of 0.62 (less than the favorable ratio 0.76) , indicating less stability of the cavity. However, at high pressures, two nitrogen molecules can occupy the $5^{12}6^4$ cavity (Sloan et al., 2008). Methane can stabilize the 5^{12} cavity of structure I with a ratio of 0.86; it occupies the $5^{12}6^2$ cavity of structure I with a ratio of 0.74. Table 1-3 demonstrates size ratios of guest diameter/cavity diameter for some hydrate formers.

Table 1-3: Ratio of molecular diameters to cavity diameter for gas hydrate formers (Sloan et al., 2008). There are more guest molecules than presented here, these are listed in Appendix A 1.

		Molecular diameter / cavity diameter for cavity type			
Guest hydrate former		**Structure I**		**Structure II**	
Molecule	**Diameter (Å)**	**5^{12}**	**$5^{12}6^2$**	**5^{12}**	**$5^{12}6^4$**
CH_4	4.36	0.855	0.744	0.868	0.655
CO_2	5.12	1.00	0.834	1.02	0.769
N_2	4.1	0.804	0.700	0.817	0.616
O_2	4.2	0.824	0.717	0.837	0.631
H_2	2.72	0.533	0.464	0.542	0.408
He	2.28	0.447	0.389	0.454	0.342
H_2S	4.58	0.898	0.782	0.912	0.687
n-C_4H_{10}	7.1	1.39	1.21	1.41	1.07
Xe	4.58	0.898	0.782	0.912	0.687

Simple hydrates are the ones which host a single type of molecule. For instance, methane can stabilize the 5^{12} cavity of structure I with a ratio of 0.855. The molecule also occupies the large cavity, $5^{12}6^2$, of the structure I with a ratio of 0.744 (Table 1-3). n-butane does not form a simple hydrate; this due to the ratio of n-butane to the largest cavity of structure II being 7% larger than the $5^{12}6^4$ free cavity diameter. But a structure II hydrates can be formed with a combination of n-butane and xenon. In this case, the xenon fills the small cages (Ripmeester et al., 1990).

1.2 Hydrate formation kinetics

Processes, in which hydrates form, dissociate and are inhabited, are time-dependent processes. Due to time dependency of such processes, one can expect decrease in accuracy of measurements and models describing them (Sloan et al., 2008). Despite efforts both theoretically and experimentally, it has been hard to find a correlation between hydrate formation conditions and hydrate initiation, in another words, it has been difficult to predict the time and condition of the onset of hydrate formation (Makogon, Y. F. et al., 1999). To better understand the hydrate formation, some of the key aspects of the phenomenon are discussed in the following sections. These are:

- Hydrate nucleation
- Induction time
- Conditions and site of hydrate formation
- Hydrate inhibition

1.2.1 Hydrate nucleation

Nucleation is the process during which hydrates form. Under nucleation, small clusters of water and gas (hydrate nuclei) grow and disperse randomly in attempt to achieve a critical cluster size, r_c, for continued growth. Before the critical size is achieved, clusters may grow or shrink as a result of density and composition fluctuations (Sloan et al., 2008). The critical cluster size and the cluster growth can be explained by the excess Gibbs free energy (ΔG) between a solid particle of solute and the solute in solution. Hydrate nucleation is a phase transition, and for a phase transition to occur, the Gibbs free energy has to be negative. The Gibbs free energy is equal to the sum of the free energy gained due to solute molecules becoming a part of the surface of the hydrate crystal (surface excess free energy), and energy lost due to solute molecules ending up in the bulk of the hydrate crystal (volume excess free energy) (Kvamme, 2012):

$$\Delta G = \Delta G_S + G_V = 4\pi r^2\sigma + \frac{4}{3}\pi r^3 \Delta g_V \qquad (1.2)$$

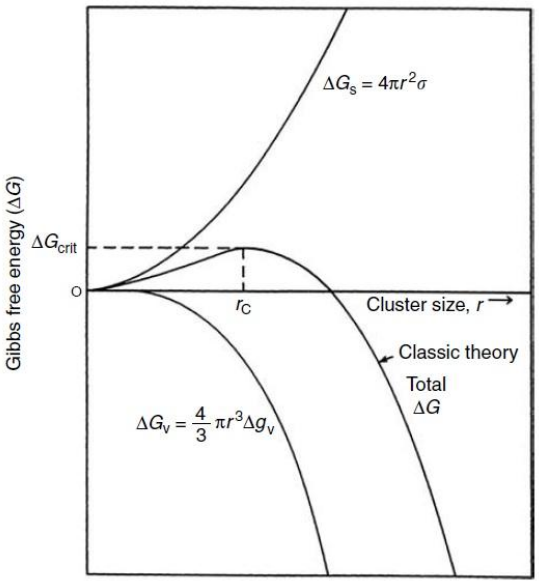

Figure 1-6 - Gibbs free energy as a function of cluster radius (Sloan et al., 2008).

Where Δg_V is the free energy unit per unit volume and σ is the interfacial tension of the crystal and the liquid. Figure 1-6 shows ΔG as a function of the cluster radius, the maximum (ΔG_{crit}) corresponds to the critical cluster radius for spherical hydrate nucleus (1.3), r_c, and can be obtained by deriving the equation (1.2) and setting the result to zero:

$$r_c = -2\sigma/\Delta g_V \tag{1.3}$$

$$\Delta G_{crit} = 4\pi\sigma r_c^2/3 \tag{1.4}$$

The hydrate nucleation process is a micro scale process and occurs down at the most left corner of Figure 1-6. The literature refers to two different types of nucleation processes, depending on the condition under which the nucleation occurs: 1. Homogeneous nucleation (HON). 2. Heterogeneous nucleation (HEN).

1.2.1.1 Homogeneous nucleation

Homogeneous nucleation is a solidification process that happens in absence of impurities. This type of nucleation is rarely encountered in the real world and is to be considered an ideal model to describe hydrate growth. Under homogeneous nucleation, hydrate forms from a single phase and there has to be enough gas dissolved in the water to build cage-like clusters, something that is unlikely to happen considering the low solubility of the non-polar gases in water (Sloan et al., 2008). In addition, aqueous solutions that are prepared in the laboratory contain more than 10^6 particles per cm^3; to achieve a solution completely free for foreign particles is impossible (Mullin, 2001).

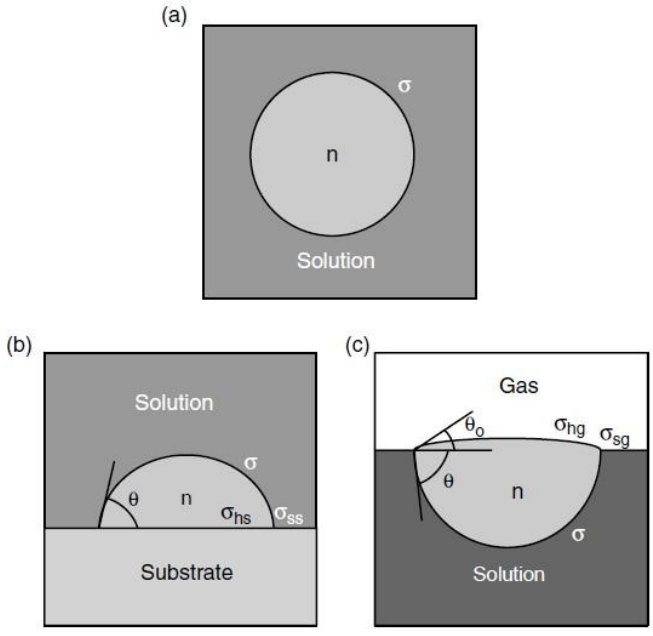

Figure 1-7 - (a) Spherical cluster of n units in HON; (b) cap-shaped cluster of n building units in HEN; (c)lens-shaped of n building units at the gas-solution interface in HEN. Modified by (Sloan et al., 2008) from (Kashchiev et al., 2003).

1.2.1.2 Heterogeneous nucleation (HEN)

The other and more usual case is when nucleation occurs in presence of foreign particles (e.g. dust micro-particles), or substrate (e.g. container, or pipeline) or at the interface between two different phases. Figure 1-7 illustrates (HON) and (HEN) schematically. Under this study methane hydrate was

formed within Bentheim sandstone core samples. Hydrate growth occurs more readily in presence of a substrate (grain surface). This is due to the fact that, when free energy is taken into account, hydrate growth is more probable to happen on a two-dimensional surface, than in the three-dimensional surface (free volume of water/gas). A contact angle (θ) between the hydrate crystal and the substrate is the result of the wettability preference of the substrate. Since (HEN) occurs in absence of impurities (e.g. substrate, surface), the critical Gibbs free energy is given by equation (1.4). But for (HEN) case, the contact angle is to be taken into consideration. Equation (1.4) is therefore modified to:

$$\Delta G'_{critical,HEN} = \emptyset \Delta G_{critical} \tag{1.5}$$

Where:

$$\emptyset = [(2 + cos\theta)(1 - cos\theta)^2]/4 \tag{1.6}$$

A contact angle of 180° (complete nonwetting of the substrate), the critical Gibbs free energy will be the same for both (HON) and (HEN). When the contact angle $\theta = 0°$ (complete wetting of the substrate), $\Delta G_{critical} = 0$. The hydrate formation experiments during this study have been conducted within Bentheim sandstone core samples which are strongly water wet (Graue et al., 2006). As shown in equation (1.5) and (1.6), presence of foreign surface effectively lowers the, $\Delta G'_{critical}$, and the critical cluster radius, that has to be achieved for continued growth. The induction time is therefore lower compared to the case where no impurities are present.

1.2.2 Induction time

A system containing water and methane under constant pressure and temperature is pressurized and brought to hydrate formation conditions (*P,T*). Methane is being added to the system to maintain constant pressure. The rate of gas consumption is the rate of hydrate formation and is controlled by kinetics, or heat or mass transfer (Sloan et al., 2008). Figure 1-8 illustrates the various stages of the hydrate formation.

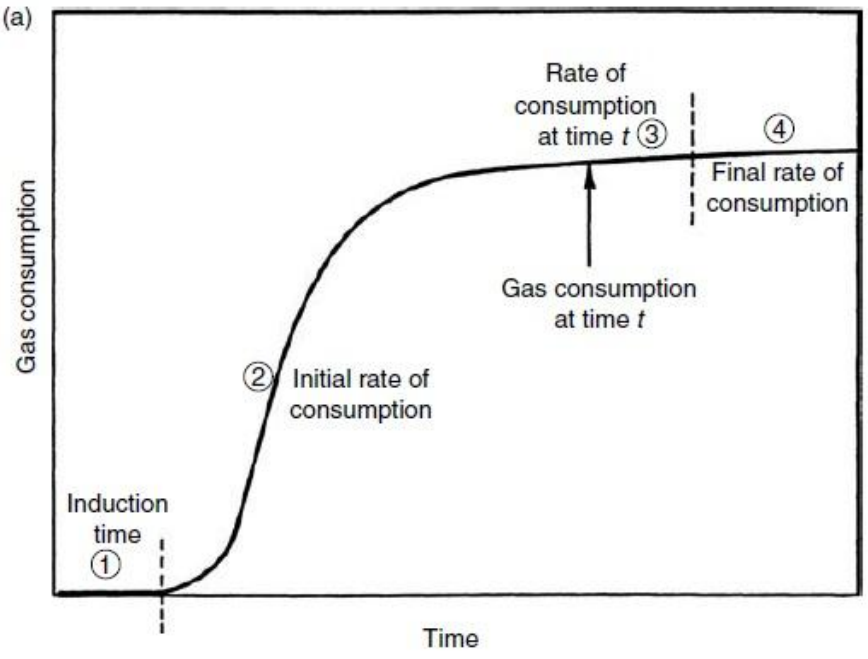

Figure 1-8 Gas consumption versus time for hydrate formation(Sloan et al., 2008)

The induction time (marked as 1 in Figure 1-8) is defined as the time elapsed until a detectable hydrate phase is observed. Or equivalently, in the case above, the induction time is the time elapsed until detectable gas volume consumed is observed. Pressure and temperature are within the hydrate stable region, but hydrate does not form before time *t* is elapsed. Kashchiev and Firoozabadi define the induction time as "a measure of the ability of a supersaturated system to remain in the state of metastability[5]" (Kashchiev et al., 2003). The induction time appears as stochastic, as if perfect control of impurities are virtually impossible (Kvamme, 2012). The growth period (marked as 2 in Figure 1-8), is rapid when hydrate formation is initiated. More methane is to be added to the system in order to maintain constant pressure. As the water is consumed the slope of the curve decreases with time. The hydrate formation experiments under this study were monitored in the same way as described over. A partly saturated sandstone core sample were pressurized with methane and brought to hydrate formation conditions. The volume of consumed gas as a function of time was constantly monitored. The procedure of hydrate formation is described in details under section 3.4.1.

1.2.3 Conditions and site of hydrate formation

Hydrate formation conditions are dictated by temperature and pressure (*T,P)* that are to be found in region left for the curve CD in figure under. As Mullin (2001) describes the crystallization regions in Figure 1-9 (Mullin, 2001) p.124:

1. The stable (unsaturated) zone to the right of equilibrium line AB where crystallization is impossible.
2. The metastable (supersaturated) zone between lines AB and CD where spontaneous crystallization is improbable. However, if a crystal seed were placed in such a metastable solution, growth would occur on it.
3. The unstable or labile (supersaturated) zone to the left if line CD, where spontaneous crystallization occurs.

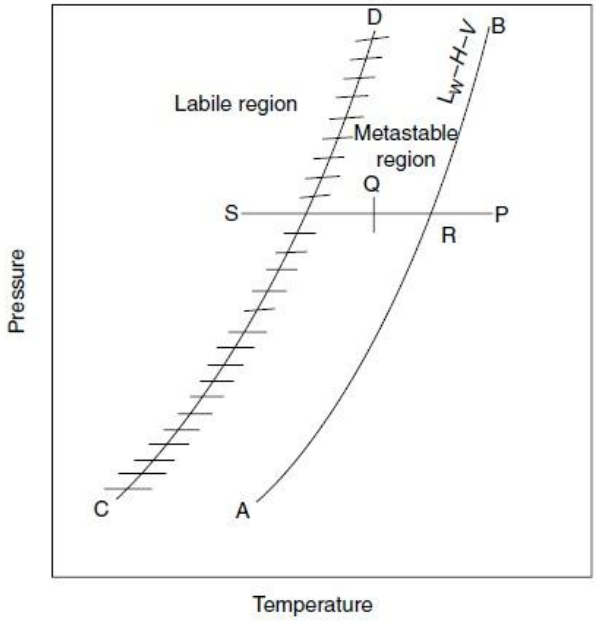

Figure 1-9 Stability region for hydrate formation (Sloan et al., 2008)

[5] Thermodynamically unstable phase that persists because the transition is kinetically hindered (Atkins et al., 2006).

Cooling the system into the region left for CD curve, results in a more readily hydrate nucleation. As the temperature is lowered, the driving force for the nucleation process to proceed is increased. However, it is not known where the CD curve is for various hydrate systems. The CD curve is shown as a broad band in Figure 1-9, because it is based on calculations and experimentally proven for a number of systems (e.g. ice but not for hydrates) (Sloan et al., 2008). Under this study, partly water saturated Bentheim sandstone core samples were pressurized with methane up to 83bar. The temperature was then lowered to 4 ^{o}C. Lowered temperature results in increased driving force for the reaction to occur. Hydrate formation was detected by a sudden increase in gas consumption.

1.2.4 Hydrate inhibition

The formation of solid masses of hydrates (plugs) from the thirties has been a source of concern to the natural gas industry (Hammerschmidt, 1934). As the pressure and temperature in gas transport lines are often within the hydrate formation conditions (Figure 1-9), presence of water in addition to abundance of guest molecules may lead to formation of hydrate plugs along the pipeline. Removing such plugs is considered as time consuming operations involved with damage to the production facilities as well as danger to the crew, as the dislodged plug can be a dangerous projectile due to the differential pressure over the plug. Since changing the temperature and pressure in the transport lines may be impractical, hydrate formation is avoided by use of hydrate inhibitors and removing the free water from the system. Inhibitors such as alcohols and glycols make the water less accessible to the guest molecules, as the water is hydrogen bonded to the inhibitor. This reduces the water activity in a way that higher pressure and lower temperature is required to form hydrates (Sloan et al., 2008). Salt can also act as a hydrate inhibitor. Water molecules are attracted to salt ions rather than hydrate structure due to their dipole nature. Previous studies at university of Bergen have looked into the relation between brine salinity and the induction time (Birkedal, 2009; Husebø, 2008). Both studies agreed on higher salinity resulting in longer induction time of the system.

1.3 Hydrates in nature

In situ gas hydrates were first discovered in 1965 in permafrost regions of the former Soviet Union. This was long after their artificial formation had been observed during laboratory studies by Sir Humphrey Davy (1811). One knows now that the *in situ* gas hydrates have existed for millions of years and are ubiquitous wherever methane and water are in close proximity under hydrates formation conditions (Sloan et al., 2008). The information about gas hydrate deposits is either based on limited direct evidence (hydrate samples) or concluded from data obtained during drilling and logging of conventional oil and gas wells. (Moridis et al., 2009). Estimates about the magnitude of the resources have varied since they were first discovered by Yuri Makogon (1965). Table 1-4 shows the estimates of the natural gas hydrates through the last four decades. Some of the early estimates of *in situ* hydrates included all areas that fulfilled sufficient pressure and temperature for hydrate formation (Milkov, 2004). Growing knowledge about *in situ* hydrates distribution and ongoing efforts to better assess the hydrate accumulations, has led to a decrease of estimates of resources. But despite the variation of the estimates, the consensus is that the quantity of the *in situ* gas hydrates is vast. The mostly cited estimate of global hydrate extent is 21×10^{15} m^3 methane at STP (or ~ 10,000 Gt of methane carbon) (Milkov, 2004). The magnitude of the estimates is better understood when compared to 1×10^{15} m^3, which is the energy consumption of the United States for 1000 years at current rate. (Sloan et al., 2008). The estimates are also comparatively large relative to world's proven natural gas reserves; OPEC reported a total of 1.9×10^{14} m^3 by the end of 2011 (Opec, 2011).

Table 1-4 Estimates of In Situ Methane Hydrates (Sloan et al., 2008)

Year	CH_4 amount 10^{15} m^3 STP	Citation
1973	3053	Trofimuk et al.
1977	1135	Trofimuk et al.
1982	1573	Cherskiy et al.
1981	120	Trofimuk et al.
1981	301	McIver
1974/1981	15	Makogon
1982	15	Trofimuk et al.
1988	40	Kvenvolden and Claypool
1988	20	Kvenvolden
1990	20	MacDonald
1994	26.4	Gornitz and Fung
1995	45.4	Harvey and Huang
1995	1	Ginsburg and Soloviev
1996	6.8	Holbrook et al.
1997	15	Makogon
2002	0.2	Soloviev
2004	2.5	Milkov
2005	120	Klauda and Sandler

1.3.1 Occurrence of methane hydrates

Gas hydrates deposits in nature are restricted to two general regions: 1) Below or at the seafloor at continental margins, and 2) permafrost regions both onshore and offshore. When it comes to global distribution of gas hydrate resources, marine hydrate systems stand for 99% of the total resources, and only 1% error in estimation of the marine gas hydrates could encompass the entire permafrost hydrates reserves (Moridis et al., 2009).

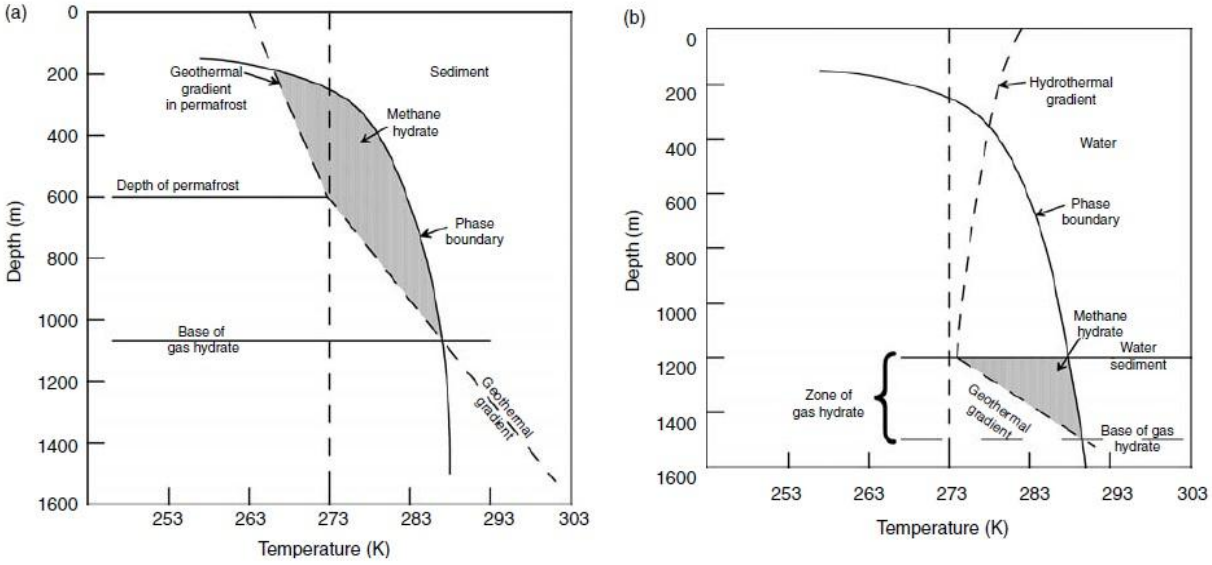

Figure 1-10 Temperature and depth conditions form methane hydrate stability (a) in permafrost and (b) in marine systems (Sloan et al., 2008).

Figure 1-10 shows examples of depth and temperature of hydrate phase stability in permafrost and in marine systems. In permafrost regions, the Gas Hydrate Stability Zone (GHSZ) can begin at 100-300 m and ranges to hundreds of meters. In Figure 1-10(a), in region bounded by phase boundary and geothermal gradient, the hydrates are stable in presence of only one other phase. This other phase is in excess and in most cases this is liquid water containing dissolved methane. Due to low concentration of methane in water, further hydrate formation is unlikely (Sloan et al., 2008). For marine systems, (GHSZ) begins at depths below 300-600 m and can range to several hundreds of meters below the seafloor, with a temperate variation of 2 - 20° C. Due to sulfate reduction and anaerobic oxidation of methane just below the seafloor, the concentration of methane is lowered and limits the hydrate formation to the Gas Hydrate Occurrence Zone (GHOZ). (GHOZ) is therefore a thinner layer owing to availability of methane (Hester et al., 2009). In Figure 1-10(b), the (GHSZ) is not included in region above the seafloor. Conditions such as, absence of porous medium in which water and gas could concentrate, and the fact that hydrates are less dense than seawater lead to a instability of hydrates (Ersland, 2013). However, small addition of heavier natural gas components such as, ethane, propane, or isobutene, in presence of H_2S in areas with high gas flux results in shallow accumulations or mound on the sea floor (Hester et al., 2009).

Knowledge about gas hydrates occurrence in continental margin sediment is concluded mainly from an anomalous seismic reflector (BSR or bottom-simulating-reflector)[6] (Kvenvolden, 1988) that

[6] "A bottom-simulating reflection (BSR) is a seismic reflectivity phenomenon that is widely accepted as indicating the base of the gas-hydrate stability zone. The acoustic impedance difference between sediments

matches with the transition boundary at the base of the gas hydrate zone. Gas hydrates have also been recovered at greater sub-bottom depth during coring by the deep sea drilling projects. Sloan and Koh (2008) report 23 locations where hydrate samples have been recovered, 3 in permafrost regions and 20 in ocean environments. Figure 1-11 shows an overview of the distribution of resources worldwide. Hester and Brewer (2009) reported up to 90 sites that have directly or indirectly identified hydrate deposits.

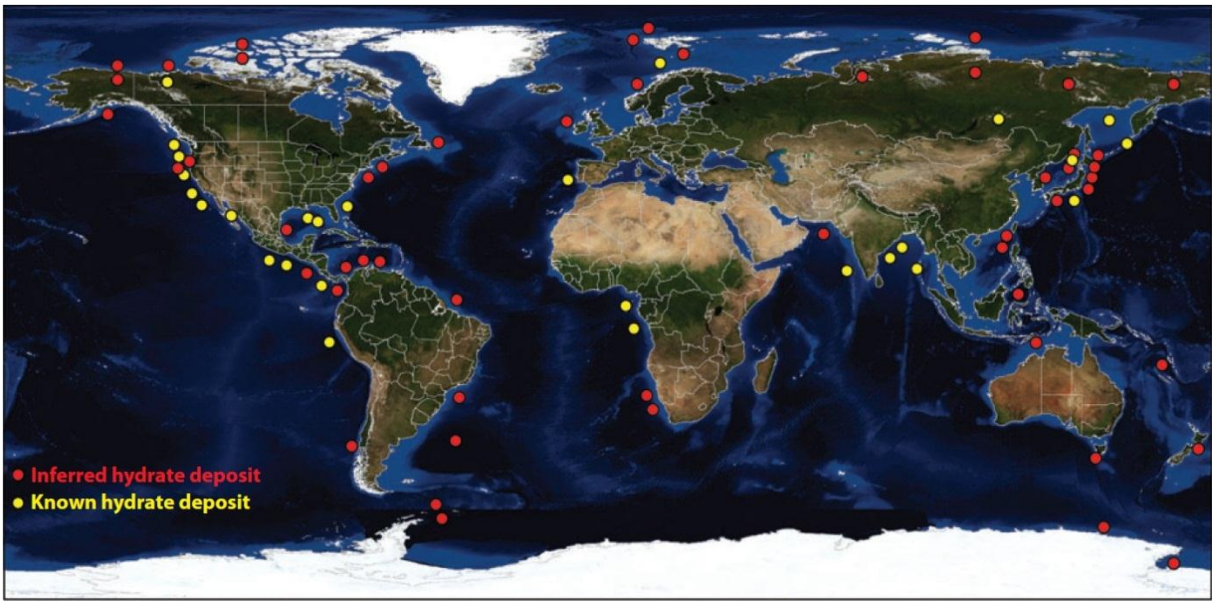

Figure 1-11 Worldwide distribution of more than 90 documented hydrate occurrences (Hester et al., 2009). Inferred hydrate deposits were concluded from indirect data, mainly from seismic reflectors and pore-water freshening in core samples. Known hydrate deposits are areas where direct data (hydrate samples) have been obtained during ocean drilling and remote-operated vehicle expeditions.

1.3.2 Classification of hydrate deposits

Natural gas hydrates have formed in different geological settings and under different temperature and pressure regimes. The result is a variety of gas hydrate occurrences with different properties. Boswell and Collet (2006), proposed a resource pyramid to portray the relative size and producibility of the different gas hydrate deposits with respect to their relative prospect for future commercialization, (Figure 1-12). According to Boswell and Collet, the hydrate deposits closed to potential production, are the ones with high hydrate saturations within quality reservoir rocks that lie closed to existing Arctic infrastructure. Such a deposit is found in the Eileen trend of the Alaskan North Slope with an estimated 9.4×10^{11} m^3 (STP) gas in place. The second largest class of hydrate deposits are the ones formed within similar geologic setting, but some distance away from the existing infrastructure. These deposits are of the less defined accumulations that are discretely trapped. The US geological survey has estimated a total of 1.3×10^{13} m^3 (STP) gas in place for the resources in North Slope. The currently less attractive reserves are the third class of the deposits. These are deposits that contain moderate to high hydrate saturations formed within high quality oceanic sandstone reservoirs. Potential production from such deposits is considered as challenging and expensive operations due to technical complexity of gas extraction from deep waters. Deposits found in Gulf of Mexico are

---

invaded with gas hydrate above the BSR and sediments invaded without gas hydrate, but commonly with free gas below, are accepted as the conditions that create this reflection" (Roberts et al., 2006).

favorable production targets belonging to this class due to their vicinity to existing oil and gas production infrastructure (Boswell, 2006).

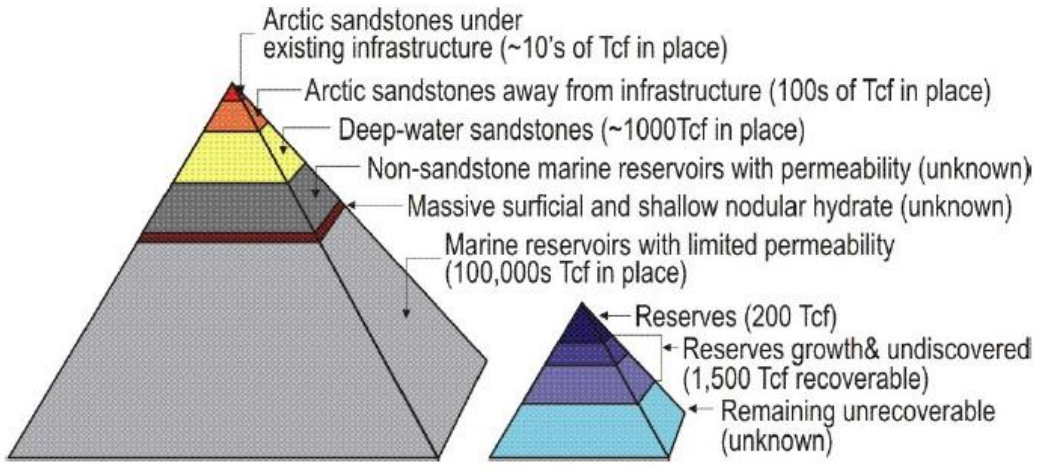

Figure 1-12 Gas hydrates reserves classification with respect to their size and relative prospects for future production (left), conventional gas reserves (right)

1.3.2.1 Types of hydrate deposits

As mentioned in section 1.3.2, there is a variety of gas hydrate deposits. Properties of the deposits are considered with respect to their thermodynamic state, hosting geological settings and trapping configuration (sealing characteristic and sealing geometry) (Ersland, 2008). Based on their properties, the deposits are divided into four main classes (Moridis et al., 2009).

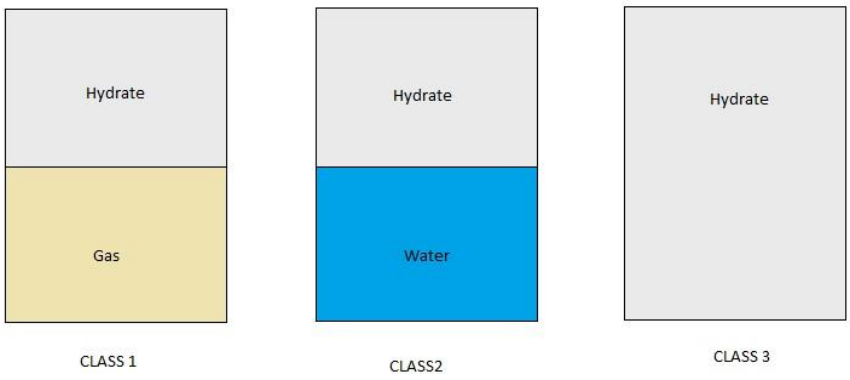

Figure 1-13 Schematic over types of hydrate deposits (Ersland, 2008), this simple classification provides insight into optimal production method.

As shown in Figure 1-13, CLASS 1 deposits are composed of a hydrate bearing layer (HBL), and an underlying 2-phase zone of free gas and connate water. If the hydrate layer is composed with water, the system is a Class 1W (gas-poor system), and if the hydrate layer involves gas and hydrate the system is a Class 1G (water-poor system). CLASS 2 deposits have a mobile water zone underling the hydrate bearing layer (HBL). Different from CLASS 1 and CLASS 2 accumulations, CLASS 3 deposits are characterized by a single hydrate zone and absence of an underling layer of mobile fluids. CLASS 4 deposits are described as scattered accumulations with low hydrate saturation, lacking a

confining geological strata and are generally not a target for exploitation (Ersland, 2008), oceanic hydrate accumulations are of such character.

1.4 Proposed production methods

Current literature refers mainly to two different groups of production methods. The first group is based on hydrate dissociation by changing the thermo-baric conditions. The proposed methods are; depressurization, thermal injection and inhibitor injection. The second group of production methods is based on replacement of guest molecule (methane) by another gas molecule resulting in thermodynamically more stable gas hydrate. $CH_4 - CO_2$ exchange has been used as a production method under the experiments for this master thesis. The method is further discussed under section 1.4.2.

1.4.1 Gas production by hydrate dissociation

The hydrate dissociation occurs either when the temperature is raised or the pressure is lowered to outside of the thermodynamic restrictions of the phase equilibrium as shown in Figure 1-14. Depressurization is considered as a promising production method as it has been applied successfully on the field scale (Messoyakha filed in Siberia and Mallik at the Mackenzie Delta, Canada), and as no energy needs to be added to the system during the process (Birkedal et al., 2010). However there are some concerns regarding the subsidence of the surface as the hydrate saturation decreases during the production. As hydrates tend to fill the pores rather than cementing them (Kleinberg et al., 2003), dissociation of hydrates may result in compaction of the formation specially in the area adjacent to the wellbore. Thermal injection is another proposed production method, using steam or hot water to increase the reservoir temperature and dissociate the hydrates. The method is less appealing as energy is required to heat up the water. Injection of an inhibitor has also been discussed in the literature as dissociation technique. An inhibitor (such as salts and alcohols) causes a shift in the hydrate formation curve. Hydrate forming region is therefore restricted to lower temperature and higher pressure than before the inhibitor was injected. All methods mentioned above result in dissociation of hydrate into its water and gas constituents and decreasing in saturation of the solid hydrate phase (Schoderbek et al., 2012).

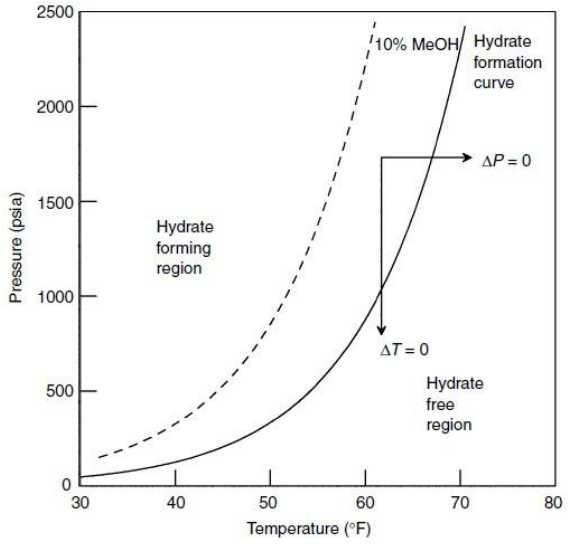

Figure 1-14 A phase diagram showing the three common hydrate dissociation methods. Depressurization is shown as $\Delta T = 0$, thermal stimulation as $\Delta P = 0$; inhibitor injection is displayed by hydrate formation curve being displaced by the dashed curve (injection of 10 wt% methanol in the free water phase) (Sloan et al., 2008).

1.4.1.1 Field example: The Messoyakha Field

The Messoyakha gas hydrate field is known as the first field producing gas from hydrate in the permafrost (Sloan et al., 2008). The field is located in northeast of western Siberia, close to the junction of Messoyakha River and Yenisei River. The hydrate reservoir in Messoyakha field has an underlying free gas layer (CLASS1 hydrate reserve, shown in Figure 1-13) which was target for production. Gas production from the lower free gas layer began in 1969 and a pressure drop was observed as predicted. But the pressure drop started to deviate from the predicted values in 1971 (Moridis et al., 2009). The hydrates began to dissociate when the pressure in the field reached the hydrate equilibrium value releasing more gas to the reservoir. The Messoyakha filed has also produced through inhibitor injection and a combination of inhibitor and depressurization. The inhibitor injections tests gave dramatic short-term increases in production rates. This because the hydrate dissociation occurred in vicinity of each injected wellbore. The inhibitor tested were methanol and a mixture of MeOH and $CaCl_2$. Production methods applied in Messoyakha are shown schematically in Figure 1-15 (a) and (b).

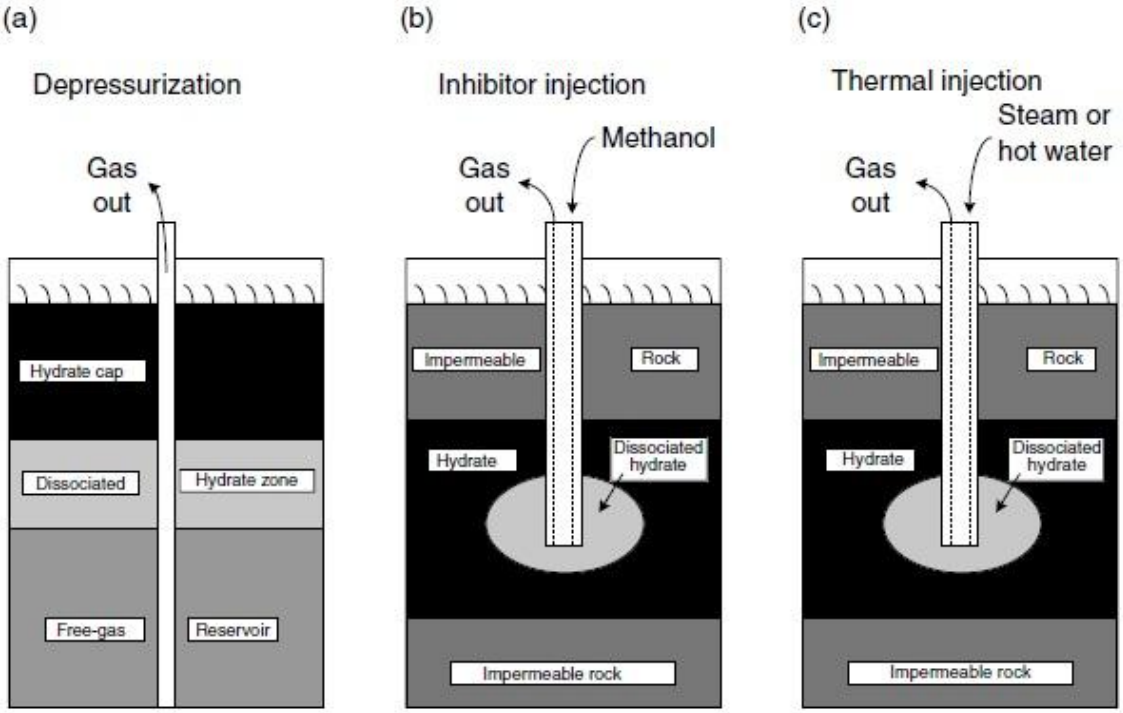

Figure 1-15 Gas hydrate production options (Makogon, I. U. F., 1997)

1.4.1.2 Field example: The Mackenzie River Delta

Gas hydrate occurrences in the Mackenzie River Delta were concluded based on data attained during exploration for conventional petroleum reserves (Alan et al., 1994). These data were later refined with data from three international scientific drilling programs in 1998, 2002 and 2006-2008 making Mallik field one of the best characterized gas hydrate deposits in the world. The gas hydrate layer in the field has a thickness of more than 110 m and underlies 600 m of permafrost. Hydrate saturations of more than 80% were concluded from well-log analysis, making the Malik field one of the most concentrated gas hydrate deposits in the world. To investigate the hydrate bearing layer's response and feasibility of production of depressurization-induced gas, short-term depressurization experiments were conducted. Thermal injection was also applied as a production method in 5 days, this involved injection of warm water in a 17-m-thick layer with high hydrate saturation. The main findings from the three drilling

project indicated that methane production from the Mallik reservoir was possible through long-term depressurization. However, sand control and handling of the produced water could be crucial. Data acquired from these test also indicated that the hydrate in the Mallik reservoir reinforced the sediment matrix. This could implicate the production as hydrate dissociation could result in less formation integrity (Moridis et al., 2009).

1.4.2 Production of CH_4 from hydrates by CO_2 exposure

The idea of accessing hydrate bound methane by introducing a thermodynamically more stable hydrate former guest molecule was first introduced by Japanese researchers (Ebinuma, 1993). CO_2 hydrate is thermodynamically more stable than CH_4 hydrate under low temperatures, below 283K, because the equilibrium pressure for CO_2 hydrate is lower than that of CH_4 hydrate (Ota et al., 2005). The pressure and temperature diagram for CH_4 and CO_2 hydrates is shown in Figure 1-16. Several experimental and theoretical studies have demonstrated the occurrence of the exchange in hydrate using pressurize CO_2 and succeeded in production of CH_4 and in storage of CO_2 (Ersland, 2008; Graue et al., 2006; Husebø, 2008; Lee et al., 2003; Park et al., 2008). The driving force for the replacement have been mentioned to be, firstly, the difference in thermodynamic stability provided by CO_2 in comparison with CH_4, and secondly the exothermic nature of CO_2 hydrate formation which in turn may accelerate the replacement rate through rapid CH_4 hydrate micro dissociations . The generated heat during formation of a mol of CO_2 – hydrate varies between 57.7 and 63.6 KJ mol^{-1} and the amount of heat needed to dissociate a mole of CH_4 – hydrate is 52.7 – 55.4 KJ mol^{-1}. Therefore, CH_4 – CO_2 exchange process is an exothermic process (Jung et al., 2010). In addition to providing more hydrate stability, CH_4 – CO_2 replacement offers the possibility of CO_2 sequestration into hydrate. The latter may be an attractive approach considering long term CO_2 storage, which may halt the possible anthropogenic global warming.

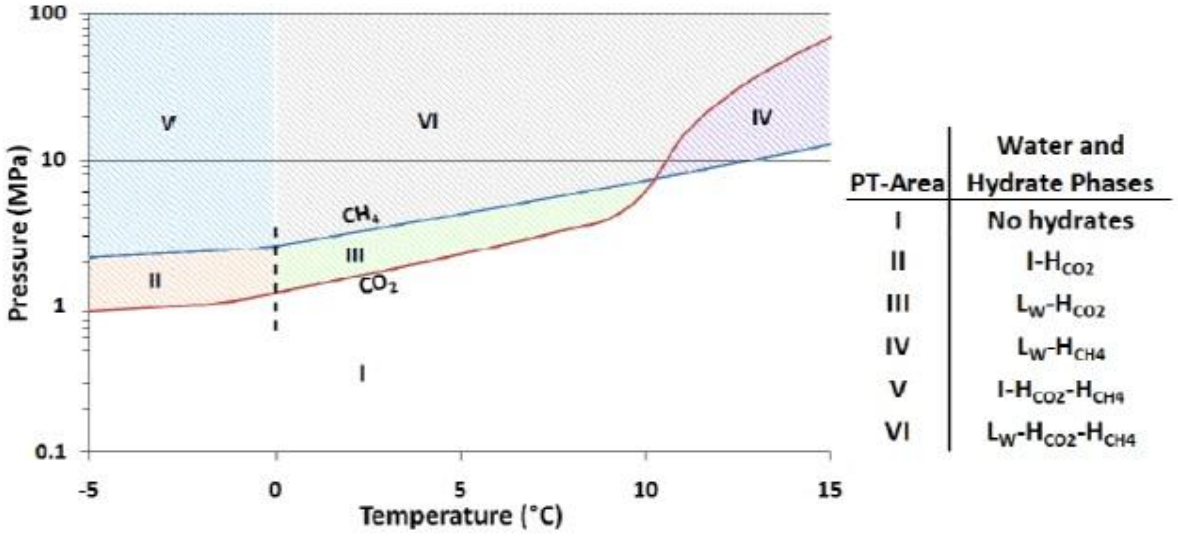

Figure 1-16 - Pressure and temperature diagram for both CH_4 and CO_2 hydrates. As the figure shows, at temperatures below 10° C, the CO_2 hydrate is stable at lower pressure values. Table to the right shows an overview over the stability regions of different hydrates as well as the water phase. (I = Ice, L_w = Liquid Water, H_{CO2} = CO_2 – Hydrate, H_{CH4} = CH_4 – Hydrate) (Husebø, 2008).

Production methods based on hydrate dissociation involve significant production of the associated water. Natural gas production by CO_2 exchange and sequestration benefits from no or little water production during this process (Graue et al., 2008). During the exchange process, CO_2 replaces CH_4 preferentially in the large cages of the structure I. CO_2 is a poor guest filling the small cages due to the ratio of guest diameter to cavity diameter (Lee et al., 2003). Figure 1-17 shows a schematic diagram of the guest molecule exchange process in the large cage and the CH_4 reoccupation in the small cage. Ratio of molecular diameter to cavity diameter for CH_4 and CO_2 in structure I and structure hydrates are listed in Table 1-5.

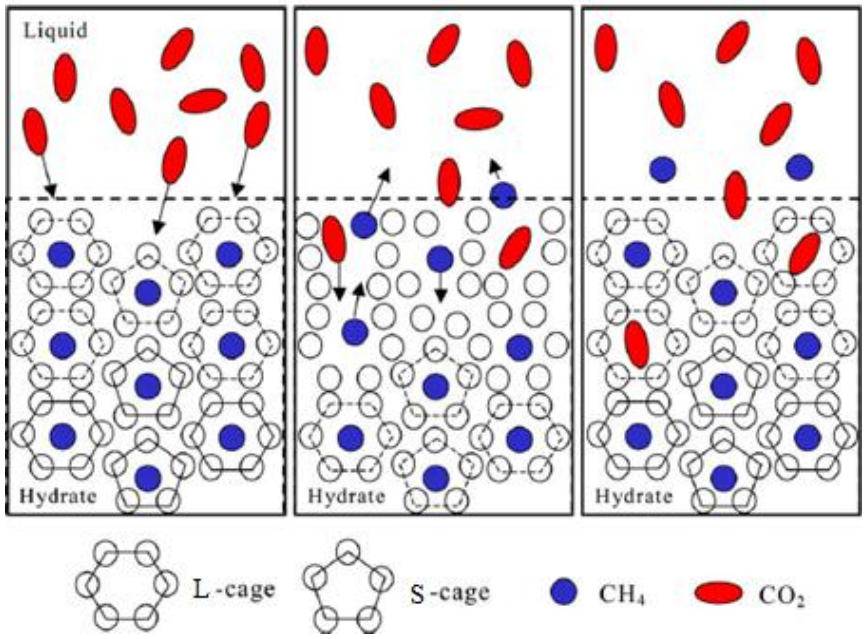

Figure 1-17 - A schematic diagram of the illustration of the guest molecule replacement in the M-cage and the CH_4 reoccupation in the S-cage. Modified from (Ota et al., 2005).

Table 1-5 - Ratio of molecular diameter to cavity diameter for CH_4 and CO_2 (Sloan et al., 2008) .

		Molecular diameter / Cavity diameter for cavity type			
Guest hydrate former		**Structure I**		**Structure II**	
Molecule	**Diameter (Å)**	5^{12}	$5^{12}6^2$	5^{12}	$5^{12}6^4$
CH_4	4.36	0.855[a]	0.744[a]	0.868	0.655
CO_2	5.12	1.00[a]	0.834[a]	1.02	0.769

[a] indicates the cavity occupied by simple hydrate former.

1.4.2.1 North Slope hydrate field trial: CO_2/CH_4 Exchange

Based on extensive research and laboratory results on CO_2 – CH_4 exchange in sandstone (Ersland et al., 2009; Graue et al., 2006; Graue et al., 2008; Husebø et al., 2009), a field trial was planned and successfully completed on the North Slope of Alaska. The goal of the field trial was to further investigate the possibility of injection of CO_2 and production of CH_4. Reviewing of log data indicated that the formation beneath the Eileen Trend was expected to contain hydrates in several sandstone layers at depth ranging from 1700 feet to 2400 feet. The well Ignik Sikumi #1 was designed to pass through a number of hydrate accumulations keeping distance from producing wells (Schoderbek et al., 2012). Data collected from the site indicated strong shows of gas at the predicted depth. Advanced analysis of open-hole wireline data as well as NMR measurements showed four hydrate bearing sediments with a hydrate saturation of 75%. The NMR log clearly indicated the remaining 25% pore volume to be free water (and not free gas) that could form additional hydrate if a hydrate former molecule was present. Based on the deposits characterization, there were two issues to be addressed: 1) liquid CO_2 operational concerns. 2) Potential loss of injectivity due to secondary hydrate formation from the free water and injectant. The simulations data indicated a composition of 23% CO_2 + 77% N_2 to be an optimal composition for the injectant in order to mitigate the secondary hydrate formation. An injection was carried on for thirteen days, resulting in a total of 210 mscf mixed gas injected at a

bottomhole pressure of 1420 psi and a temperature of 5 °C at the perforations. A production test was conducted at four phases: 1) Unassisted flowback 2) Production at pressure above the CH_4 hydrate stability pressure 3) Production at pressure near the CH_4 hydrate stability pressure 4) Production at pressure below the CH_4 hydrate stability pressure. A total of 998 mscf of gas was measured and analyzed. The total gas measured at the well head was consisted of 22 mscf CO_2, 155 mscf N_2 and 821 mscf CH_4, shown in Figure 1-18 (Schoderbek et al., 2012).

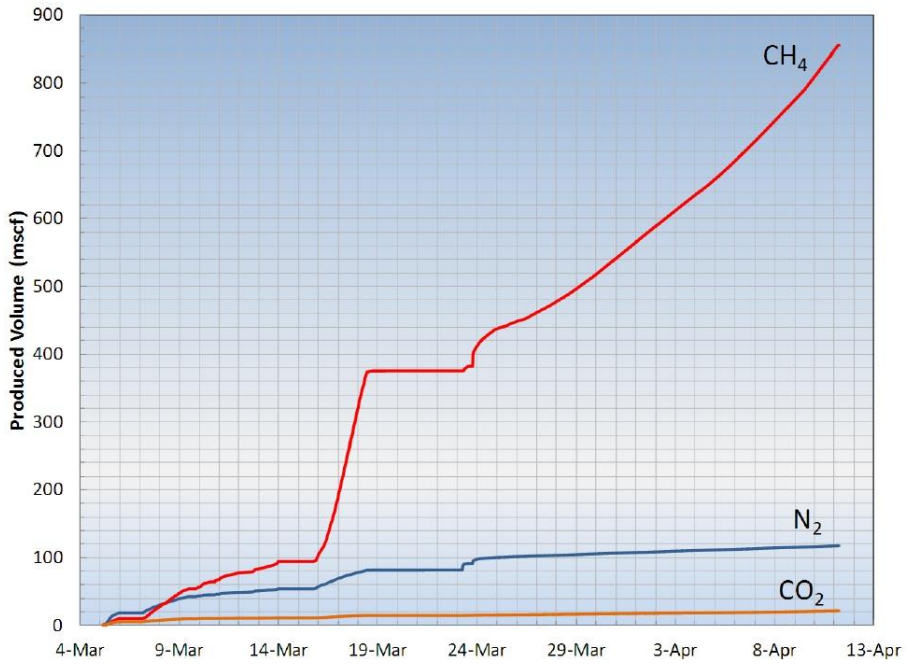

Figure 1-18 Composition of gas produced at Ignik Sikumi #1 during the various phases of the production. (Schoderbek et al., 2012).

One of the key achievements of the field trial was the identification of the N_2/CO_2 composition that would mitigate CO_2 hydrate formation of excess water. Analyzed data indicated that nearly 1000 mscf was produced with rates as high as 175,000 scf/day over a five week period of time. Most of the 162 mscf of injected N_2 was recovered during the production stages and more than half of 48 mscf of CO_2 injected remained in the formation. The results from the Ignik Sikumi field trial showed that CO_2 could be injected into a hydrate reservoir resulting in CH_4 production. The also showed that CO_2/CH_4 exchange process may be commercially feasible in the future (Schoderbek et al., 2012).

1.4.3 Production impacts on geomechanical stability of hydrate deposits

There are mainly two approaches to produce natural gas from natural gas hydrate reservoirs. One can either bring the hydrate out of hydrate stability, or expose the hydrate to a substance that will form a more thermodynamically stable hydrate. A serious concern with bringing hydrate of out hydrate stability conditions is that the dissociation of hydrate frees the water bound in hydrate and destabilizes the reservoir sediments. The dissociated water causes production problems while decreased reservoir stability could trigger large scale subsidence. These problems can be avoided by exposing hydrate to a thermodynamically more stable hydrate former. An induced replacement process will increase the reservoir stability by maintaining hydrates in solid state (Graue et al., 2008). Natural gas hydrates can be found in consolidated sediments, but natural gas hydrates that are considered attractive targets for commercialization, are hydrates formed in unconsolidated sediments. Geomechanically, gas hydrates play an important role in formation strength, giving support to the overlying sediments (Birkedal et al.,

2010). NMR studies of methane hydrate growth habit in porous media have shown that the methane hydrate is mainly pore-filling and not grain-cementing (Kleinberg et al., 2003). This may be a reason to believe that the shear strength of the hydrate saturated matrix would be much less if not for the hydrate filling the pores. So if hydrates are dissociated, the matrix will no longer be able to support the overlying sediments, which in turn could trigger uncontrolled pore-collapse. The latter could potentially result in major release of methane into the water column and the atmosphere. Uncontrolled subsidence of the sea floor represents a threat to production facilities and infrastructures at the well site.

2 Fundamental petrophysics

Since natural gas hydrate deposits are formed in sediments, it is sensible to study formation of methane hydrates and conversion of carbon dioxide to its hydrate in porous media. Outcrop of sedimentary rocks have been used under the experiments for this study. A basic understanding of core analysis terminology is to be revised for further studies of hydrate formation and dissociation in porous medium.

2.1 Effective porosity

Porosity is the measure of a sedimentary rock's capacity of containing fluids. The porosity is defined as the void part of the rock's total volume. Absolute porosity is the fraction of the total void space V_{pa} within a rock to the bulk volume of a rock sample, V_b:

$$\emptyset = \frac{V_{pa}}{V_b} \tag{2.1}$$

Equation (2.1) defines the porosity regardless of whether the voids are interconnected or not. One defines an effective porosity as a measure of interconnected pores. The effective porosity is given by the fraction of the total volume of interconnected pores, $V_{p,}$ to the bulk volume of a rock sample:

$$\emptyset = \frac{V_p}{V_b} \tag{2.2}$$

2.2 Permeability

2.2.1 Absolute permeability

Permeability is the porous medium ability to transport fluids through its interconnected pores and may be related to the effective porosity in some cases. When a single fluid is flowing through the porous medium, the permeability is absolute and may be considered as a constant property of the porous medium. Permeability is a direction orientated parameter, this means that, the permeability of a porous medium depends upon the flow direction. But for practical reasons, it is often reduced to one value in one direction. Permeability for a porous medium such as one in Figure 2-1, where pressure is equal to *Pa* at the inlet side and *Pb* at the outlet side may be defined through the empirical Darcy's law for the linear, horizontal flow of an incompressible fluid can be written as equation (2.3):

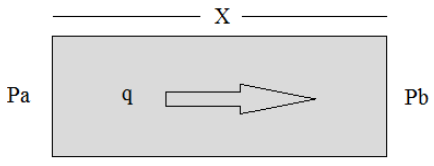

Figure 2-1 – Fluid flow along x-direction through a porous medium with a length x and cross-section areal A.

$$q = -A\frac{k}{\mu}\frac{dp}{dx} \tag{2.3}$$

Where q is the flow rate [m^3/s], k is the permeability [m^2], A is the cross-sectional area of flow [m^2], μ is the viscosity of the fluid [Pa.s], and dp/dx is the pressure drop per meter [Pa.s].

2.2.2 Relative permeability

As stated in preceding section, the permeability is absolute when only a single fluid is flowing through the pores. The situation is different when multiple non-miscible fluids flow through the porous medium, as each fluid occupies the flow area of the other fluids and hinders flow throughout the porous medium. As a result of this, each fluid will have a reduced effective permeability compared to their absolute permeability. The effective permeability of a porous medium to a fluid is given by a modification of Darcy's law:

$$k_{i,eff} = -q_i\frac{\mu}{A}\frac{dx}{dp} \tag{2.4}$$

Where i is a specific fluid. The relative permeability is then given by:

$$k_{r,i} = \frac{k_{i,eff}}{k_{abs}} \tag{2.5}$$

Where $k_{r,i}$ is the relative permeability of fluid i, $k_{i,eff}$ is the effective permeability of fluid i and k_{abs} is the absolute permeability. As each fluid hinders the free flow of the other fluids, the effective permeability is always less than the absolute permeability. The effective permeability is significantly influenced by each fluid's saturation of the porous medium. The high saturation of a fluid results in easier flow giving increased permeability.

2.3 Capillary effects

Capillary effects arise when immiscible, mobile phases coexist within a porous medium. Capillary equilibrium occurs when difference in pressure in phases either side of the interface is supported by a surface tension force in the interface region (Clennell et al., 1999).

2.3.1 Capillary pressure

The pressure and temperature conditions for hydrate formation in a porous medium are in under impact of capillary pressure (Goel, 2006) which is given by equation (2.6):

$$P_{nw} - P_w = \frac{2\sigma_{hw}\cos\theta_{hw}}{r} \tag{2.6}$$

Where Pnw is the internal pressure of the non-wetting phase [Pa], Pw is the internal pressure of the wetting phase [Pa], σ_{hw} is the interfacial tension between hydrate and water [mN/m], θ_{hw} is the wetting angle between hydrate-water and the solid's surface, and r is the effective pore entry radius [m] (Zolotukhin et al., 2000). Capillary pressure affects the distribution of different phases. According to Clennel *et al.* (1999), in a capillary equilibrium gas will reside in the larger pores in a gas-water system (Clennell et al., 1999). In Bentheim sandstone core samples, water is continuous and wetting to the sediment grains. Given that gas bubbles reside in the large pores, hydrate formation initiates in the large pores and at the gas-water interface.

2.3.2 Properties of methane

CH_4 is a gas at standard conditions and also at experimental conditions used under present study (83bar 4ºC). Density, viscosity and solubility of methane in present of other phases have to be evaluated in order to better understand both the hydrate formation and CH_4 – CO_2 replacement phenomena. Density and viscosity as function of pressure are respectively shown in Figure 2-2 and Figure 2-3.

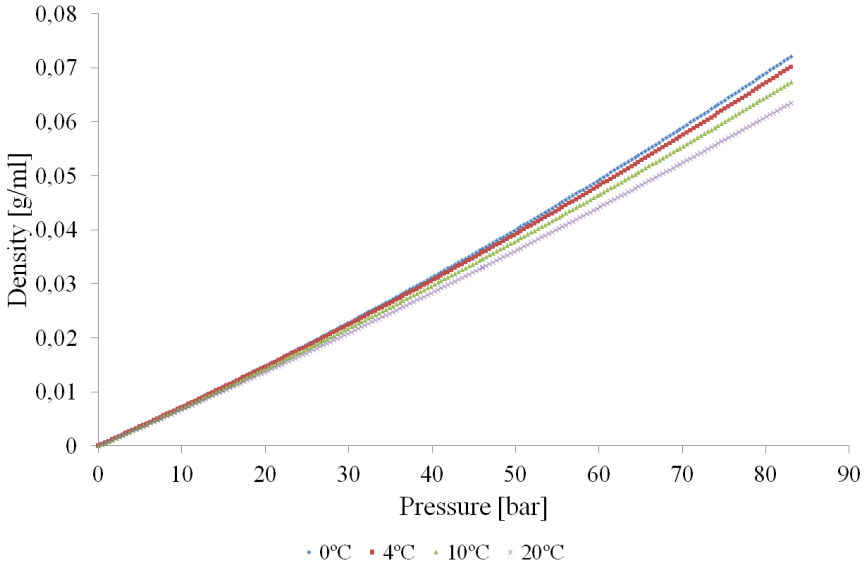

Figure 2-2 – Density of CH_4 as function of pressure at different temperatures (NIST, 2013).

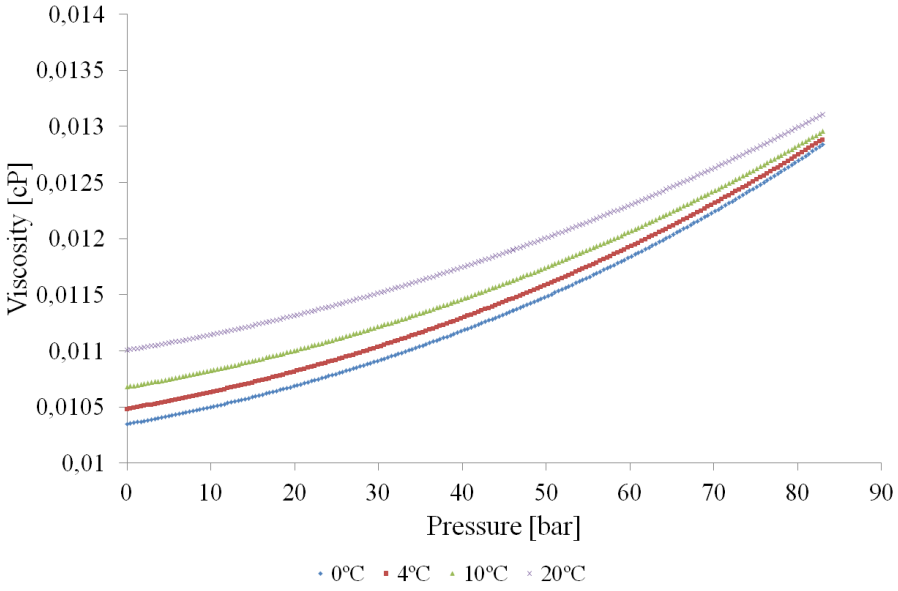

Figure 2-3 – Viscosity of CH_4 as function of pressure at different temperatures (NIST, 2013).

Solubility of methane in liquid water is very small at pressures both below (0.11 mol Kg^{-1} at 3MPa, 273K) and above (0.12 mol Kg^{-1} at 6.6 MPa, 274K) the hydrate formation point (Sloan et al., 2008). But CH_4 is highly soluble in liquid CO_2, for example, a molar mixture of 12% CH_4 and 88% CO_2 remains liquid above a line defined between [6.6 MPa, 273.1 K] and [7.2 MPa, 278.1 K] (Jung et al.,

2010) and a mixture of these two components will be less dense with increasing CH_4 fraction. Density of mixtures of CO_2 and CH_4 as function of CH_4 fraction is shown in Figure 2-4.

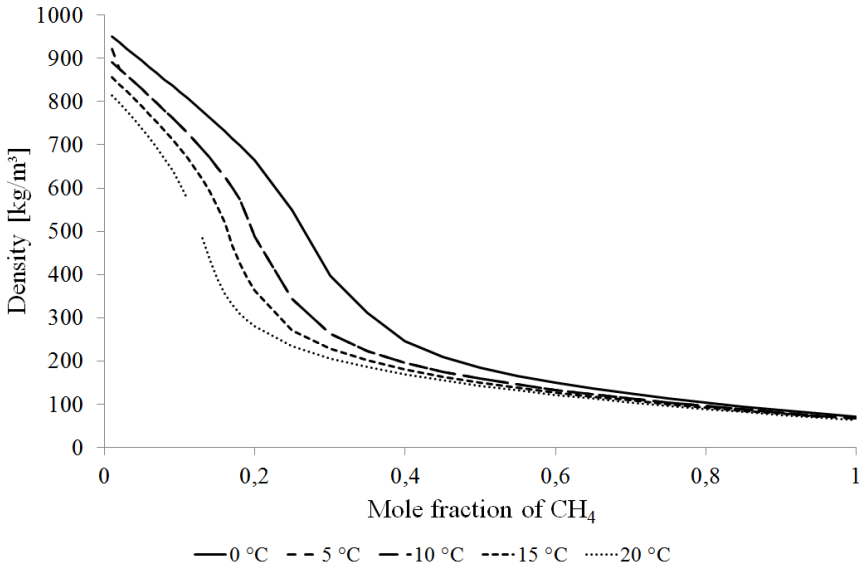

Figure 2-4 – Density of mixtures of CH_4 and CO_2 as function of CH_4 fraction at different temperatures (NIST, 2013).

2.3.3 Properties of Carbon Dioxide

Gaseous or liquid, viscosity, density and solubility of CO_2 in present of other phases are of great importance during CO_2 exchange experiments. CO_2 is in gas phase under standard conditions, but under experimental conditions (83bar and 4ºC) CO_2 is in liquid state. Under experimental conditions, CO_2 has a density of 0.9427 [g/ml]. Under such conditions, CO_2 is over 10 times denser than CH_4. The density of CO_2 as function of pressure under different temperatures is shown in Figure 2-5. As shown in, the change in density is huge when CO_2 becomes liquid at higher pressure. At experimental conditions, CO_2 has a higher viscosity than CH_4. Viscosity of CO_2 as a function of pressure at different temperature is shown in Figure 2-6.

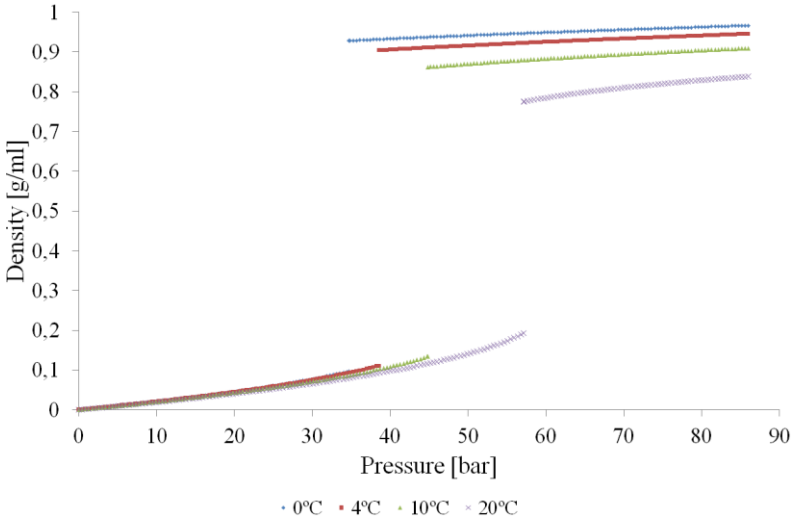

Figure 2-5 - Density of CO_2 at different temperatures [ºC]. (NIST, 2013)

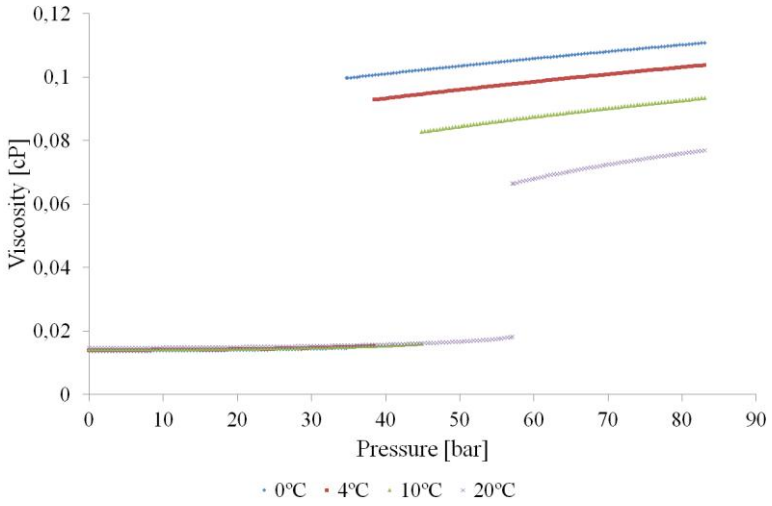

Figure 2-6 – Viscosity of CO_2 as function of pressure under different temperature. (NIST, 2013)

Solubility of CO_2 in water is also important as it affects gas transport, hydrate formation and hydrate dissolution in water which is undersaturated with gas. The solubility of CO_2 in water is about 10 times larger than the solubility of CH_4 in water (Jung et al., 2010). The solubility of both methane and carbon dioxide increase as pressure increases and temperature decreases.

Mutual diffusivities

Diffusion controls both hydrate formation and CH_4 – CO_2 replacement (Kvamme, 2012). Both CH_4 and CO_2 have about the same diffusivities in water, but the diffusivity of H_2O in liquid CO_2 is up to 2 orders of magnitude larger. The diffusivity of H_2O, CH_4 and CO_2 through the solid hydrate mass is a slow process compared to diffusion in liquids. Transport of CH_4 or CO_2 molecules through hydrate is therefore a much slower process compared to through liquid water (Jung et al., 2010).

2.3.4 Monoethanolamine (MEA) & Methyldiethanolamine (MDEA)

Under this study enhancement of the CH_4 – CO_2 replacement process by use of slugs of MEA and MDEA was studied. A more detailed description of CO_2 – CH_4 exchange process is provided under section 1.4.2. Both MEA and MDEA are used for removal of carbon dioxide in natural gas industry(Farmahini et al., 2011; Li et al., 2007; McCann et al., 2009; Xie et al., 2010; Zhang et al., 2010). MEA and MDEA belong to Alkanolamines which are a group of ammonia derivatives that are consisted of at least one hydroxyl group and one amine group. The amine group is divided into different subgroups based on the number of substituents on the nitrogen atom. These are the primary, secondary and tertiary alkanolamines. MEA belong to the subgroup of primary alkanolamines while MDEA belong to tertiary alkanolamines.

- Primary alkanolamines: Nitrogen atom carries one substituent group (ethanol group) and two other hydrogen atoms that are bonded to the nitrogen atom. MEA (Monoethanolamine) is an example for the primary alkanolamines.

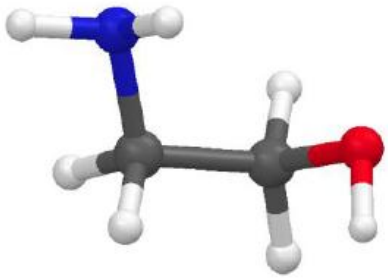

Figure 2-7 - Molecular structure of Monoethanolamine, C_2H_7NO (NIST, 2013).

- Tertiary alkanolamines: These alkanolamines have no hydrogen atoms directly bonded to the nitrogen. The hydrogen atoms have been replaced by the substituent groups (alkyl or alkanol groups). MDEA is an example for the tertiary alkanolamines. (MDEA) is a viscous aqueous amine at standard condition and has a density of 1.008 [g/ml] and viscosity of 101 [cP] (Derks, 2006).

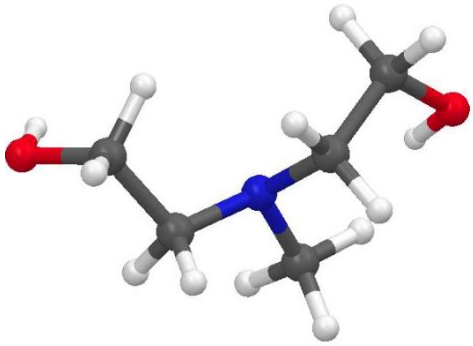

Figure 2-8 – Molecular structure of Methyldiethanolamine, CH_3N $(C_2H_4OH)_2$ (NIST, 2013)

Reaction of primary alkanolamines such as MEA with CO_2 follows the overall reaction **(2.7)** which results in formation of carbamates (Derks, 2006):

$$2Am + CO_2 \leftrightarrows AMH^+ + AmCOO^- \quad (2.7)$$

While reaction between a tertiary alkanolamines such as MDEA with CO_2 does not result in formation of carbamates and follows the overall reaction (2.8) (Derks, 2006):

$$Am + CO_2 + H_2O \leftrightarrows AMH^+ + HCO_3^- \quad (2.8)$$

Both MEA and MDEA are highly soluble in water and can act as hydrate inhibitors. Both MEA and MDEA can be hydrogen bonded to water making water less accessible for the guest molecule. This way, the water activity is reduced in a way that higher pressure and lower temperature is required to form hydrate.

The exothermic nature of the reactions between CO_2 and (MEA) and CO_2 and (MDEA) in presence of water (Kvamme, 2013) was the reason these additives were injected during CH_4 – CO_2 exchange process. The generated heat from the reactions above has the potential of triggering hydrate dissociation. Methyldiethanolamine (MDEA) has relatively low heat of reaction compared to (MEA) when it reacts with CO_2 (Kvamme, 2013; Zhang et al., 2010). Heat of reaction between MDEA and CO_2 has been measured to be in the range of 48 KJ mol^{-1} (Kierzkowska, 2007), while heat of reaction between MEA and CO_2 has been measured to be 1900 KJ mol^{-1} (Prakash et al., 2006). It is important to mention that heat adsorbed during the dissociation of a mole of CH_4 hydrate is 52.7 – 55.4 KJ mol^{-1}(Jung et al., 2010). The heat generated during the reaction between MEA and CO_2 is several orders of magnitude greater than the heat generated during reaction between MDEA and CO_2 which indicates that such reaction has the potential of dissociating methane hydrate. In order to investigate feasibility of enhancing the CH_4 – CO_2 reaction, slugs of both pure (>99%) (SIGMA-ALDRICH, 2013) MDEA and MEA were injected both prior and post CO_2 injection to investigate if the generated heat could assist methane production from the core.

Part II

Experimental Description

3 Material and methods

The different hydrate experiments presented in following section were conducted using two setups at the hydrate laboratory at the University of Bergen. One was a completely new setup that was made based on experiences from previous studies (setup c). The other one was a simpler setup existing from previous studies. Both setups generated PVT measurements for analysis. As for this master thesis, most of the experiments have been conducted using setup c. The possibility of monitoring the phase transition during hydrate formation and $CO_2 - CH_4$ exchange process has been absent under this study, however a mass flow meter was implemented in production line which provided quantification of the produced effluent. Previous extensive hydrate studies were conducted using magnetic resonance imaging (MRI) (Birkedal, 2009; Ersland et al., 2009; Graue et al., 2008; Husebø, 2008).

3.1 Properties of the sandstone core sample

The porous rock samples used under this study are Bentheim sandstone core plugs with a porosity of 22%, absolute permeability of 1100mD and a grain density of 2.65 g/cm^3. This type of sandstone has a mineralogy of 99% quarts with traces of the clay mineral kaolinite (Graue et al., 2006). The core samples are strongly water wet and are characterized by uniform pore geometry with an average pore diameter of 125 microns (Husebø, 2008). The outcrop Bentheim sandstone core plugs were 14.5cm long and were 5.0cm in diameter. Further details, such as weight, length and diameter on each sample core can be found in Appendix B1.

3.2 Experimental Setups

The early experiments in this study were conducted on existing setups used during previous hydrate studies (Birkedal, 2009; Bringedal, 2011; Hauge, 2011). These setups were further modified in order to extent the experimental possibilities. In Addition a mass flow meter was installed enabling quantification of the production. Three setups, shown in Figure 3-1 were available at the hydrate laboratory at the University of Bergen. Setup C was mainly used for experiments conducted under this study.

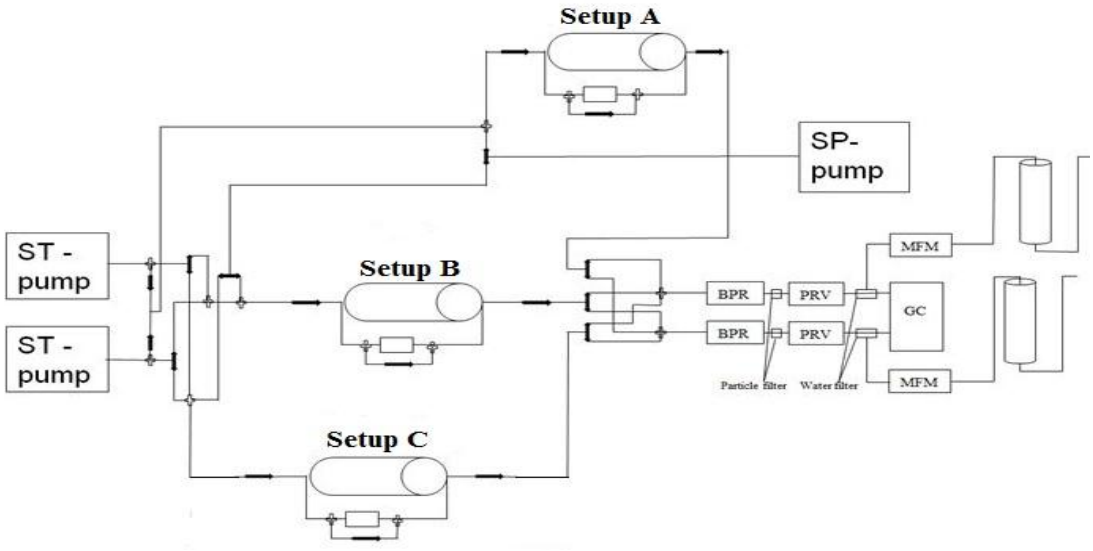

Figure 3-1 - Overview of all three available setups at hydrate laboratory at University of Bergen. Setup C was mainly used for the experiments conducted under this study.

3.2.1 Experimental setup with cooling pool

Early experiments were conducted using available setup from previous hydrate studies (Birkedal, 2009; Bringedal, 2011; Husebø, 2008). This setup consisted of a high pressure Hassler core holder that was cooled by being submerged into an open external bath. A STIGMA 3000 pump from Sanchez Technologies was used for CH_4 injection into the core. Generated PVT data were logged using a computer. These data were used to monitor hydrate formation. A haskel pump provided confining pressure by injection of high viscosity oil into the core holder. The external open bath was cooled by circulating antifreeze from a Thermo Neslab RTE-17.

Pressure Cell (core holder)

The pressure cell is a chamber in which the experiments have been conducted. The pressure cell used under this study is a Hassler type core holder designed and manufactured by Temco Inc ©, Tusla, OK. Hassle type core holder applies radial pressure to the core sample. The unique design of the core holder makes it easy to interchange core test samples without completely disassembling the core holder. The enclosure is made of aluminum in order to reduce the weight of the core holder. The two end lugs stabilizing the core sample are made of stainless steel and allow access to the core sample through four connection ports. N-decane was used as confining liquid. By applying confinement pressure a sleeve seals the core sample. A schematic illustration of the pressure cell is shown in Figure 3-3.

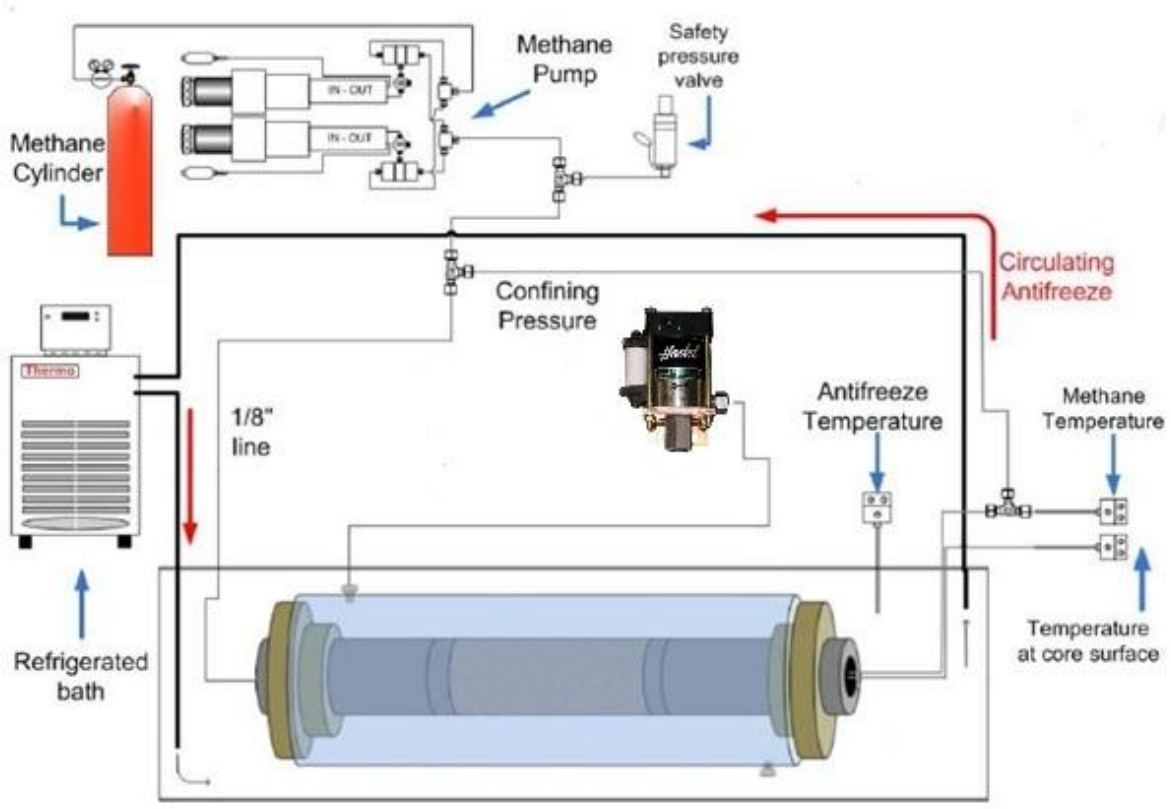

Figure 3-2: Illustration of the old setup C, modified from (Birkedal, 2009). The blue core holder is submerged into an open bath which is cooled by refrigerated bath.

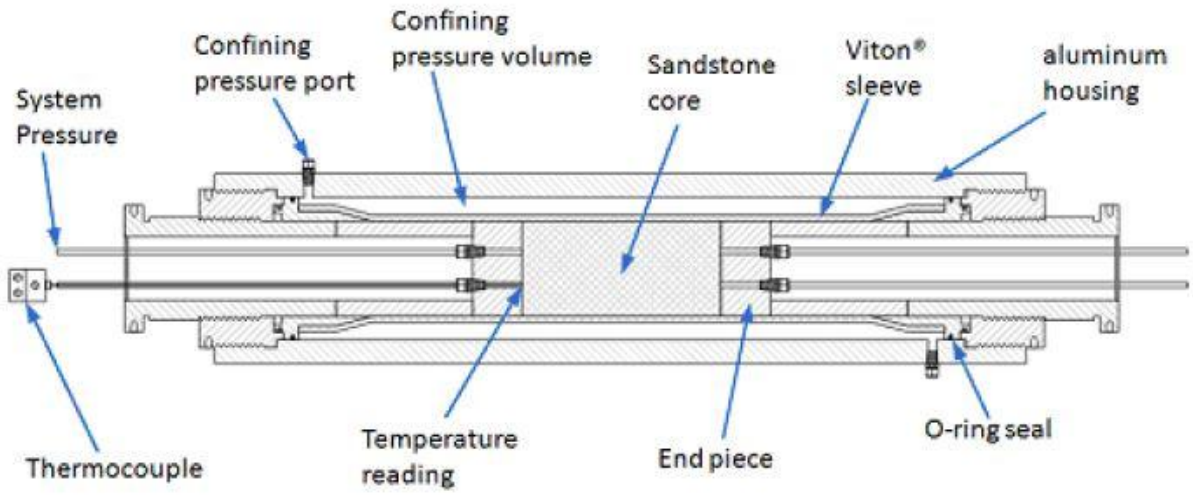

Figure 3-3 – Cross-sectional illustration of core holder used in experimental setup based on external cooling bath (Husebø, 2008).

3.2.2 Experimental setup based on cylindrical cooling jacket (Setup C)

A new setup, setup C, was designed and built during spring 2012. To avoid flooding problems, a cylindrical cooling - jacket was customized to cover around a Hassler core holder (Hassler core holder) is shown in Figure 3-3. The core holder was cooled by circulating antifreeze from a Thermo Neslab RTE-17. An illustration of setup C is shown in figure. Not the whole core holder is covered by the cooling jacket, but the part covered are sufficient in order to keep the whole core sample under desired temperature. Confinement pressure system was also modified for setup C. An Isco D-series pump was used to pressurize the confinement oil. When the desired confinement pressure, 120bar, was reached, an already pressurized (up to 120bar) confinement buffer was connected to the system and the pump was disconnected. A STIGMA 3000 pump from Sanchez Technologies was used for injection of CH_4 and CO_2 into the core sample. The new design allowed for gas injection from both sides (inlet and outlet) through a bypass valve. In addition, two pressure sensors of type UNIK 5000 were installed enabling differential pressure measurements over the core sample. Temperature measurements were taken at the end of the end-piece using a thermocouple. The implemented thermocouple passed through the end-piece and was in contact with the core during the experiment. Moreover, inlet, outlet pressure sensors and the bypass valves were installed on a control panel which provided better stability for the connected tubing lines as well as better overview of the connected lines. In addition, the setup was modified to allow for slug injection. Figure 3-4 and Figure 3-5shows an illustration of the high pressure core holder used in setup C.

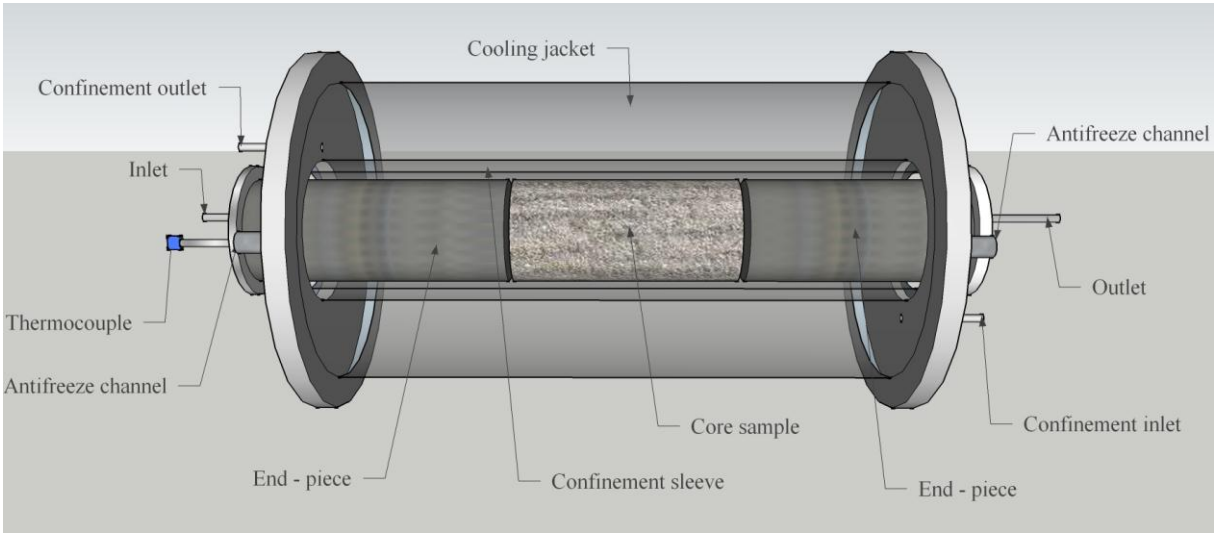

Figure 3-4 - Illustration of high pressure core holder, the cooling jacket and the way the core is placed inside the core holder. The two end-pieces hold the core steady inside the core holder. Inlet and outlet lines pass through the end-pieces and are in contact with the core sample. The cooling jacket, core holder and confinement sleeve are made transparent in this illustration enabling an insight of how the setup is constructed. During experiments, temperature measurements could be taken at the inlet side of the core. A thermocouple in the end of the end-piece measured the temperature.

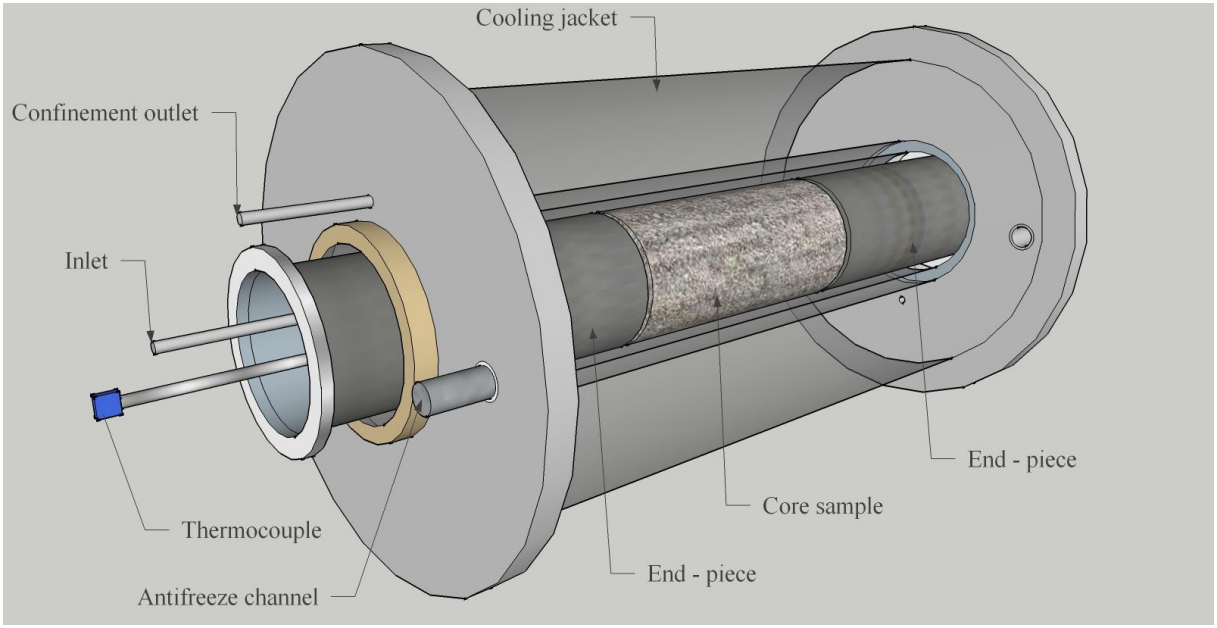

Figure 3-5: Illustration of high pressure core holder, the cooling jacket and the way the core is placed inside the core holder. The two end-pieces hold the core steady inside the core holder. Inlet and outlet lines pass through the end-pieces and are in contact with the core sample. The setup is equipped with a thermocouple measuring the temperature at the inlet side of the core.

The effluent from the core was sent to a gas chromatograph first through a back pressure valve (BPV) and then a pressure regulator. Due to pressure limitations on GC, the production pressure had to be lowered. This was done using a back pressure valve (BPV). BPV released effluent from the production side towards GC whenever the production pressure exceeded the BPV pressure. In addition, a pressure regulator was used to adjust the pressure down to 1.6 – 1.7bar (GC inlet pressure limit). The gas chromatograph used under this study was of type Agilent Technologies 3000 Micro Gas

Chromatography (GC). Installing a mass flow meter (MFM) was also part of the modification process. This was done to improve recovery measurements as well as production quantification. The analyzed effluent was sent towards mass flow meter (MFM) where flow rate (g/h) was measured. Generated data from MFM in conjunction with gas composition data from GC made it possible to quantify production during the CO_2 exchange process. An overview of experimental setup C is shown in Figure 3-6.

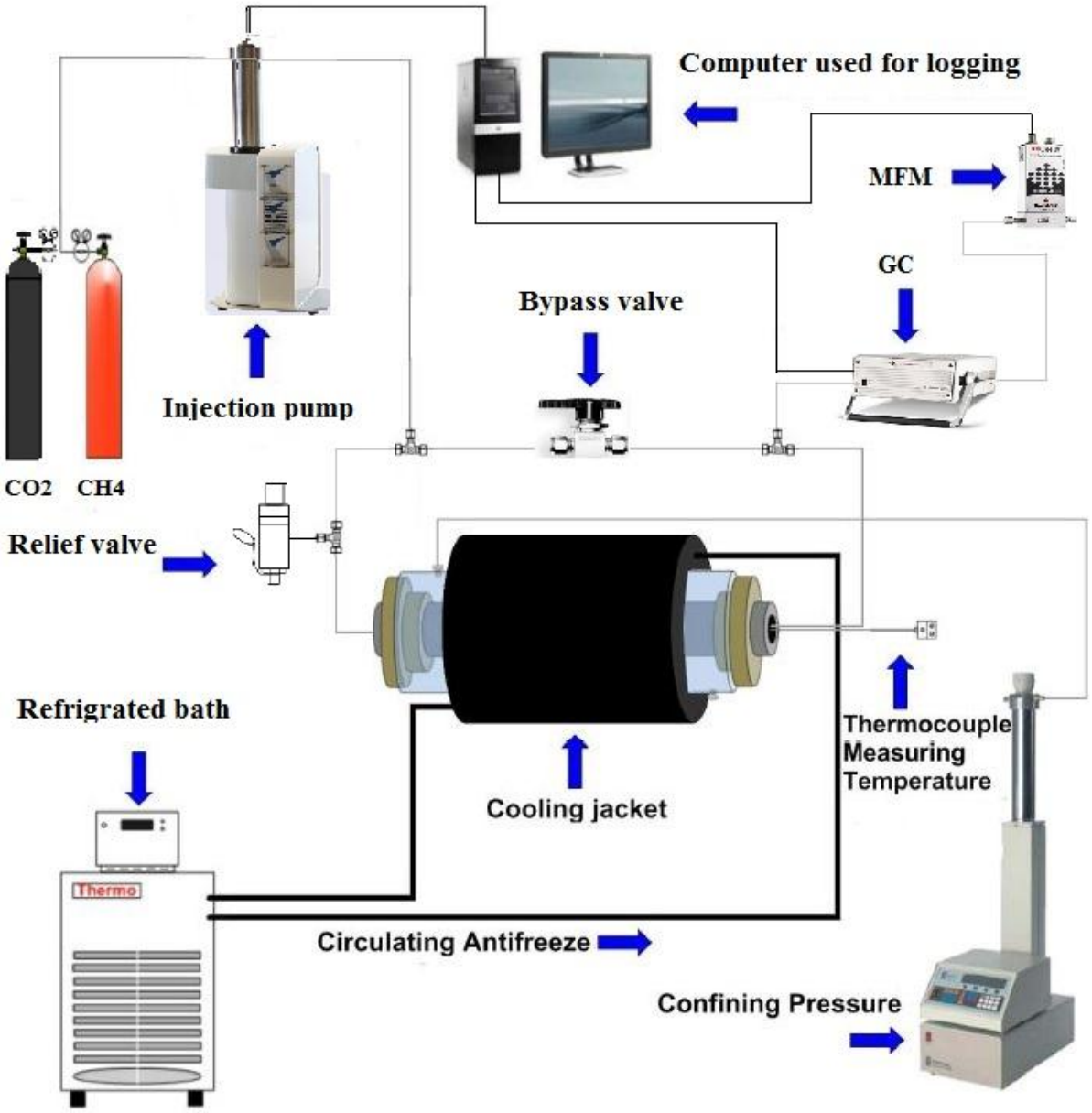

Figure 3-6 – Experimental setup C. Antifreeze was circulated in a cylindrical cooling jacket. A gas chromatograph and a mass flow meter were used to analyze the recovery.

Slug injector

The setup c was modified in order to allow for injection of additives during the CO_2 – CH_4 exchange process. This was done by installing a loop valve at the inlet side of the system. The loop was connected to the system through a three-way valve, which made it possible to exclude the loop when not needed. When the three-way valve *was* open towards the loop, CO_2 was injected through the loop

and into the core plug from the inlet side. The loop was able to inject a volume of 250µl of chosen additive. This volume was flushed with CO_2 once the volume was connected to the loop. One could connect the volume inside the loop to the upstream side of the system using a valve.

3.2.3 Experimental setup based on separate injection of MEA and CO_2 (Setup b)

In order to allow for separately injection of MEA and CO_2 setup b was modified. Setup b is similar to setup c and offers the same functionalities. However in addition to one thermocouple at the inlet side of the setup, two thermocouples were implemented allowing for temperature measurements at outlet side of the core and the confinement liquid. End-pieces stabilizing the core inside the core holder allow for two injection lines at each side of the core. In order to inject MEA separately at the inlet side of the core, one had to compromise temperature measurements at the inlet side of the core. The thermocouple was replaced by a separate injection line. The modified setup is shown in Figure 3-7.

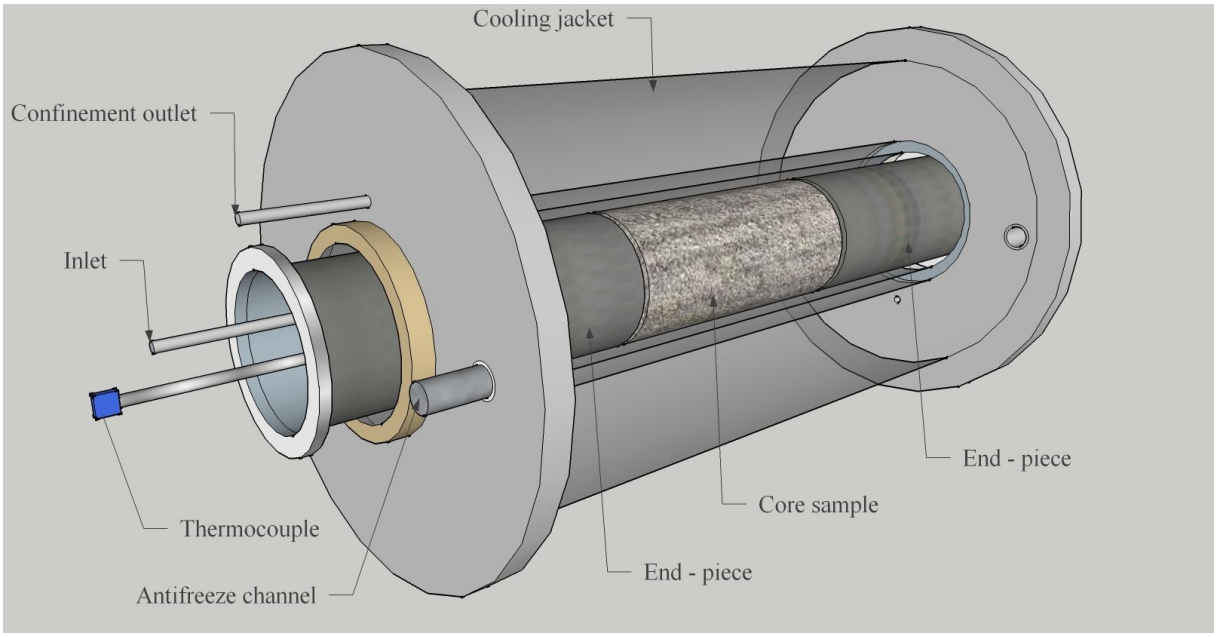

Figure 3-7 - The figure illustrates how the setup was modified. Note that thermocouple that was in contact with the core is replaced by an injection line for MEA. However, two extra thermocouples were implemented enabling temperature measurements of the confinement fluid and outlet side of the core. The figure shows where the thermocouple measuring temperature of the confinement fluid is located. Note the distance from the thermocouple to the core. The thermocouple measuring temperature at the outlet side of the core is not illustrated in the figure.

3.3 Modification of experimental setup

Experimental setup used for experiments during this study was improved and modified in various occasions. A mass flow meter was implemented along the production line in order to better quantify the production during the experiments. Several meter of tubing and lines were changes, safety valves were installed in order to meet the safety standards during experiments. A whole new setup was designed and assembled through collaboration within the hydrate group at the University of Bergen. The experimental setup benefited from use of cool jacket instead of being submerged into a cool bath. This resulted in more accurate temperature control during the experiments. In addition, all the control valves were installed on a control panel which offered better stability for the lines connected to the system.

An idea of measuring of the cumulative mass produced was proposed as a backup to measurements taken by mass flow meter. The idea was based on the produced gas displacing water. The weight of the displaced water could be related to the cumulative mass produced during the experiment. The equipment was purchased and the apparatus was made at the workshop at the Institute for physics and technology, University of Bergen. The apparatus was made the very end of this study and therefore could not be used during the experiments.

In order to inject chemical additives into the core, an injection site had to be implemented along the upstream side of the system. This was done after baseline experiments were conducted. The so called loop valve was installed and was able to inject a total volume of 250µl during each injection. Heat loss along the upstream side of the core, between the injection site and core, was an issue during the injection experiments and had to be handled. Upstream lines of the system were isolated to minimize the heat loss. This was done on the experimental setup used mainly during most of the experiments conducted in this thesis.

Another experimental setup was modified in order to being able to inject CO_2 and chemical additive separately. The end pieces stabilizing the core inside the core holder allow for two intakes, one of which was used to inject gas and the other to allow for temperature measurements. Since temperature measurements could be taken at the outlet side of the core and also from the confining liquid, one could compromise temperature measurements at the inlet side. The temperature sensor at the inlet side of the core was replaced by an injection connected to a separate pump. This made is possible to inject slugs of chemical additive separately. This was a breakthrough during the experimental work which could ensure that the target reaction could occur at short distance from the hydrate saturated core sample.

3.4 Experimental Procedures

Under present study, gas hydrate was formed under controlled laboratory conditions in Bentheim sandstone core plugs. Methane was produced using both depressurization and thermal stimulation as dissociation methods. Methane production induced by a $CH_4 – CO_2$ replacement was also investigated. Lastly, potential of MDEA and MEA for enhanced exchange rate was studied during three experiments.

3.4.1 Experimental procedures for hydrate formation

All the hydrate formation experiments under this study occurred in an excess methane gas system with water as the limiting phase. To saturate the core samples with appropriate brine, a predetermined amount of NaCl was added to deionized water. The hydrate experiments under this study were conducted using brine with a salinity of 0.1 wt%. The strongly water wet core samples were partially saturated through spontaneous imbibition when submerged into the brine. The cores were then placed inside a glass chamber. Vacuum was applied to remove undesired water from the core in order to reach predetermined water saturation level of 40%. This step was repeated two or three times and the cores were weighted and turned upside down at the end of each time in order to achieve a relatively uniform water distribution throughout the core. The perfectly saturated cores where placed into the core holder. The core was then pressurized up to 83bar with CH_4. A confinement pressure was applied incrementally as the core was being pressurized. The confinement pressure was kept 20bar more than the pressure within the core during this step and had a final value of 120bar. To estimate the leakage rate, the system was controlled for a period of time. Once the system was pressurized, the temperature was lowered to 4.0 ^oC from the ambient conditions. This was done by circulating a cooling agent (antifreeze) around the core holder. Hydrate formation started spontaneously when the temperature was brought towards gas hydrate equilibrium conditions and was detected as a sudden increase in rate of CH_4 consumption. All generated PVT data were monitored and recorded during the hydrate formation process. These data were further processed and fixed for a possible leakage. Leakage rates during experiments investigated varied between 0.01 ml/h and 0.05 ml/h.

3.4.2 Experimental procedures during CO_2 injection

When hydrate formation ceased (low methane consumption shown in pump log), the system was isolated by closing inlet and outlet valves. CH_4 in injection and production lines was drained towards the ventilation cabinet. Vacuum was applied in order to remove the remaining CH_4 in the lines. CO_2 was introduced to the system by setting the pump to deliver CO_2 at a rate of 1.2 ml/h from the inlet side. This was done with a closed bypass valve to make sure that CO_2 was only injected from the inlet side. The effluent was run through a gas chromatograph (GC) to measure the composition of the gas mixture produced from the core. The process went on for 140 – 200 hours where diffusion of CO_2 seemed to be the dominant driving force in providing CO_2 to the methane hydrate reaction sites (Ersland et al., 2009). An important aspect of this process (as stated under 1.4.2) is the absence of large-scale dissociation of hydrates during the replacement process of $CO_2 – CH_4$. This has also been confirmed by MRI – observation during the previous hydrate studies (Graue, A. et al., 2006; Husebø, 2008). All generated PVT data were monitored and recorded during the process.

3.4.3 Experimental procedures during depressurization

Depressurization has been proposed as a production method from natural gas hydrates, see section 1.4. In this study, methane production by depressurization was studied and acquired production data were compared with simulated results from CSMGem (Sloan et al., 2008). When hydrate formation came to the end, the pressure was reduced isothermally at a constant rate in a period of 1 hour until it reached

42bar. Confinement pressure was reduced incrementally and was 30bar over the pore pressure during the experiment. At 42.5bar, the system was given a period of 30 minutes to stabilize. At this point, the bypass valve was closed to make sure that the production happened from the inlet of the system. Pressure was reduced to 32.5bar rapidly (32.5bar is lower than dissociation pressure, 38.9bar for methane hydrate at 4ºC and brine salinity of 0.1wt%). All generated PVT-data were monitored and recorded during the experiment. The system was left at this condition for a long period of time. When no further production was observed, the pressure was lowered to 20bar.

3.4.4 Experimental procedure during thermal stimulation

Dissociation of hydrate by increasing the temperature is proposed as a production method from hydrate reservoirs. During present study, a series of hydrate dissociation by thermal stimulation experiments were studied where the threshold dissociation temperatures was compared with data acquired from computer simulations by CSMGem (Sloan et al., 2008). After hydrate formation, temperature was increased incrementally while the system was kept under constant pressure, 83bar. The system's temperature was from 4ºC to 9ºC in a time period of 10 hours. The system was stabilized at 9º in 12 hours before the temperature was further increased. When no volume changes were observed, the temperature was increased to 10ºC. System was given 30 minutes to stabilize, before the temperature was increased to 11.3ºC. Volume, pressure and temperature changes were monitored and recorded during the experiment.

3.4.5 Experimental procedures during injection of chemical additive

When the exchange process ceased (no further methane production was observed), slugs of MDEA or MEA were injected into the core plug to investigate the possibility of enhanced methane production. A volume of 250µl of the desired additive was injected with 15 minutes intervals. A 15 minute interval was chosen in order to make sure that the whole volume of the additive was flushed with CO_2. This process was repeated 4 times for each experiment resulting in a total injection volume of 1ml for each injection round. A loop valve was used to inject the desired chemical additive. Loop valve was connected to the injection line through a three way valve and could be disconnected when not needed. A volume of 250µl could be filled with the desired additive. This volume could be connected to the injection line using a valve. This volume could be flushed with the injected CO_2.

4 Literature survey

Experimental and theoretical studies have shown that replacement of CH_4 by CO_2 is a thermodynamically favorable process upon which CH_4 is released and CO_2 is sequestrated in a stable hydrate. This section reviews some of the early and recent studies of $CH_4 – CO_2$ reformation process to provide the reader a fundament for the work presented in chapter 4 of the present study.

The idea behind the exchange process was presented by Japanese researchers (Ebinuma, 1993), where heated CO_2 was injected to a hydrate reservoir in order to induce hydrate dissociation. A hydrate reformation was expected to occur with CO_2 as the guest molecule as CO_2 is preferred as hydrate former over CH_4 within a certain P-T range. Based on the knowledge of increased thermodynamic stability offered by CO_2 over CH_4, some of the early experimental works investigated the process of $CO_2 – CH_4$ exchange (Hirohama et al., 1996; Ohgaki et al., 1996). These early studies looked into the rate of the $CO_2 – CH_4$ exchange process as a function of the thermodynamic driving force in bulk methane hydrate. Hirohama exposed bulk methane hydrate to liquid CO_2. The rate of the $CO_2 – CH_4$ process could be determined of the mass transfer of CO_2 in hydrate solid. The exchange process was limited by CO_2 – hydrate formation at the interface which inhibited further conversion (Hirohama et al., 1996).

Yoon *et al.* (2005) studied conversion of methane hydrate to carbon dioxide hydrate in high pressure cell using powdered methane hydrate. Rapid rate of initial $CO_2 – CH_4$ exchange was observed within the first 200 minutes and then became relatively slow. This retardation was explained to do with layers of CO_2 – hydrate being a strong barrier against the diffusion of carbon dioxide into hydrate solid phase. They also used Raman spectroscopy to study the coexistence of methane and carbon dioxide hydrates and water in phase. They proposed that the water phase produced during the replacement reaction allowed the reaction to proceed rapidly by enhancing the diffusion of both methane and carbon dioxide, resulting in complete and relatively fast recovery of methane gas from methane hydrates (Yoon et al., 2005). Next step was taken towards improvement of the methane recovery from the hydrates. The recoverable amount of CH_4 from structure I CH_4 – hydrate by $CO_2 – CH_4$ exchange process may be as high as 64% (Lee et al., 2003). This because CO_2 preferentially replaces CH_4 in large cavities and CH_4 in small cavities remains untouched. Park *et al.* proposed a method where a gas mixture of N_2 and CO_2 was injected instead of pure CO_2. As nitrogen molecular size almost coincides with methane (N_2 molecular diameter = 4.1 Å, CH_4 molecular diameter = 4.36 Å (Sloan et al., 2008)) it could compete with methane for the small cages in structure I. The result from experiment indicated that 23% of methane was replaced by nitrogen and 62% was replaced by CO_2, resulting in a total recovery of 85%. Drawback with use of N_2 during the exchange process was the decrease in driving force for the exchange process. Lee *et al.* studied the conversion of CH_4 hydrate to CO_2 hydrate in porous silica. They used NMR-measurements to study the ratio of $CH_4 – CO_2$ replacement in small and large cavities of structure I hydrate. The study demonstrated poor replacement of CH_4 by CO_2 in small cages of structure I hydrate as these were too small for CO_2 to fit in. The study did not cover variables such as porous media and permeability changes into account.

$CH_4 – CO_2$ exchange in porous media

Graue *et al.* (2006) used MRI measurements to visualize the kinetics of both hydrate formation and the $CH_4 – CO_2$ replacement process within a Bentheim sandstone core samples. The study demonstrated clearly that CO_2 storage in gas hydrate formed in porous rock resulted in spontaneous methane production with no associated water production. Methane hydrate formed within a fractured core held by polyethylene space was exposed to liquid CO_2. Polyethylene spacer with to connected

compartments was used in order to increase the exposure contact area between the methane hydrate and the injected CO_2. In addition, spacer improved the fluid flow through the core as well as it provided an accumulation volume for the produced methane (Graue et al., 2006). Experimental work by McGrail *et al.* (2007) measured the penetration rate of CO_2 into bulk hydrate, where a greater penetration depth was measured at 4ºC compared to 2.5 and 0ºC. In addition, they studied $CH_4 - CO_2$ replacement by exposing methane hydrate formed within a sand packed column to a two-phase emulsion formed of CO_2 and water. The temperature of the injectant was significantly higher than methane hydrate causing decomposing of the gas hydrate lattice and release of encaged gas. The released gas was displaced ahead of the emulsion front and collected. When the injection was over the system was cooled into stability region for CO_2 hydrate. Formation of CO_2 hydrate was verified by Raman spectroscopy (McGrail et al., 2007). An experimental study of gas permeability in gas-hydrate-water systems was done by Ersland *et al.* (2008) where gas permeability was measured during hydrate growth. The study showed that the measured gas permeability was affected by initial water saturation and the corresponding hydrate saturation after hydrate formation, where increasing initial water saturation and hydrate saturation after hydrate formation resulted in decrease gas permeability. Ersland *et al.* (2008) indicated also that the permeability drop was due to hydrate expansion as hydrate act as an extension of the solid grain space. The concluded that a given amount of water occupied 26 percent more of the pore space when converted from liquid to hydrate (Ersland et al., 2008). An extensive study by Jung *et al.* (2010) throws a light on some of the important coexisting processes such as; heat liberation, mass transport, and gas production during $CH_4 - CO_2$ replacement process(Jung et al., 2010).

Gas hydrates are currently not considered as economically feasible energy resource. Extensive research is being done in order to address different issues related to technical viability of producing from such deposits. An extensive publication by Moridis *et al.* (2008) provides an overview on the assessment of the resources as well as the policies, focus and priorities being taken on the gas hydrates as a potential energy resource.

5 Experimental Results and Discussion

In the present study, methane hydrate was successfully formed within Bentheim sandstone core plugs. Both pressure depressurization and thermal stimulation as production methods were studied. Hydrate decomposition was numerically simulated (Birkedal et al., 2013) where production data from the simulation was compared with the data achieved during the experiment. Data acquired during thermal stimulation were used to test the computer program CSMGem that predicts thermodynamic equilibrium data for a hydrate system. During $CH_4 - CO_2$ exchange process, a gas chromatograph (GC) and a mass flow meter (MFM) were used to quantify methane production initiated by CO_2 exposure. No external heating was applied in order to dissociate the hydrate. Potential of various additive agents for enhanced $CO_2 - CH_4$ exchange rate was also investigated under this study. Table 5-1 shows an overview of the experiments conducted under this master thesis. This master thesis emphasizes first the difficulties during the injection of the selected additives.

Table 5-1 – Overview of hydrate formation and $CH_4 - CO_2$ experiments conducted under this study.

Core name	Initial water saturation	Brine salinity [wt%]	Temperature under exchange [°C]	Amine used
CO2_19	0.62	0.1	-	-
CO2_20	0.42	0.1	-	-
CO2_21	0.41	0.1	9.6	-
CO2_22	0.38	0.1	-	-
CO2_23	0.41	0.1	4.0	MDEA
CO2_24	0.41	0.1	4.3	MEA
CO2_25	0.41	0.1	4.3	-
CO2_26	0.43	0.1	9.6	-
CO2_27	0.40	0.1	4.0	MEA
CO2_28	0.40	0.1	-	-
DEP_5	0.43	0.1	-	-
HR48	0.40	3.5	-	-

5.1 Results from hydrate formation

In controlled laboratory experiments gas hydrate were successfully formed within Bentheim sandstone core plugs. All core samples were saturated up to 40% water saturation using brine with salinity of 0.1 wt%. Previous hydrate studies (Birkedal, 2009; Husebø, 2008) have investigated the effect of brine salinity on the hydrate growth. Both studies agreed on less methane consumption under hydrate formation at high brine salinities (> 4.0wt %). Since hydrates form out of water and gas, an increased salt concentration in the brine is expected at the hydrate formation front throughout the core. Hydrate formation experiments in this study were conducted with the water being the limiting hydrate forming component. Due to low solubility of methane in liquid water, the site of hydrate formation has been suggested to preferentially be at gas – water interface (Sloan et al., 2008). This is due to the availability of both hydrate formers, methane and water (Kvamme, 2012). Hydrate's growth pattern has also been the subject of previous hydrate studies (Ersland et al., 2009), where MRI observations confirmed various growth patterns. These varied between a frontal growth and uniform distribution of hydrate growth throughout the core samples. The experiments also indicated low water saturation (< 3%) post to hydrate formation for cores with initial water saturation of 50% and salinity of 0.1 wt%. Water saturation post hydrate formation for experiments conducted during present study has also been calculated. The results vary between 0 – 5%, which agree with results from experiments conducted by

Ersland et al., (2009). Some lower final water saturation was expected for experiments conducted under present study due to lower initial water saturation. Table 5-2 shows water, gas and hydrate saturation distribution pre and post hydrate formation.

Table 5-2 – Overview of saturation distribution after hydrate formation for conducted experiments.

Core ID	Brine salinity [wt%]	Initial water	Final water saturation	Final hydrate saturation	Final gas saturation	Pore volume [ml]
CO2_19	0.1	0.62	0.11	0.71	0.24	52.2
CO2_20	0.1	0.416	-	0.53	0.47	64.2
CO2_21	0.1	0.415	0.032	0.48	0.51	65.8
CO2_22	0.1	0.379	0.001	0.48	0.52	66.2
CO2_23	0.1	0.412	0.034	0.48	0.49	70.3
CO2_24	0.1	0.410	0.032	0.48	0.49	68.9
CO2_25	0.1	0.41	0.003	0.56	0.44	73.8
CO2_26	0.1	0.43	0. 05	0.41	0.59	67.7
CO2_27	0.1	0.40	0.06	0.43	0.51	68.7
CO2_28	0.1	0.40	0.08	0.4	0.52	68.1
DEP5_1	0.1	0.43	0.06	0.46	0.48	69.5
DEP5_2	0.1	0.43	0.07	0.45	0.48	69.5
DEP5_3	0.1	0.43	0.08	0.44	0.48	69.5
HR48	3.5	0.40	0.08	0.42	0.5	62.1

Previous hydrate studies (Ersland et al., 2009; Graue et al., 2008; Husebø, 2008)at University of Bergen used MRI-visualizations and PVT-data to detect and monitor hydrate formation. The consistency of PVT-data was proven by comparing MRI-measurements with normalized methane consumption rate(Birkedal, 2009). Previous master study (Hauge, 2011) at the University of Bergen used resistivity measurements to detect hydrate formation where resistivity over the core sample increased with increasing hydrate saturation. This method has not been used during present study. Monitored and recorded PVT-data were used to evaluate hydrate formation experiments during this study.

5.1.1 Temperature impacts on hydrate growth

During hydrate formation experiments, all generated PVT data were monitored and recorded. All hydrate formation experiments during this master study were conducted at pressure and temperature conditions of 83bar and 4°C. However, an additional hydrate formation experiment was conducted at same pressure but at a temperature of 9 °C to further investigate temperature effect on hydrate growth. As stated under 3.4.1, Bentheim sandstone core samples were saturated using brine with a predetermined salinity of 0.1 wt%. The system was pressurized with up to 83bar using methane. The temperature was then lowered from the ambient conditions to desired temperature (4 °C and 9 °C). The cooling lasted for approximately 5 hours. Hydrate formation was observed as an increase in gas consumption rate. Figure 5-1 shows a typical pump log curve for hydrate formation under pressure and temperature conditions of 83bar and 4°C. For simplicity, the illustrated pump log starts from the time which cooling from the ambient temperature was initiated.

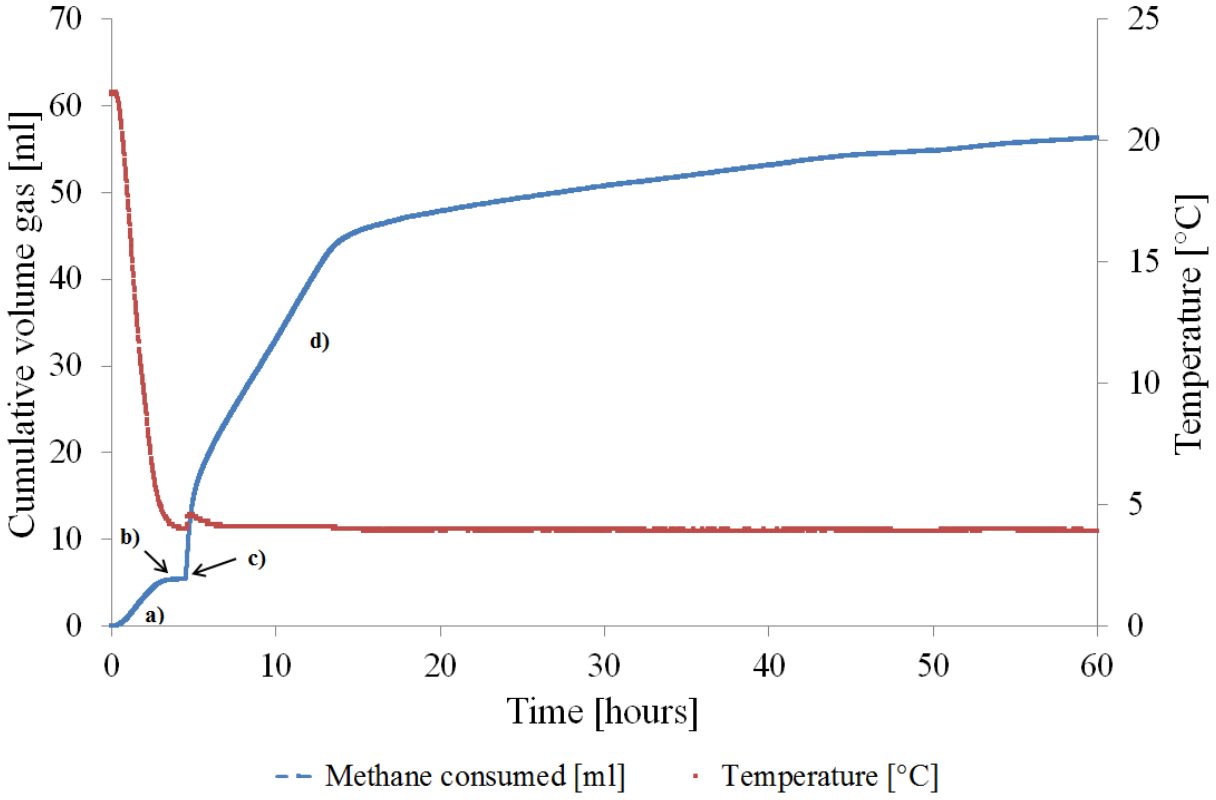

Figure 5-1 - CH_4 consumption as function of time during hydrate formation. At the corner of the figure, the system is already pressurized up to 83bar. a) Represents methane consumption during the cooling from ambient temperature to 4ºC. This is due to compaction of gas as a result of decrease in temperature. The pump has to deliver more methane in order to keep the pressure constant. During period b) the system is stabilized at 83bar and 4ºC (induction time). At c) the induction time for the system is over. Red circle Steady growth of methane hydrate occurs during d) and continues until there is sufficient amount of reactants to form methane hydrate.

Hydrate formation initiates when the system is within the hydrate stability area and the induction[7] time is over. As shown in Figure 5-1, during the first 5 hours of this experiment, temperature was lowered (from ambient temperature of 22ºC to 4ºC). Gas delivery occurred to compensate for compression due to increased density during cooling is about 5ml. Hydrate initiation did not occur at hydrate formation conditions due to the induction time of the system. No or very little methane is being injected into the system at this point. Although the actual nucleation occurs might have occurred much earlier and not been detected. When the induction time is over, the period of steady hydrate growth starts and continues for another 120 hours. The experiment continued for another 40 hours. This was done to make an estimate on the leakage rate. It has not been possible to measure the temperature along the core sample during hydrate formation experiments and temperature measurements are only from the inlet side of the core sample. A temperature increase of 0.5ºC was observed at the inlet side of the core at 4 hours. The time of the temperature increase coincides with start of period of steady hydrate growth. The temperature increase is expected due to the exothermic nature of the hydrate formation process. Bringedal (2011) reported temperature increase of approximately 1 ºC at the start of hydrate formation for the same system as system used during present study. Zhou (2009) reported a temperature increase of 2.5 ºC (Zhou et al., 2009) for a system where a total of 413 L of methane were consumed during hydrate formation compared to 50ml methane consumed during experiments studied here. Temperature measurements during hydrate formation were taken at the inlet side of the core

[7] Induction time was explained in detail under section 1.2.2.

sample. The relatively small increase in temperature indicates effective cooling during the experiments. To further investigate the temperature increase as result of hydrate formation, one should eliminate the cooling during the process.

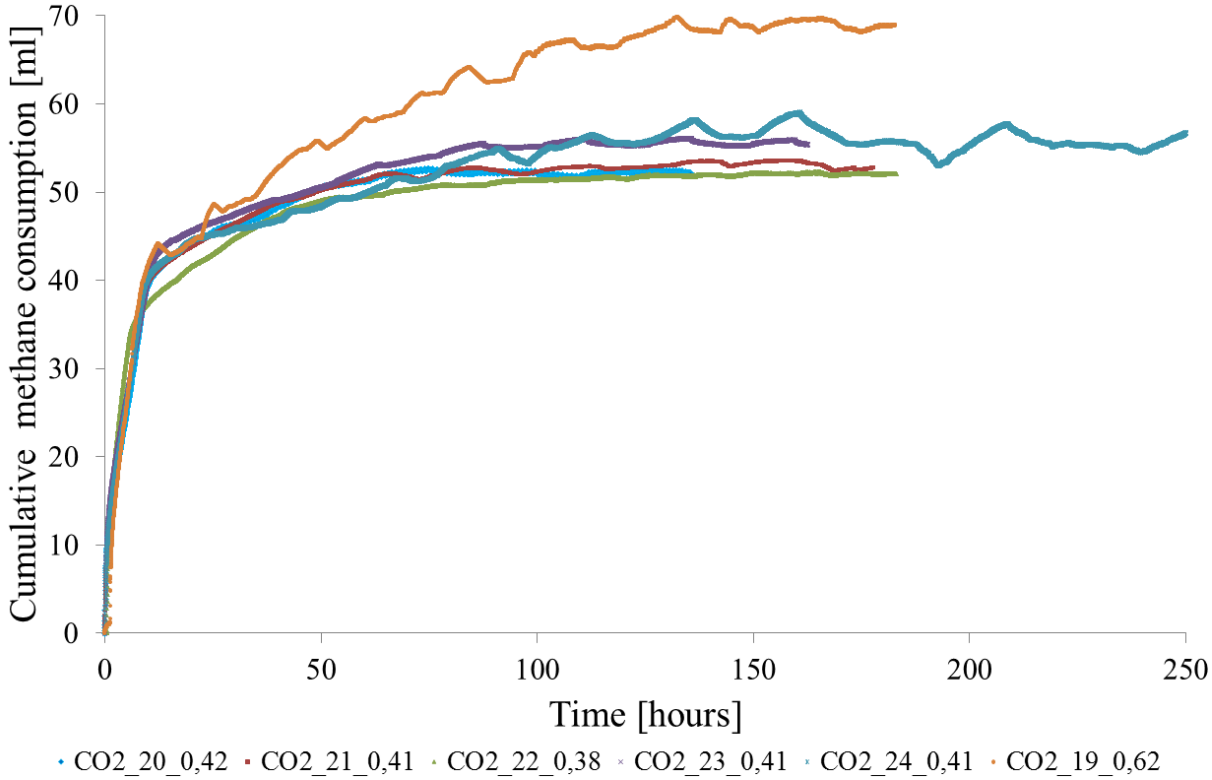

Figure 5-2 – Methane consumption during hydrate formation for a number of experiments conducted during this study.

Methane consumption as a function of time, for a number of experiments conducted under present study is shown in Figure 5-2. Core samples used under this study were saturated up to 40% with a brine salinity of 0.1 wt%. Experiments CO2_20, CO2_21, CO2_22 and CO2_23, were conducted at 83bar and 4 ºC. These show almost the same exponential hydrate growth. However, CO2_22 shows lower methane consumed during the experiment. This is consistent with the fact that the core was saturated to a lower saturation compared to the other experiments. Initial water saturation was 0.379 which is lower compared to for the other hydrate formation experiments. CO2_19 showed highest methane consumption due to high initial water saturation. Water has been the limiting factor for the hydrate formation experiments conducted during present study. This means that lower water saturation may result in lower methane consumption, and relatively lower final hydrate saturation. Results from earlier hydrate formation experiments (Birkedal, 2009; Bringedal, 2011; Hauge, 2011), showed the same tendency for core samples with lower initial water saturation. A comparison plot from in house data where methane hydrates were formed at higher salinity is shown in Figure 5-3. Initial water saturation for the studied cores varied between 0.4 – 0.74 and all the cores were saturated using brine with salinity of 3.5 wt%. The results demonstrate a tendency for longer induction time for experiments with higher initial water saturation. Cores with lower initial water saturation (HR47 and HR48) exhibited lower methane consumption compared with experiments with similar initial water saturation and salinity of 0.1 wt% studied in this study. Less methane consumption can be explained by high salinity as at higher salinity the extent of hydrate inhibition is higher and can affect the hydrate growth.

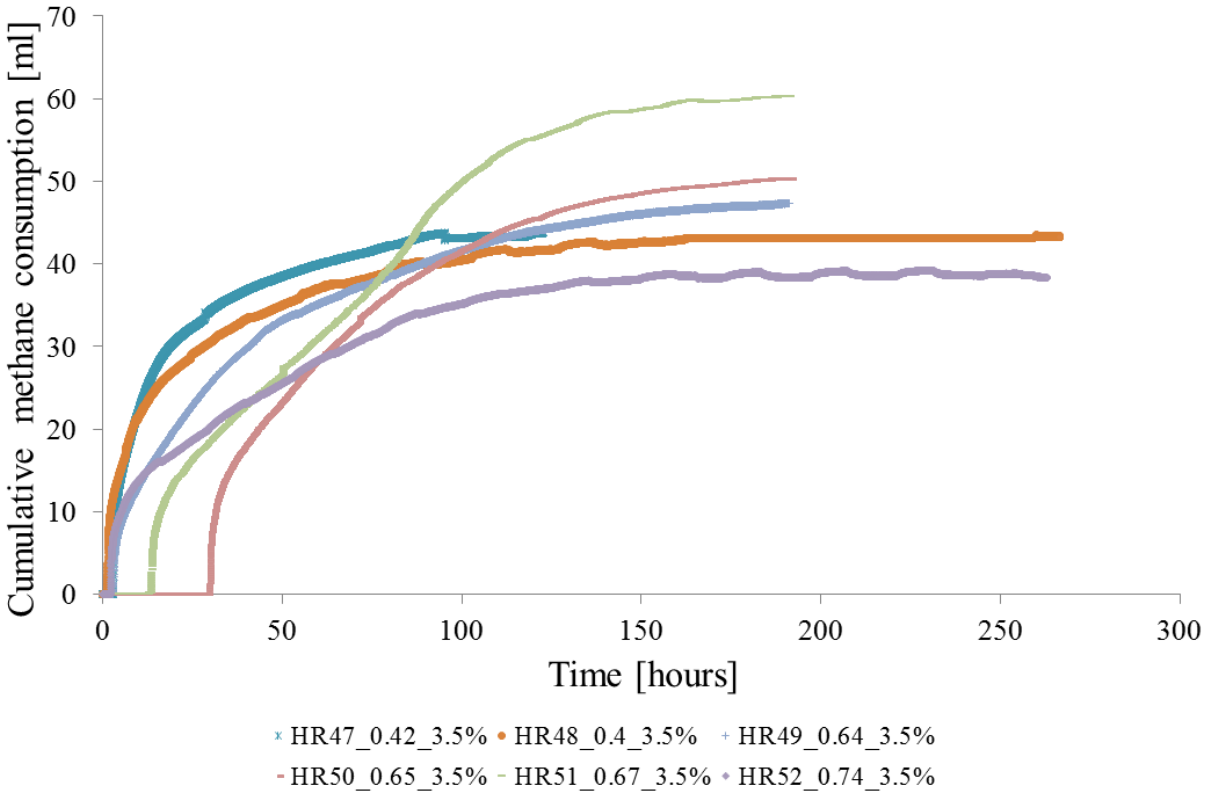

Figure 5-3 – Methane consumption during hydrate formation for a series of in house hydrate formation experiments. Longer induction time was observed as a result of higher brine salinity.

Core HR52 showed methane consumption. Core HR52 was saturated up to 74% water saturation which is higher than the other cores. Hydrate growth for this core may have been affected by such high initial water saturation. Higher initial water saturation results in less surface area between water and methane. High water saturation leaves less pores space for the gas which could result in reduced relative gas permeability. Less surface area and reduced relative gas permeability may have contributed to less methane consumption.

Experiment CO2_24 was conducted to investigate how higher temperature affects the driving force for the hydrate formation process. During this experiment, the core was saturated using the same method described under 3.4.1 and was pressurized up to 83bar using methane. The temperature was lowered to 9 ºC instead of 4 ºC. Computer simulation results from CSMGem indicate that methane hydrate could form at 83bar, 9ºC and a brine salinity of 0.1 wt%. The results from computer simulation are shown in Figure 5-4. Lowering the temperature from the ambient conditions to 9 ºC took 3 hours. 3ml methane was consumed in order to maintain the pressure at 83bar during this stage. The system was then kept at 83bar and 9 ºC for another 70 hours. Some fluctuations in gas consumption rate are seen during this stage. This may have been caused by temperature fluctuations in the laboratory. Moreover the pump contained more methane compared to earlier experiments (about 500ml), which may be the reason to drastic fluctuations compared to earlier pump logs. The methane consumption and temperature as function of time are shown on Figure 5-5.

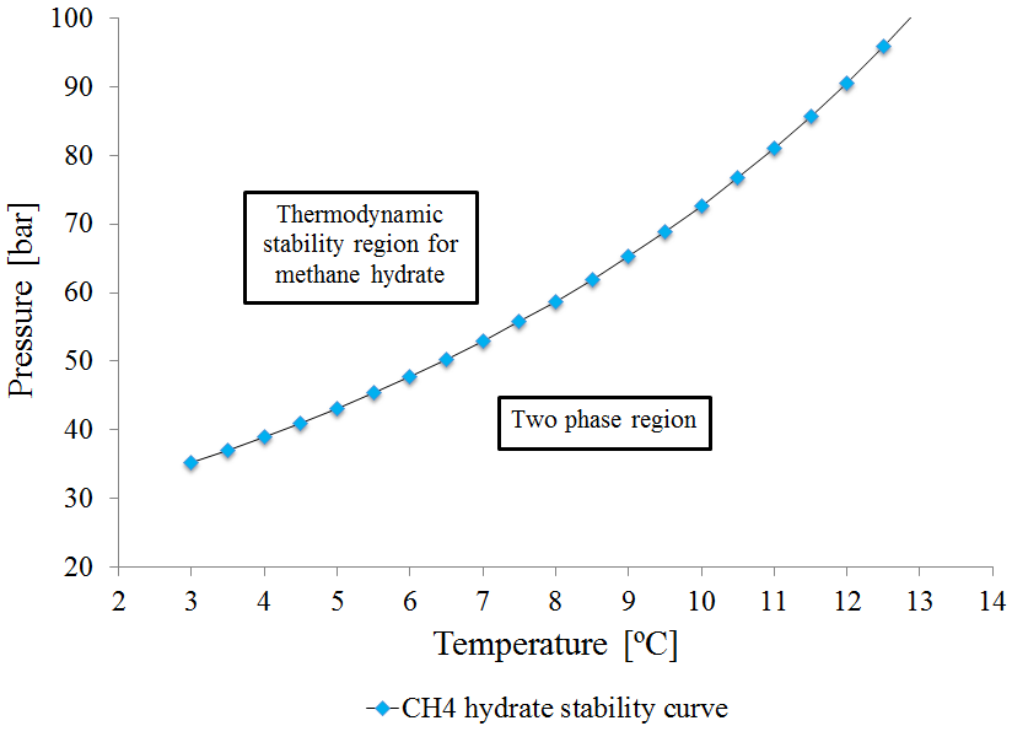

Figure 5-4 – Thermodynamic stability region for methane hydrate. The area above the line displays the stability region for methane hydrate. The calculations are done for a brine salinity of 0.1wt%. CSMGem (Sloan et al., 2008) has been used to calculate the equilibrium values.

Based on simulation results from CSMGem, hydrate formation may occur at 83bar 9ºC, but lower driving force for the reaction to proceed may lead to longer induction time. After 70 hours, no rapid methane consumption was detected for this experiment. Hydrate growth would occur at some later time, but due to time limitations the temperature was lowered to 4ºC and the result was an immediate response from the system and by a period of rapid hydrate growth. The immediate response from the system may be explained by long period of induction time at 9ºC which ended as a result of the further cooling. Hydrate formation was detected as a sudden increase in methane consumption rate. 45ml methane was consumed in 20 hours (70. – 90. hour). The consumption rate levels out gradually. Estimated leakage rate for this experiment was ~0.04 ml/h.

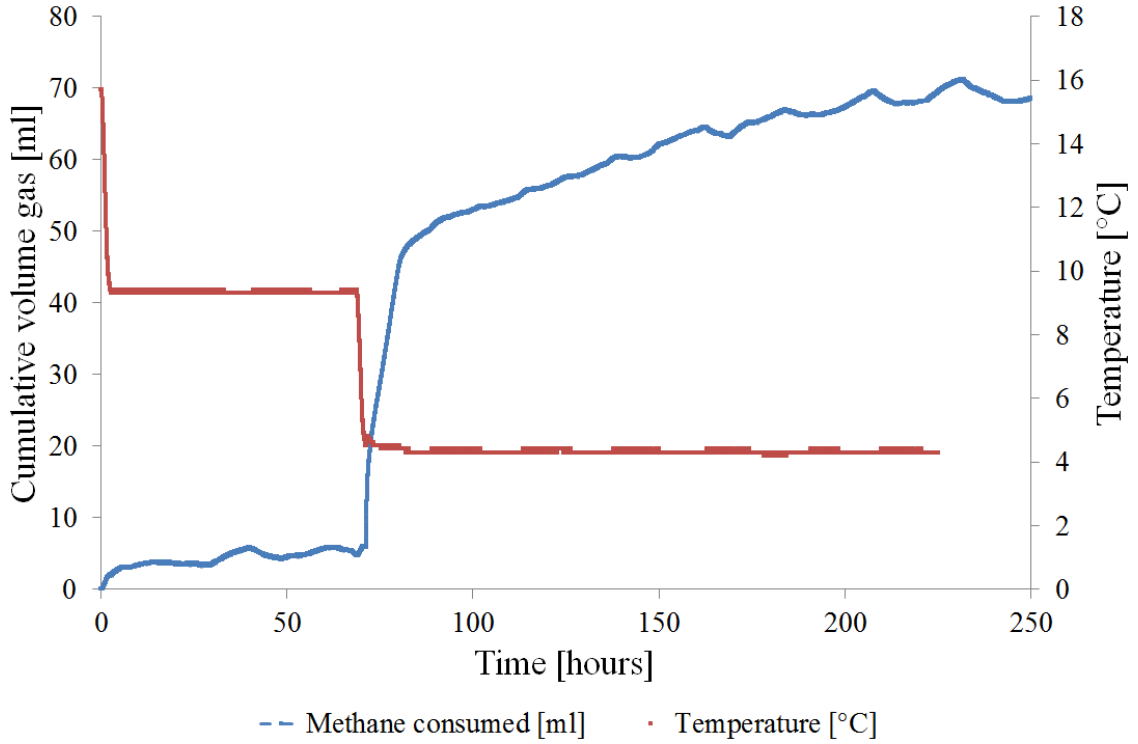

Figure 5-5 – CH_4 consumption and temperature as function of time. About 3ml methane is consumed during the first cooling from 16 ºC to 9 ºC. No hydrate formation is observed until temperature is lowered to 4 ºC.

5.1.2 Hydrate growth in an excess gas system

During hydrate formation experiments studied during present study, Bentheim sandstone core samples were saturated up to a predetermined water saturation using brine at salinity of 0.1wt%. Hydrate formation experiments were therefore conducted with water being the limiting component as core samples were pressurized using a reservoir with infinite amount of methane. Bentheim core samples have exhibited strong water wettability (Graue et al., 2006). Result of such wetting preference is water occupying the smallest pores and being in contact with a majority of the rock surface. In such system the non-wetting phase, methane, will occupy the centers of the larger pores and form globules that extend over several pores (Clennell et al., 1999). Studies have shown that hydrate forms in the center of the large pores (Kleinberg et al., 2003) and at the gas-water interface (Kvamme, 2012). Hydrate formation is unlikely to occur in small pores due to extensive capillary forces (Clennell et al., 1999). Hydrate growth in the excess gas system used in this study starts at the gas-water interface, grows towards the pore wall and expands towards the center. Period of steady hydrate growth continues until the mass transport of the reactants to the nucleation site has stopped, leaving a thin layer of water wetting the pore wall (Ersland et al., 2009). Ersland *et al* (2009) indicated that the thickness of the water layer could be dependent on the salinity of the formation brine. As hydrate formation continues, salt is increasingly concentrated in the remaining water. Phase composition of gas hydrate formed in sediments is illustrated in Figure 5-6. Such behavior can also be seen on methane consumption curve retrieved during hydrate formation experiments. As shown in Figure 5-2, methane consumption rate is high during the first 10 hours of experiment. During this period, hydrate grows as a result of a high thermodynamic driving force and availability of both reactants. It can be seen on the Figure 5-2 that methane consumption rate flattens out despite the thermobaric conditions being within the hydrate stability zone. The latter may be explained by both reduced gas permeability and reduced mass transport of the reactants to the nucleation site being restricted as the hydrate layer thickens. Gas permeability drops with increasing hydrate saturation. Hydrates will expand and act as an extension of

the solid grain blocking the gas flow (Ersland, 2008). The hydrate growth process ceases when methane and water can no longer be transported to the nucleation site leaving residual post hydrate water saturation. Chuvilin *et al.* (2011) refers to two types of residual pore water saturation post to hydrate formation; pore-water that cannot transform into hydrate under given thermodynamic conditions (equilibrium water) and pore water that can transform into hydrate but does not do so because of kinetic reasons (Chuvilin et al., 2011).

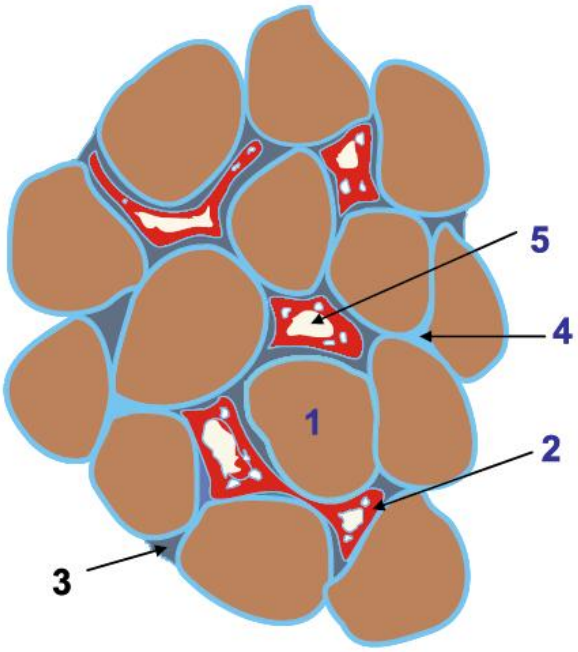

Figure 5-6 – The figure shows phase composition of gas hydrate formed in sediments. 1. Mineral particles. 2. Gas-hydrate enclosures. 3. Metastable pore water that may be transformed to hydrate phase but takes a long time to do so as there is no direct gas-water contact. 4. Equilibrium part of pore water that cannot contribute to form cavities that encapsulate the gas molecules. 5. Gas in pores. Figure modified from (Chuvilin et al., 2011).

As listed in Table 5-2, hydrate formation experiments studied during present studied exhibited final water saturation varying between 0-10 percent. The remaining water may be water that has not transformed into hydrate due to kinetic reasons such as high salinity or restricted mass transport, or water that is not in direct contact with gas, such as capillary bound water in small pores. Comparison of final water saturation values achieved during present study with in house data shows that final water saturation increases with increasing initial water saturation and increasing brine salinity. Final water saturation as a function of initial water saturation for a series of hydrate formation experiments is shown in Figure 5-7. Note the initial water saturation of 37% which resulted in the lowest final water saturation at brine salinity of 0.1 wt%.

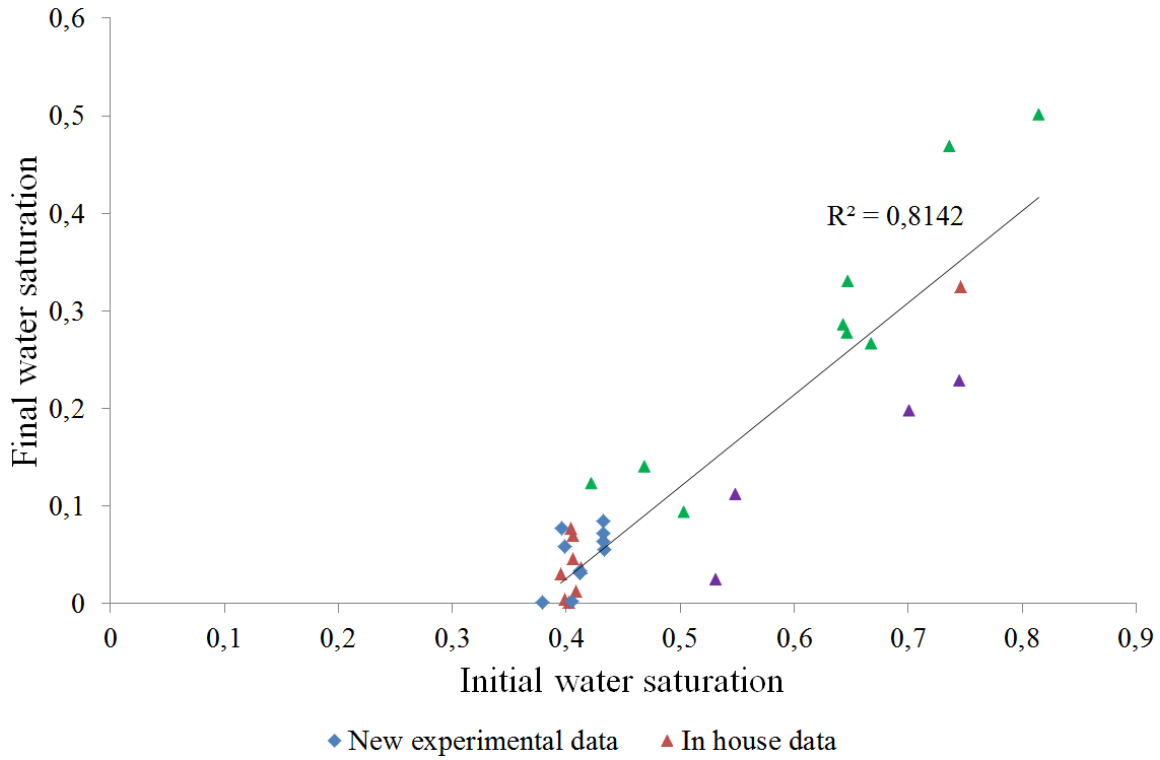

Figure 5-7 – A comparison of experimental data achieved during this study and in house data for final water saturation as a function of initial water saturation for hydrate experiments. Note the green triangles are experiments with brine salinity of 3.5 wt% and purple ones are experiment with brine salinity of 1 wt%, red triangles are experiments with brine salinity of 0.1 wt%. All hydrate formation experiments investigated during present study were conducted have an initial water saturation of 0.4 and brine salinity of 0.1 wt%. Note the initial water saturation of 0.37 resulting in lowest final water saturation of 0.001. In house data collected by (Hauge, 2013).

5.2 Memory effect of water structures

To investigate the memory effect of water structures prior to hydrate formation and after dissociation, a series of hydrate formation experiments were performed. Methane hydrate was first formed within a single Bentheim sandstone core sample and then dissociated by pressure depletion. A total of four hydrate formation experiments studied the so called *memory effect* of the water structure. The memory effect can be described as the phenomenon whereby a clathrate hydrate forms more readily from gas and water which have been attained by melting the hydrate, compared with water with no previous hydrate formation history (Buchanan et al., 2005). A Bentheim core sample was saturated using brine with salinity of 0.1wt%. Methane hydrate was formed at 83bar and 4ºC using method described under section 3.4.1. When hydrate formation ceased, methane hydrate was decomposed by depressurization. Pressure was reduced to 42bar at constant rate. The system was given time to stabilize before the pressure was reduced rapidly to 32.5bar, below the hydrate dissociation threshold. A STIGMA 3000 pump from Sanchez Technologies was used to receive the produced gas from the system. When no more methane production was observed, the pressure was reduced to 20bar to see more methane could be produced from the system. Results from depressurization are discussed in section 5.3. Hydrate was formed within the same system that was decomposed. Figure 5-8 shows hydrate saturation as a function of time for the four hydrate formation experiments studied.

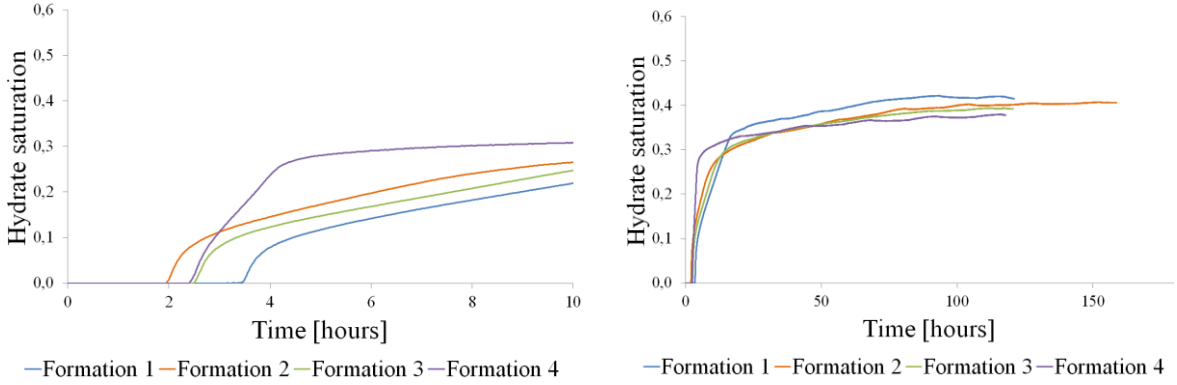

Figure 5-8 – Hydrate saturation as a function of time, where the plot in left shows hydrate saturation during 10 first hours of the hydrate formation process and the plot in right shows the hydrate saturation as a function of time during the whole experiment time. In the left plot, note the shorter induction time for formation 2, 3 and 4 compared to induction time for formation 1. In the right plot, note the decreasing final hydrate saturation for each experiment. Formation 2 was initiated 758 hours after formation 1 was taken down. Formation 3 was carried out 24 hours after formation 2 was taken down. Formation 4 was conducted 92 hours after formation 3 was taken down.

As shown in Figure 5-8, the induction time is longest for the first hydrate formation. During the first hydrate formation, methane hydrate was formed from water and gas with no previous hydrate history. After the first hydrate formation, the system was taken down and left at atmospheric pressure and room temperature for a period of 24 hours. The induction time formation 2 ended after 2 hours compared to 4 hours for formation 1. However, the final hydrate saturation for formation 2 is lower compared to the one for formation 1. This may be explained by water production that occurred in association with hydrate decomposition after the first hydrate formation. In words, less water was available to form a hydrate during formation 2. Formation 3 showed an anomaly whereby the induction time was longer compared to formation 2. The longer induction time may have been caused by the heating rate at which the system was brought to ambient temperature after formation2. Lower heating rate may cause a greater degree of equilibrium for the system. Tohidi *et al.* demonstrated that the observed formation and dissociation temperatures can be up to ~6 K different at the same pressure, depending on the degree of mixing and the rate of heating (Tohidi et al., 2000). Although the "memory" effect of the water structures have been observed during four hydrate formation experiments, the neutron diffraction studies done by Buchanan *et al.* could confirm that the water structure remained largely unchanged from its structure before the hydrate formation, and the hypothesis of memory effect may mainly be ascribed due to nonequilibrium effects and does not exist in a system in a fully equilibrated system (Buchanan et al., 2005).

5.3 Results from CH_4 production through pressure depressurization

As established under section 1.4.1, depressurization is considered as an economically viable method of gas production from gas hydrate deposits. The method involves reduction of pressure below the hydrate dissociation threshold pressure (Zhou et al., 2009). Depressurization method has been proposed to be the best suited method to produce from CLASS 1 (section 1.3.2) deposits containing either gas hydrates and free water (CLASS1W) or gas hydrates and free gas (CLASS1G) (Moridis et al., 2009). The benefit from this production method is to produce the whole amount of gas stored in hydrates without need of adding energy to the system opposed to thermal stimulation method where heat is to be added to system in order to dissociate the hydrate. Depressurization as a production method from a hydrate reservoir with excess gas was studied during a series of experiments. Depressurization occurred as pressure was reduced stepwise until no further dissociation could be detected. When hydrate formation ceased, the pressure was reduced isothermally with a constant rate during a period of 1 hour until it reached 42bar. The system was given time to stabilize at 42bar and 4ºC. CSMGem calculations show that, at 4ºC, methane hydrate dissociates at pressures below 38.9bar (Figure 5-4). The pressure of the system was further reduced to 32.5bar from the inlet side of the core (bypass valve closed). A total volume of 170ml methane was produced in a time period of 30 hours. When no further production was observed at 32.5bar, the pressure was reduced to 20bar to see if more gas could be produced. 4ml methane was produced as a result of the pressure reduction to 20bar. This experiment was conducted as a part of collaboration within the hydrate group to acquire experimental data which could be compared with data acquired from simulation.

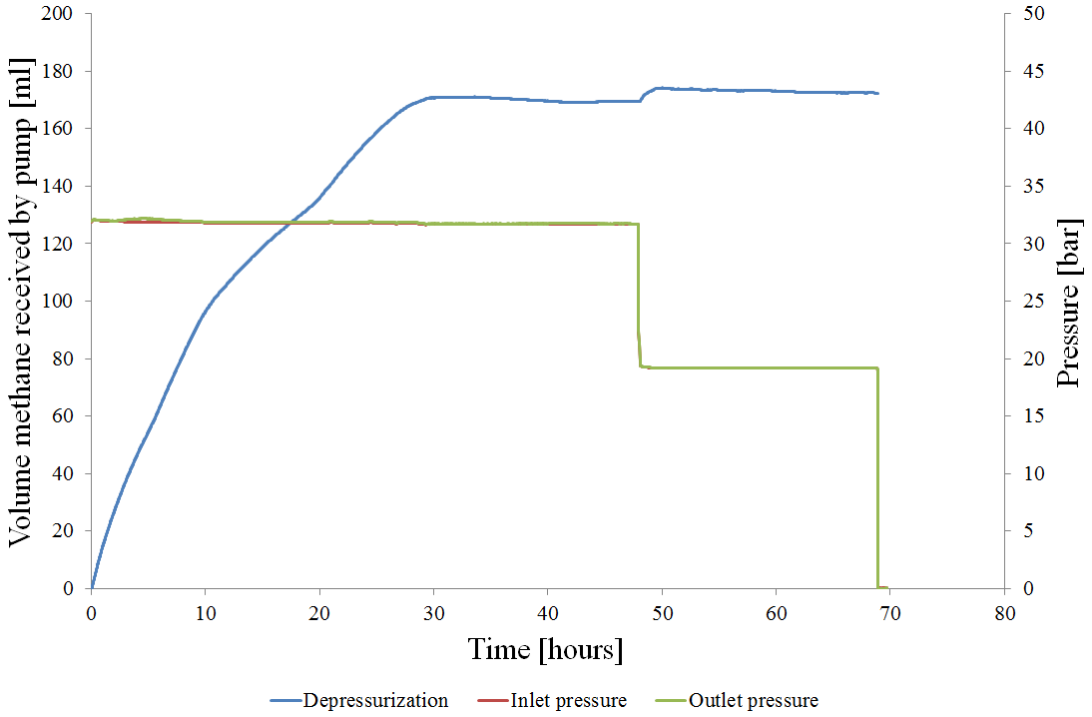

Figure 5-9 – CH_4 production from gas hydrate through depressurization at 32.5 and 20bar. A total of 170ml methane was recovered during the 30 first hours of the production. 4ml methane was recovered when pressure was reduced to 20bar.

During depressurization, temperature measurements were taken at inlet side, outlet side of the core and also from the confining liquid. Due to the endothermic nature and rapidity of the dissociation during depressurization, the induced cooling and low thermal conductivity may lead to formation of solid phases (secondary hydrate and ice) complicating the production severely (Moridis et al., 2009). Rate

of the hydrate dissociation is therefore dependable on the heat transfer during the depressurization process. In experiment mentioned over, the experimental dissociation rate was sensitive to temperature fluctuations even though the dissociation driving force was high. Methane production was simulated using TOUGH+HYDRATE which demonstrated an agreement with the experimental data (Birkedal et al., 2013). These results are also available in a recent publication by Birkedal (2013).

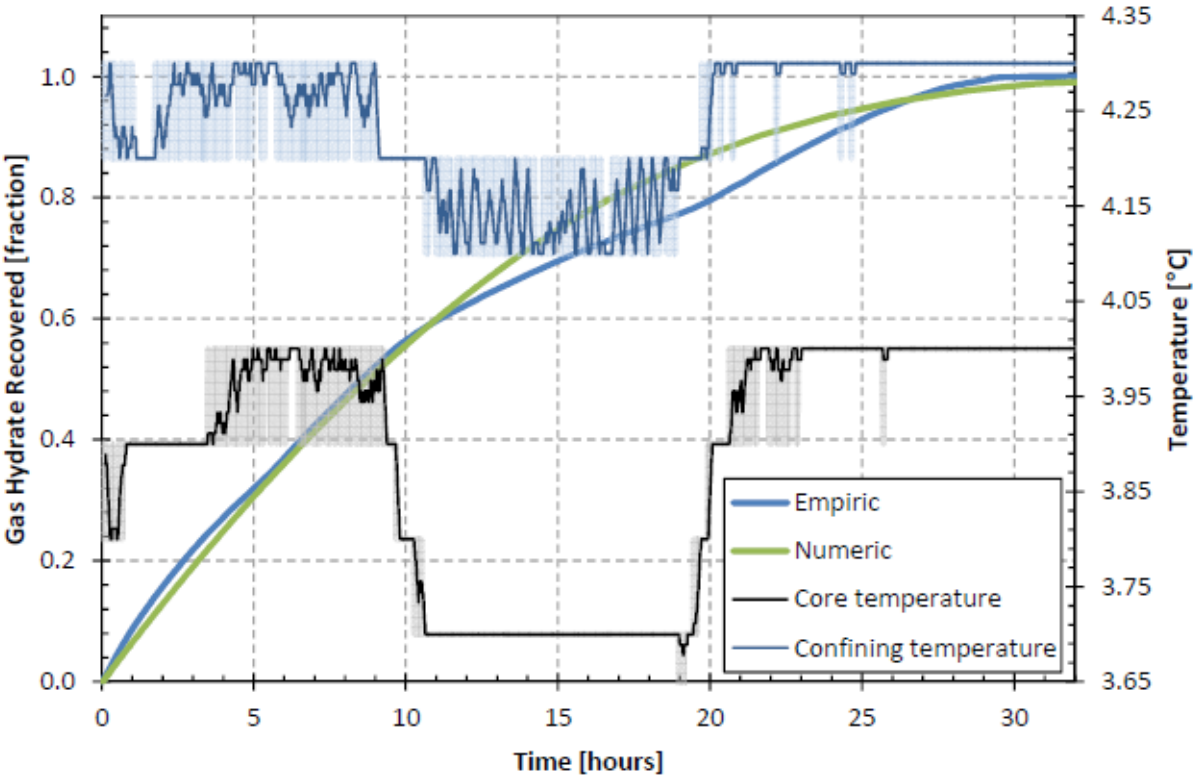

Figure 5-10 – Comparison of experimental and numerical hydrate dissociation by depressurization. Rate of hydrate decomposition was sensitive to temperature variations even though the driving force for hydrate dissociation at 32.5bar is high. This indicates that heat transfer is controlling mechanism during decomposition (Birkedal et al., 2013).

Production of associated water and loss of geomechanical stability are limitations with depressurization as a production method. The former could not be observed as the produced gas was sent to the pump through metal tubing, but data analysis after experiment indicated water production. Bentheim sandstone is a consolidated piece of rock that is unlikely to deform or be compacted despite large confining pressure. However, this may not be the case for unconsolidated porous medium. Sand production during production from Mallik has been reported which may indicate production from unconsolidated hydrate saturated rock. The geomechanical hazards as a result of depressurization as a production method have to be addressed before such method can be used.

5.4 Results from CH_4 production through thermal stimulation

Methane hydrate dissociation in Bentheim sandstone by thermal stimulation was examined. The thermal stimulation strategy typically involves *in situ* heating using steam or hot gas/liquid injection or down-hole combustion (Castaldi et al., 2006). Heat loss during the transit of the steam or hot gas from the surface to the hydrate region on one hand, and production of the associated water on the other hand are the major issues that have to be addressed before such production method could be implemented. However, the thermal stimulation as a production method has shown great recovery ratios (Fitzgerald et al., 2013). Stepwise thermal stimulation was conducted to study the production ratio from a methane hydrate system. The data were also studied in conjunction with computer calculations from CSMGem (Sloan et al., 2008), to see if the experimental data could match the simulated values. CSMGem calculations showed a dissociation threshold temperature of 11.3 ºC for a methane hydrate system at 83bar with a brine salinity of 0.1wt%, see Figure 5-11. In an attempt to acquire experimental data for dissociation threshold temperature for such system, methane hydrate was formed using method described under section 3.4.1. When hydrate formation came to end, the temperature was incrementally increased while the system was kept under constant pressure at 83bar. The isobaric temperature increase is shown in Figure 5-11. The temperature of the system was increased to 9ºC. The system was stabilized at 9º C for a period of 12 hours before the temperature was increased to 10ºC. The system was stable at 10ºC and 83bar for 30 minutes. The temperature of the system was then increased to 11.3 ºC. The temperature increase occurred over 4 hours. The system responded when temperature reached 10.1ºC. Methane hydrate was no longer stable and started dissociating. The produced methane was received by the pump. The system was kept at 11.3ºC for 24 hours. A total of 18ml methane was received by the pump during this stage. The temperature was further increased to 12ºC. System responded when the temperature reached 11.4ºC. Rapider hydrate dissociation was observed on the pump log. By the time system's temperature reached 12ºC, 52ml methane was produced. The temperature was increased further first to 12.5ºC and then to 13ºC. The experiment was ended when no further methane production was observed. Volume methane received by the pump and the temperature as functions of time are shown in Figure 5-12. Water production was expected during the experiment, but could not be observed due to limitations on the apparatus used.

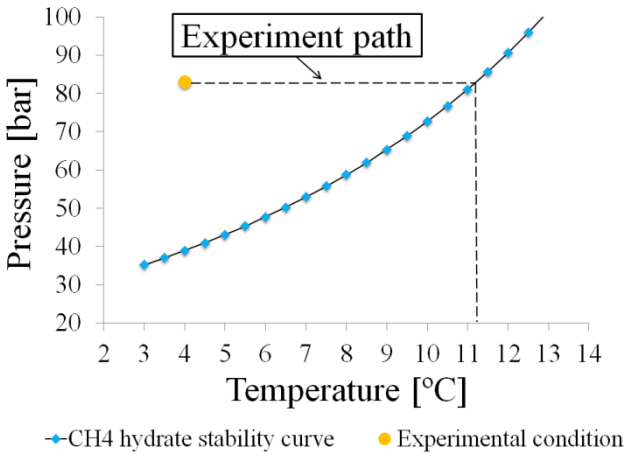

Figure 5-11 – Methane hydrate stability curve based on CSMGem calculations and experiment path during thermal stimulation of methane hydrate. The temperature was raised isobaric during the experiment.

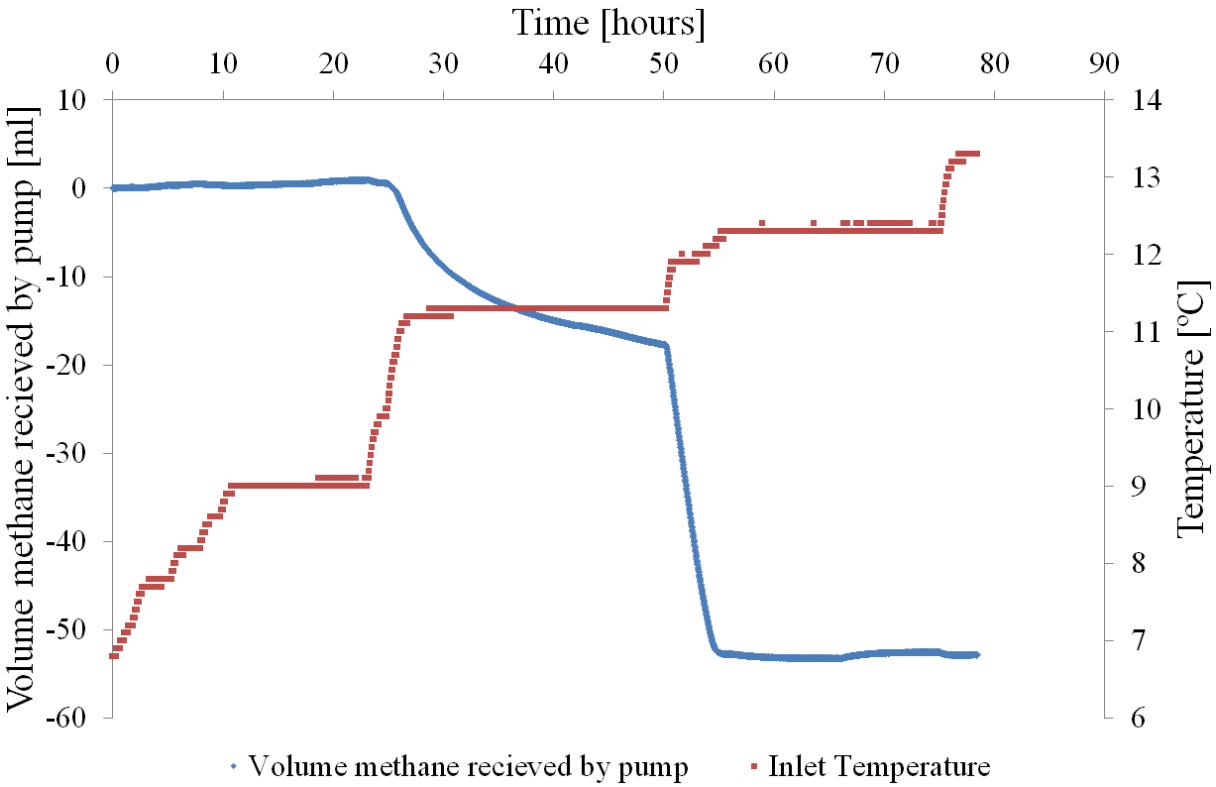

Figure 5-12 – Cumulative methane received and the temperature as functions of time are shown in the figure. Note hydrate dissociation on the figure when temperature reaches 10.1ºC. Further temperature increase to 12ºC resulted in rapider dissociation. 52ml methane was produced during the experiment. The negative volume values on the y-axis are due to the pump retracting in order to keep a constant pressure.

Methane hydrate dissociation temperature at 83bar and brine salinity of 0.1 wt% was found experimentally. In our system, methane hydrate started dissociating at 83bar and 10.6 ºC, while computer calculations using CSMGem showed a dissociation temperature of 11.2ºC at 83bar.

5.5 Results from CH_4 production through CO_2 injection

As stated under 1.4.2, CO_2 provides more thermodynamically stable hydrate than CH_4 at experimental conditions used during this study. CH_4 production is therefore a result of an exchange process in which CO_2 replaces CH_4 bound in hydrate. Methane production through CO_2 injection into hydrate bearing sandstone, along with the possibility of sequestration of CO_2 within the formation has been central in gas production from hydrates at the University of Bergen. Earlier studies have looked into the kinetic of the exchange process using MRI visualizations techniques. A methane recovery of 50-85% was estimated based on volume of methane produced (Husebø, 2008). During the present study, a gas chromatograph (GC) and mass flow meter (MFM) were implemented, tested, and used to quantify the methane production from hydrate bearing sand stone core samples. The main focus during this master thesis has been to investigate the feasibility of enhancing the exchange process by using chemical additives. Therefore, experiments CO2_20 and CO2_21 were conducted as base line experiments with an initial water saturation of 0.4 and CO_2 injection without any chemical additives. Experiment CO2_20 was lost due to problems with the cooling bath (cooling was lost). Experiment CO2_21 was conducted at 83bar and 9.6ºC. Primarily, the injection of chemical additive was done after a period of time with CO_2 injection. The reason for this was to see if more methane could be recovered from the core. Experiments CO2_23 and CO2_24 were conducted at 83bar and 4ºC, using additives after CO_2 injection. For CO2_23, slugs of MDEA were injected after 168 hours of CO_2 injection. Slugs of MEA were used for experiments CO2_24. These were injected after 177 hours of CO_2 injection. Experiment CO2_26 was done at exchange temperature of 9.6ºC without any injection of chemical additives. Experiment CO2_27 investigated the recovery when MEA was injected into the core before CO_2 injection. Table 5-3 shows an overview of water, gas and hydrate saturation prior to CO_2 injection.

Table 5-3 – Saturation distribution before CO_2 injection in experiments studied in this thesis.

Core name	Initial water saturation	Final water saturation	Final hydrate saturation	Final gas saturation	Pore volume injected	Chemical additive used
CO2_20	0.416	-	0.53	0.47	-	-
CO2_21	0.415	0.032	0.48	0.51	2.06	-
CO2_22	0.379	0.001	0.48	0.52	-	-
CO2_23	0.412	0.034	0.48	0.49	4.51	MDEA
CO2_24	0.410	0.032	0.48	0.49	2.95	MEA
CO2_25	0.41	0.003	0.56	0.44	2.76	-
CO2_26	0.43	0.055	0.41	0.59	2.33	-
CO2_27	0.40	0.06	0.43	0.51	1.11	MEA

5.5.1 CO_2 injection into a whole core plug

During present study, methane hydrate was formed within whole core samples prior to CO_2 injection. Earlier hydrate formation experiments have used both mechanically fractured cores (Graue et al., 2006) as well as whole cores (Bringedal, 2011). The idea of fracturing the core was proposed by Graue *et al.* (2006) in order to improve the surface area of CO_2 exposure to the hydrate in the pores. The fractured core was kept open using a POM spacer. The spacer also provided accumulation volume for MRI monitoring the produced methane during CO_2 – exchange experiments. This possibility has been absent during this study as CO_2 injection experiments has been conducted within a whole core plug. In experimental conditions (83bar and 4 ºC) the CO_2 is in liquid phase and has a higher viscosity than free methane. Injection of CO_2 will therefore result in a viscous displacement and mixing of the free methane in pores where CO_2 flows through, rather than diffusion driven mass transport (Ersland, 2013).

5.5.2 CH_4 production during CO_2 injection

CO_2 provides thermodynamically more stable hydrate under experimental conditions, 83bar and below 10ºC. Earlier studies conducted by the hydrate group at the University of Bergen used MRI – visualizations to confirm the CO_2 – exchange process within the hydrate bearing sandstone core plugs (Ersland et al., 2009; Graue et al., 2006; Husebø, 2008). Formation of CO_2 – hydrate induces a micro scale CH_4 – hydrate dissociation. The dissociated CH_4 is the target of this process and may be produced. When hydrate formation ceased, CH_4 was vacuumed from the injection and production lines, except the volume between the inlet valve and the core, and the volume between the core and outlet valve. CO_2 was injected with a rate of 1.2 ml/h from the inlet side (bypass closed under injection). Higher injection rate could result in CO_2 channeling throughout the core sample which in turn could lead to less methane hydrate being contacted. Low injection rate would allow for longer exposure time. It is likely to assume that the injected CO_2 displaces free CH_4 effectively (not hydrate bound). However, CO_2 is a very mobile phase and it is therefore likely that the volumetric sweep would suffer where there are heterogeneities either in core permeability or saturation. Therefore, it is unknown whether all free CH_4 is displaced by CO_2. Recovery from hydrates was calculated under assumption that all free gas was produced. Injection of CO_2 continued for a period of 140 – 240 hours for the different experiments listed in table under. Table 5-3 shows saturation distribution of different phases within the core sample prior to CO_2 injection. Results acquired during the CO_2 – exchange experiments are presented in this section. As listed in Table 5-3, CO_2 injection failed in experiments CO2_20 and CO2_22 due to a hydrate formation (plug) inside the production line. This was detected as differential pressure over the inlet and outlet side. The first results from the CO_2 injection is therefore from core CO2_21.

Results from CO_2 injection into core CO2_21

Experiment CO2_21 was conducted at 83bar and 9.6ºC, as a base line experiment where no chemical additives were injected. When hydrate formation ceased (no methane injection was observed on the pump log), the core sample was isolated by closing the inlet and outlet valve. The excess methane in injection and production lines were vacuumed. Injection and production lines were then pressurized by CO_2 up to 83bar. The pump was then set to deliver CO_2 at rate of 1.2 ml/h. Injection was done with closed bypass valve which assured injection from the inlet side. The effluent was run through a gas chromatograph and gas composition was measured as a function of time. GC analyzed CO_2, CH_4 and N_2 fraction in produced gas. The gas composition in effluent as function of time is illustrated in Figure 5-13. At 0 hour, CO_2 was introduced to the system at a rate of 1.2 ml/h. Two processes are expected to occur once CO_2 is introduced to the system. A spontaneous CH_4 – CO_2 replacement process occurs once CO_2 is in contact with methane hydrate. CO_2 provides thermodynamically more stable hydrate. CO_2-hydrate formation generates heat which induces a local CH_4 – hydrate dissociation with subsequent free methane which may be produced. The other process is displacement of excess methane (not hydrate bound) from the pores. Displacement process occurs as CO_2 advances throughout the core sample. After approximately 5 hours of CO_2 injection, a drop in the CO_2 fraction in effluent is seen on the graph. The drop may be caused by remaining methane that has not been properly vacuumed from the system. It may also be caused by free methane which is trapped between the core sample and outlet valve. At 10 hour, a sudden drop in CO_2 fraction, and an increase in CH_4 fraction is seen on Figure 5-13. The volume between core outlet and BPR on the downstream end was pressurized with liquid CO_2 prior to injection. When methane appears on GC after ~ 10 hours, this must originate from the core sample, either from free gas or hydrate bound gas. The major part of the first methane produced is most likely from free mobile gas. An increase in N_2 fraction is also observed

at 10 hour. This may be due to production of N_2 from the air that was trapped within the pores during the core preparation. This could mean that CO_2 was contacting some of the free gas occupying residual pore volume out of the core. Not all free CH_4 is likely swept by CO_2. But when calculating recovery from hydrates, the assumption has been that all free methane is produced during CO_2 injection. Therefore the calculated recovery is likely underestimated.

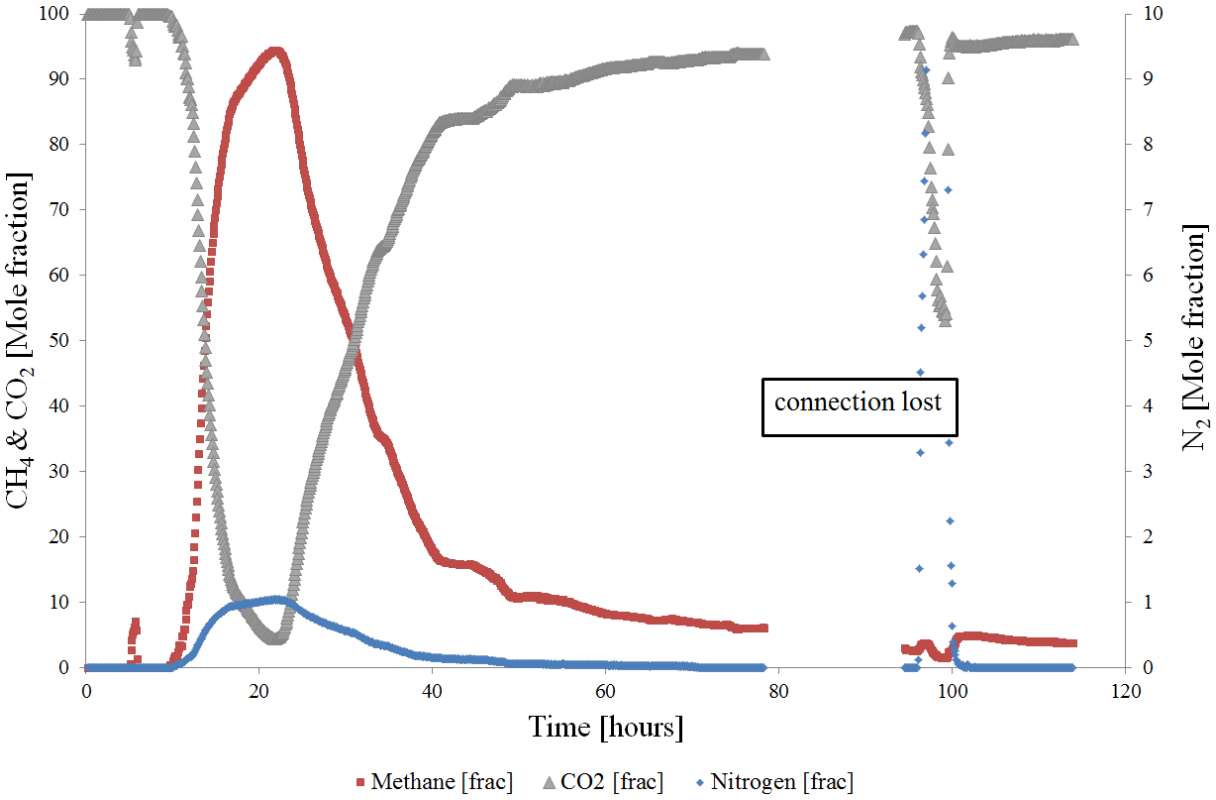

Figure 5-13 - Fluid fraction in effluent are shown for experiment CO2_21. Mole fraction of CH_4 and CO_2 are plotted on primary axis while N_2 fraction is plotted using secondary axis.

Production of non-hydrate bound methane in combination with released methane as a result of a CH_4 – CO_2 replacement is the reason to high fraction of methane until 22 hour. As CO_2 advanced throughout the core sample, more CH_4 (free methane) occupying residual pore volume was displaced. As listed in Table 5-3, final gas saturation for this experiment (before CO_2 injection) was 0.51 which constituted a volume of 33ml excess methane in pores. Assuming CO_2 injection at a rate of 1.2 ml/h, it would take at least 27 hours to displace excess methane from the pores. Advancement of CO_2 throughout the core results also in CO_2 contacting more CH_4 hydrate which may lead to higher methane production. As shown in Figure 5-13, methane fraction in effluent decreases after almost 25 hours of CO_2 injection. This is due to less free methane available for production, and also because CO_2 has to diffuse through already formed CO_2 hydrate in order to access CH_4 hydrate, less surface area between CO_2 in liquid phase and methane hydrate results in decrease in exchange rate. As it can be seen on Figure 5-13, methane fraction in effluent keeps dropping until 80 hour. Connection with GC was lost for a period of 15 hours. Contact with GC was reestablished at 95 hour. An increase in nitrogen fraction in effluent is seen at 95 hour which may be explained by analyzing the existing air in outlet line of GC. Analysis of the gas fraction in effluent restarted in 100 hour. As shown in Figure 5-13, methane fraction is down at 4% after 115 hours of CO_2 injection. Injection, production and differential production during the CO_2 injection are shown in Figure 5-14. Both the injection and production pressure build up to reach the pressure limit of the back pressure valve during the ten first hours of injection. The back pressure

valve had a limit of 86.5bar and would release the produced gas towards GC if the production pressure surpassed this pressure. A drop in both injection and production pressure can be seen at 12 hour. This may be due to a decrease in room temperature during the night, or a CO_2 leakage through the sleeve and into confining oil. A pressure build up is observed during 30 – 40 hour. This may have been caused by periodic flow through back pressure valve. A differential pressure ($P_{INJECTION} - P_{PRODUCTION}$) in range of 0 – 0.1 [bar] indicates good permeability during the injection.

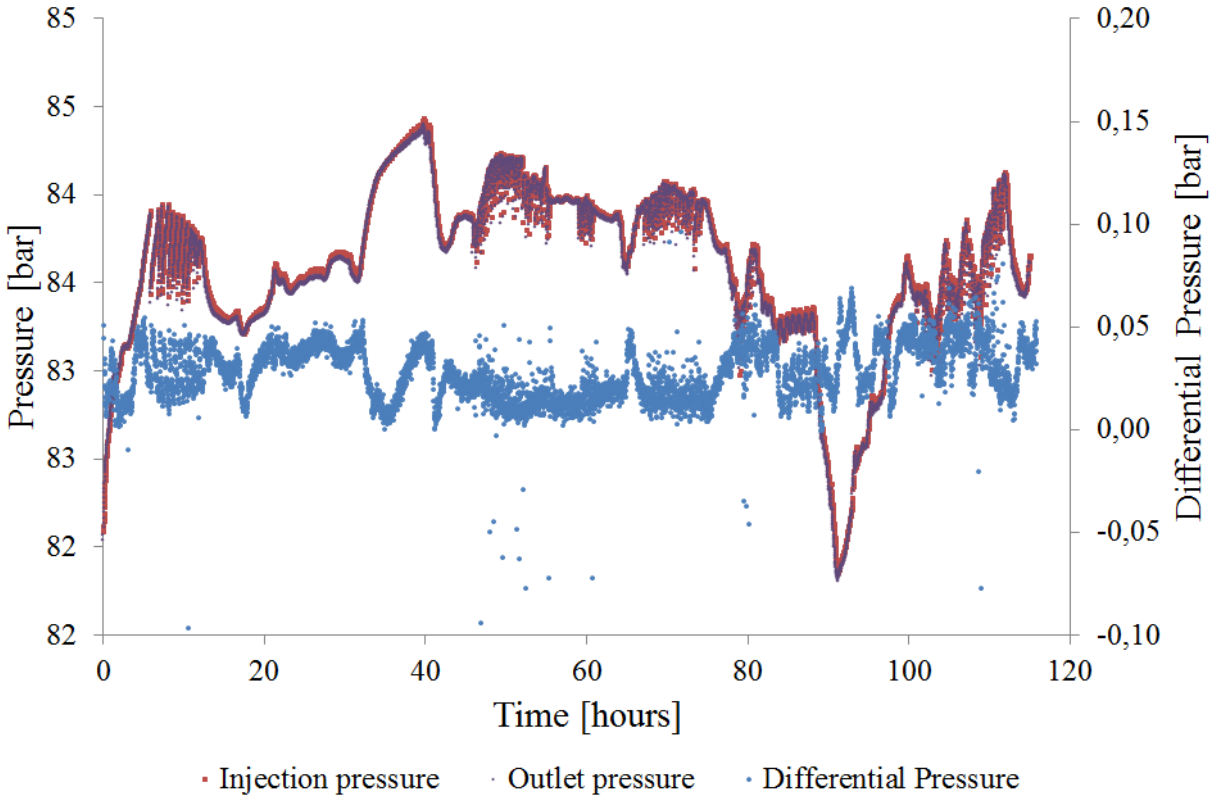

Figure 5-14 – Injection, production and differential pressure as function of time during CO_2 injection for core CO2_21. Differential pressure plotted using secondary axis.

Figure 5-15 shows methane recovery from the core CO2_21 as function of time. As shown in the figure, a recovery of almost 28% was achieved during the first 40 hours. This may be explained by production of free methane in the pores as well as the production of methane released as a result of $CH_4 – CO_2$ replacement. The exchange rate is expected to decrease as mass transport is limited when CO_2 has to diffuse through an already established CO_2-hydrate in order to reach the CH_4-hydrate (Jung et al., 2010; Lee et al., 2003; Yoon et al., 2005). Another aspect to note is the CO_2's poor ability to replace methane in small cavities of the hydrate structure allowing a theoretical maximum recovery (methane recovery from hydrate) value of 0.64 (Park et al., 2008). Park et al., (2003) suggested that an injection of a mixture of CO_2 and N_2 could improve the methane recovery as nitrogen also could replace methane in the small cavities.

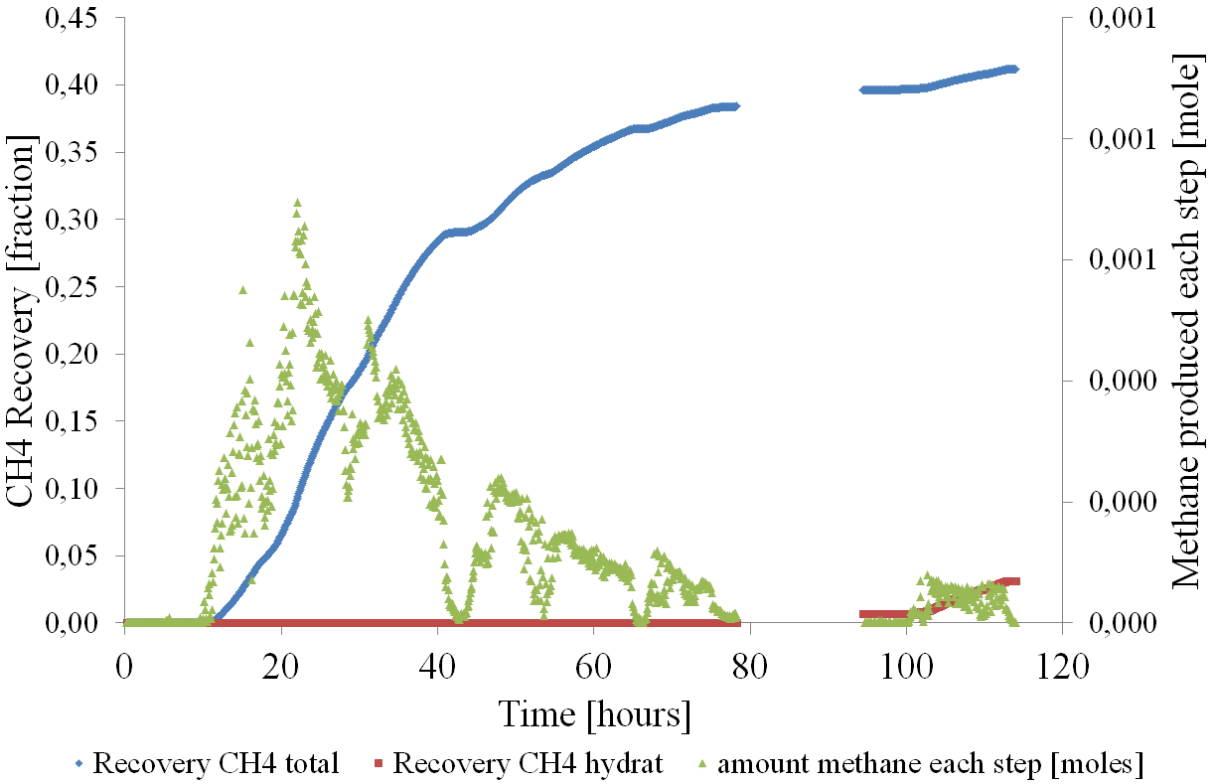

Figure 5-15 –Total recovery, recovery from hydrate and amount methane produced each step as a function of time are shown in the figure. Total recovery is given by the amount of methane produced divided by the total amount of methane in the core prior to CO_2 injection. Total amount of methane includes methane bound in hydrate, free methane in the core and the amount of methane trapped between the core and inlet and outlet valves. Recovery from hydrate is given by the amount of methane produced when all free methane is assumed produced.

As shown in the **Figure 5-15**, at 45 hour, methane production drops. This was due to a pressure build-up at the upstream side of the back pressure valve. The pressure build-up is shown in Figure 5-14 at 45 hour. The flow rate on the flow control valve (sitting in between GC and MFM) was increased at 46 hours resulting in effluent flowing through the GC and MFM. As a result of this, more methane production was measured during next four hours. Looking at the Figure 5-15, the recovery seems to cease after 70 hour. Connection with GC was lost between 80 and 95 hour. The recovery was therefore extrapolated and starts at 0.39 at 95 hour. A total recovery of 0.41 and a recovery of 0.04 from hydrate were achieved after 115 hours of CO_2 injection. Recovery from hydrate value may be underestimated due to the assumption that all free methane was produced during the experiment.

Results from CO_2 injection into core CO2_23 and injection of MDEA slugs

As stated under previous section, the rate of exchange is expected to decrease by time during CH_4 – CO_2 experiments. It is therefore of high interest to investigate the possibility of production enhancement during the exchange process. Lee et al., (2003) reported a better recovery by injecting a mixture of CO_2 and N_2. Since the injected nitrogen could also be produced, separation of injected nitrogen at the production site leads to economically less attractive production enhancement scenario (Kvamme, 2013). The feasibility of exchange enhancement by use of chemical additives was therefore investigated during two exchange experiments. Recovery enhancement by the use of MDEA slugs was studied during experiment CO2_23. Saturation distribution prior to CO_2 injection was the following, S_{Water} = 0.03, S_{Gas} = 0.49 and $S_{Hydrate}$ = 0.48. Final gas saturation of 0.48 constituted a volume of 31ml excess methane. Injection and production lines were vacuumed and then flushed with CO_2 pressurized up to 83bar. CO_2 was injected from the inlet side at rate of 1.2 ml/h (bypass valve closed under injection). A total of 4.51 pore volumes of CO_2, as listed in Table 5-3, were injected during the experiment that lasted for 225 hours. Gas fraction in effluent is shown in Figure 5-16.

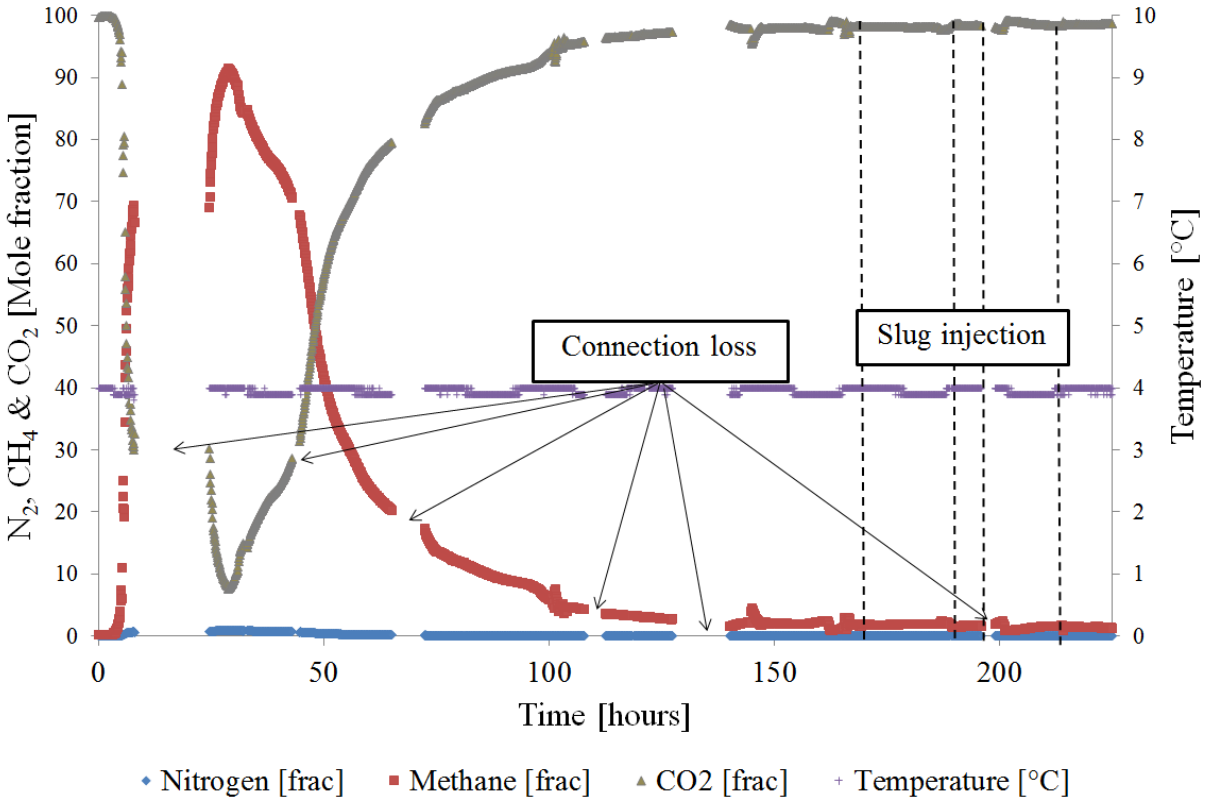

Figure 5-16 - Fluid fraction in effluent and temperature as function of time for experiment CO2_23. The time of slug injections are marked with the dashed lines.

CO_2 injection started and continued for 8 hours before it was stopped because connection with GC could not be established. When connection with GC was reestablished, the system had already been pressurized with CO_2 for 24 hours. The interaction and diffusion of CO_2 into the core during the GC downtime may already have led to some production of methane which could not be analyzed due to loss of connection with GC. Connection with GC was lost several times during this experiment and had to be reestablished, the time period for these are marked on the figure. As shown in Figure 5-16, methane fraction in effluent starts decreasing at 28 hour. Methane fraction drops gradually and flattens out at 0.02 after 160 hours of injection. Exchange rate is expected to decrease as the surface area

between CO_2 in a liquid phase and methane hydrate decreases (Yoon et al., 2005). The potential of the chemical additives to enhance methane production could be examined at this point. To investigate the latter, 16 slugs of MDEA were injected in 4 rounds with a total volume of 4ml. Each injection was divided into 4 slugs that were injected into the core with 15 minutes intervals. 15 minutes was chosen due to time it would take to push the slug into the core with an injection rate at 1.2 [ml/h]. The slugs were injected at 167, 188, 194 and 216 hour. During this experiment, temperature measurements were continuously taken (1 minute intervals) at the inlet side in order to detect the possible reaction between the MDEA and the injected CO_2. As stated under section 2.3.4, the reaction between CO_2 and MDEA has an exothermic nature and the generated heat may trigger hydrate dissociation. MDEA slugs were injected using the method described under section 3.4.5. Methane recovery both before and after slug injection, is shown in Figure 5-17. The time steps where slugs were injected are marked in the figure.

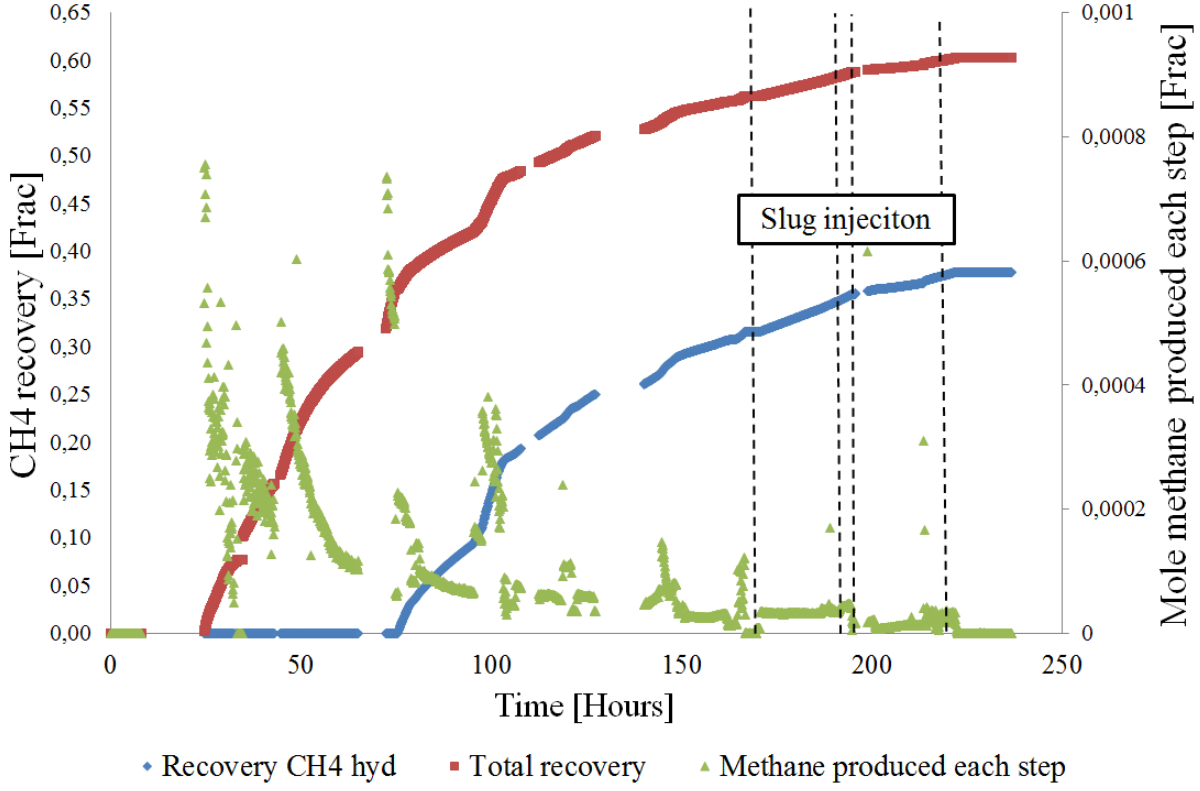

Figure 5-17 – Total methane recovery and methane recovery from hydrate during CO_2 injection both before and after slug injection for experiment CO2_23 is shown in the figure. Both recoveries were extrapolated for time periods where connection with GC was lost. Mole methane produced as a function of time, and the time steps where slugs of MDEA where injected are also shown in the figure. The times of injection are marked with dashed lines. Note mole methane produced in time period after slug injection. No significant increase in methane produced can be seen.

As shown in Figure 5-17, the slug injection intervals are different. The first injection was done to investigate the response from the system while the second and third slugs were injected with 6 hours interval to study if the volume of the injected slug and the injection intervals could have an effect on the response from the system. Finally, the fourth injection was done to see if the effect from the previous slugs could be repeated. It is important to note that analyze of the system's behavior was not possible during the experiments and the data presented here are based on calculations done when the experiment was over. No increase in temperature at the injection site was observed during the slug injections which may indicate that reaction between slugs of MDEA and the injected CO_2 did not occur at the inlet site and close enough to the core sample. Slugs may have reacted with the injected

CO_2 once they were in contact with it. Slugs were added to the injected CO_2 at distance from the core through a 60cm long 1/8" tubing. The generated heat from the reaction may have been lost along the tubing and not reached the core and subsequently not assisted the production. As shown in figure, there is an increase in amount of methane produced approximately 3 hours after the first slug was injected. Interestingly, at this point the rate on the flow control valve on downstream side of the GC and towards the MFM was increased. The rate on the flow control valve was increased due to pressure buildup on the upstream side of the pressure regulator. The increased flow rate out of GC and towards mass flow meter resulted in more effluent flowing towards the mass flow meter and could be the reason to the increased mass measured. The high mass measured may be the reason to increased methane produced at that point. Two other injections were conducted at 188 and 194 hour. As shown in Figure 5-17, there was a decrease in mole methane produced just after the third injection occurred (194 hour). The decrease was caused by lowering the rate on the flow control valve towards the mass flow meter which resulted in less effluent flowing towards the mass flow meter and subsequently less mass measured by the MFM. This could be the reason to the decrease in mole methane produced at this point. The last injection was done at 216 hour. The last injection had minor or no impact on the mole methane produced. This can be seen on the graph at 216 hour, where no increase in methane production was detected. The anticipated effect from the slug injection on the methane production was absent during the experiment due to heat loss along the injection line. The 1/8" tubing connecting the injection site and the inlet side of the core suffered from not being isolated. This may have resulted in loss of the generated heat along the injection line. This is confirmed by temperature measurements taken at the inlet[8] side of the core as the temperature did not change during the experiment. As shown in Figure 5-16, temperature was relatively constant at 4ºC during the experiment. Experiment CO2_23 had a final recovery value of 0.6 which is higher than CO2_21. Pore volume CO_2 injected for CO2_21 was 2.10 while 4.51 for CO2_23 which may be the reason to the higher recovery from core CO2_23. Increased recovery by the injected additive was not achieved due to either low heat generated as a result of the reaction between CO_2 and slugs of MDEA or loss of the generated heat along the injection line. MEA has been proven to be able to generate more heat in reaction with CO_2 (Prakash et al., 2006). The potential of MEA to assist methane production was studied during experiment CO2_24. The results from experiment CO2_24 are presented in next section.

[8] The temperature sensor sits on the end lug at the inlet side of the core enabling temperature measurements closed to the core sample.

Results from CO_2 injection into core CO2_24 and injection of MEA slugs

Saturation distribution prior to CO_2 injection for core CO2_24 was the following, S_{Water} = 0.03, S_{Gas} = 0.49 and $S_{Hydrate}$ = 0.48. Final gas saturation of 0.49 was a volume of 33.7ml excess methane. During this experiment, the potential of assisted methane production through injection of MEA slug was investigated. As stated earlier, MEA generates more heat in reaction with CO_2 than MDEA (Kvamme, 2013; Zhang et al., 2010). The assumption before slugs of MEA were injected was that, the generated heat from the reaction between MEA and the injected CO_2 would be able to dissociate methane hydrate up to a greater extent compared to MDEA. The main target was to thermally dissociate methane hydrate that was not being contacted by the injected CO_2 due to less surface area between the CO_2 and methane hydrate. In order to study the latter, slugs of MEA were injected into the core using the method described in section 3.4.5. Due to plugged pressure regulator the gas fraction in effluent could not be analyzed for a period 70 hours during experiment. During this time, the system was pressurized with CO_2 up to 85bar. When flow was reestablished, slugs of MEA were injected at 193 and 201hour. Gas fraction in effluent as a function of time is shown in Figure 5-18.

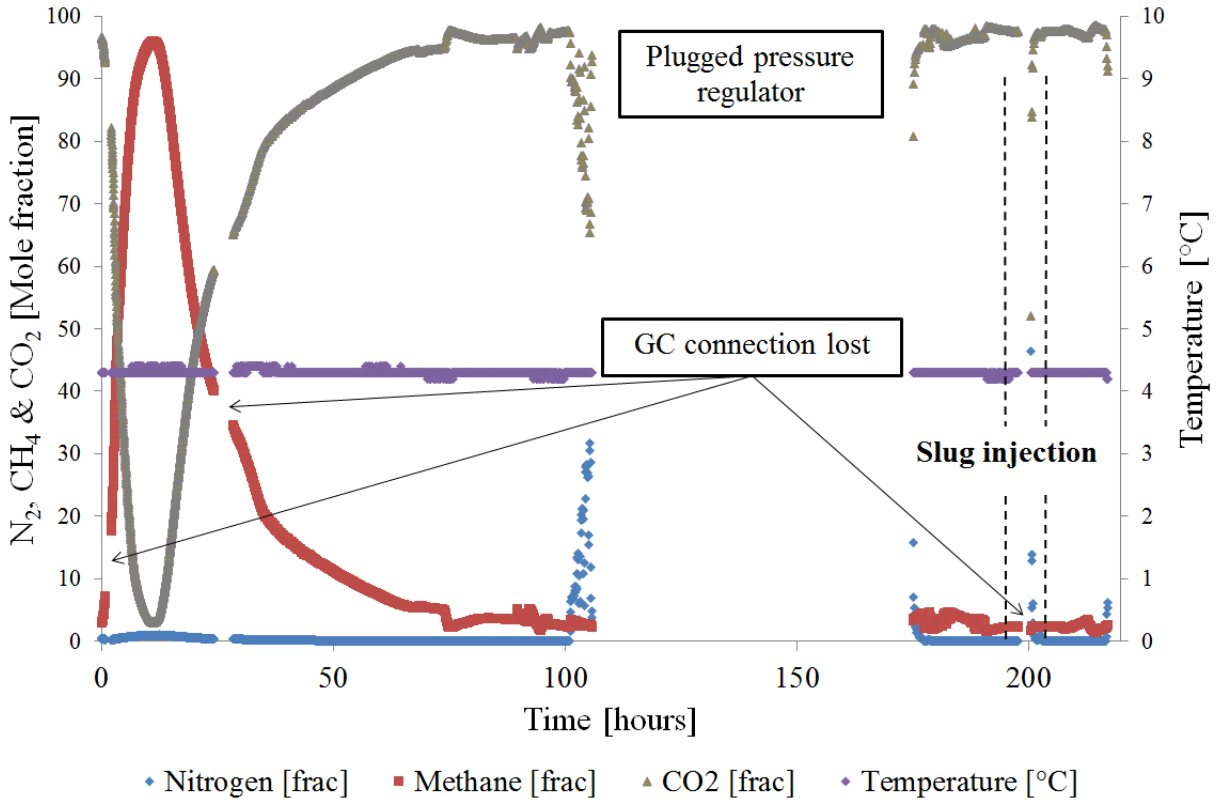

Figure 5-18 - Fluid fraction in effluent and temperature as function of time for experiment CO2_24 are shown in the figure. The time of slug injections are marked with the dashed lines. Gas fraction could not be analyzed due to plugged pressure regulator. Pressure regulator was placed between the downstream side of the system and upstream side of the GC regulating effluent pressure towards GC. When pressure regulator was blocked effluent could not flow towards GC.

During both slug injections, one could feel the generated heat from the reaction between CO_2 and MEA. This was not the case during injection of MDEA slugs. But the temperature measurements taken from inlet side of the core confirm no temperature change as a result of reaction between CO_2 and MEA. This may be due to the distance between the injection site and the core sample. The generated heat may have been lost before it reached the core sample. Methane recovery and moles methane produced as function of time are shown in Figure 5-19. A total recovery of 0.48 and a

recovery of 0.11 from the hydrate were achieved after 215 hours of CO_2 injection. As shown in Figure 5-19, no significant changes can be seen on the curve, and the curve seems to be flattening out both before and after slug injections. Due to a plugged pressure regulator the experiment was ended. No more measurements could be taken to further investigate the production. 2.95 pore volumes of CO_2 were injected during the experiment which is lower than 4.50 pore volumes injected during experiment CO2_23. Lower recovery values compared to experiment CO2_23 may be explained by the less pore volume CO_2 injected. Problems with the pressure regulator should also be taken into consideration.

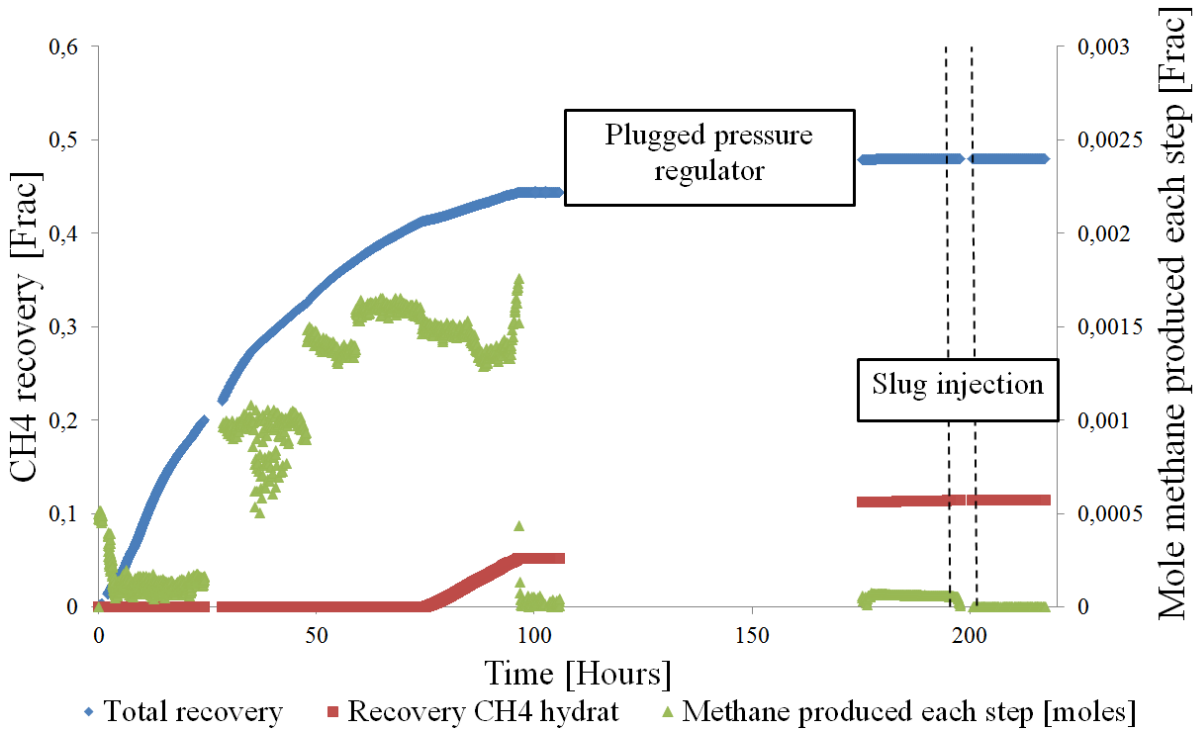

Figure 5-19 – Total methane recovery and the recovery from hydrate during CO_2 injection both before and after slug injection of experiment CO2_24 is shown in the figure. The recovery has been extrapolated for time periods where connection with GC was lost. Mole methane produced as a function of time, and the time steps where slugs of MDEA where injected are also shown in the figure. The times of injection are marked with dashed lines.

Result from the experiment CO2_24 indicate that no significant production enhancement was achieved from injection of MEA slugs. The relatively constant temperature at the inlet side of the core sample shows that the generated heat from the reaction between MEA and CO_2 had no impact on the temperature at the core inlet and subsequently could not have induced hydrate dissociation. The big lesson learnt from this experiment was that if the generated heat from the reaction between CO_2 and MEA was to assist the production, either the injection lines would have to be thermally isolated or the reaction had to occur at a shorter distance from the core. Therefore, the experimental setup was modified enabling injection of both reactants (MEA and CO_2) from two separate pumps. This way, the reaction between CO_2 and MEA could happen at shorter distance from the core. This could result in more of the generated heat reaching the core sample.

Results from CO_2 injection into experiment CO2_26

Saturation distribution prior to CO_2 injection for core CO2_26 was the following, S_{Water} = 0.055, S_{Gas} = 0.59 and $S_{Hydrate}$ = 0.41. Final gas saturation of 0.41 was a volume of 27.7ml excess methane. No chemical additives were injected during experiment CO2_26. The experiment was conducted at 83bar and 9.6ºC. Gas fraction in effluent as a function of time is shown in Figure 5-20.

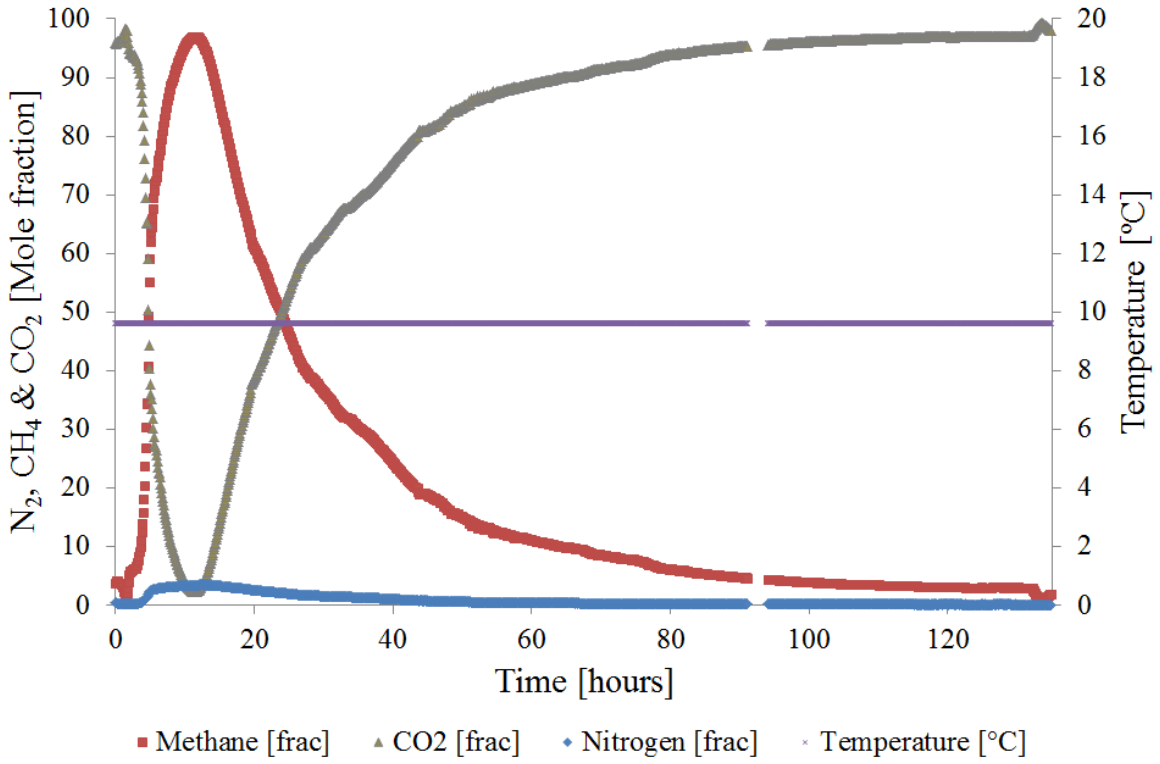

Figure 5-20 - Fluid fraction in effluent and temperature as function of time for experiment CO2_26 are shown in the figure. Note that methane's fraction is over a longer period of time during to experiments conducted at 4ºC.

Oppose to experiments mentioned above, no GC problem occurred during CO_2 injection into core CO2_26. The injection lasted for 136 hours resulting in a total recovery of 0.62 and a recovery of 0.35 from the hydrate. The total methane recovery, the recovery from the hydrate and methane produced each step are shown in Figure 5-21. Core CO2_26 demonstrated a higher methane fraction during the first 100 hours compared to the previous experiments. This may have been due to the higher driving force of the exchange process. The experimental condition of 83bar and 9.6ºC is closer to the methane hydrate's equilibrium boundary. Methane hydrate is less stable close to its equilibrium boundary. At such condition CO_2 is still a more stable hydrate former and may potentially replace methane in the hydrate more readily.

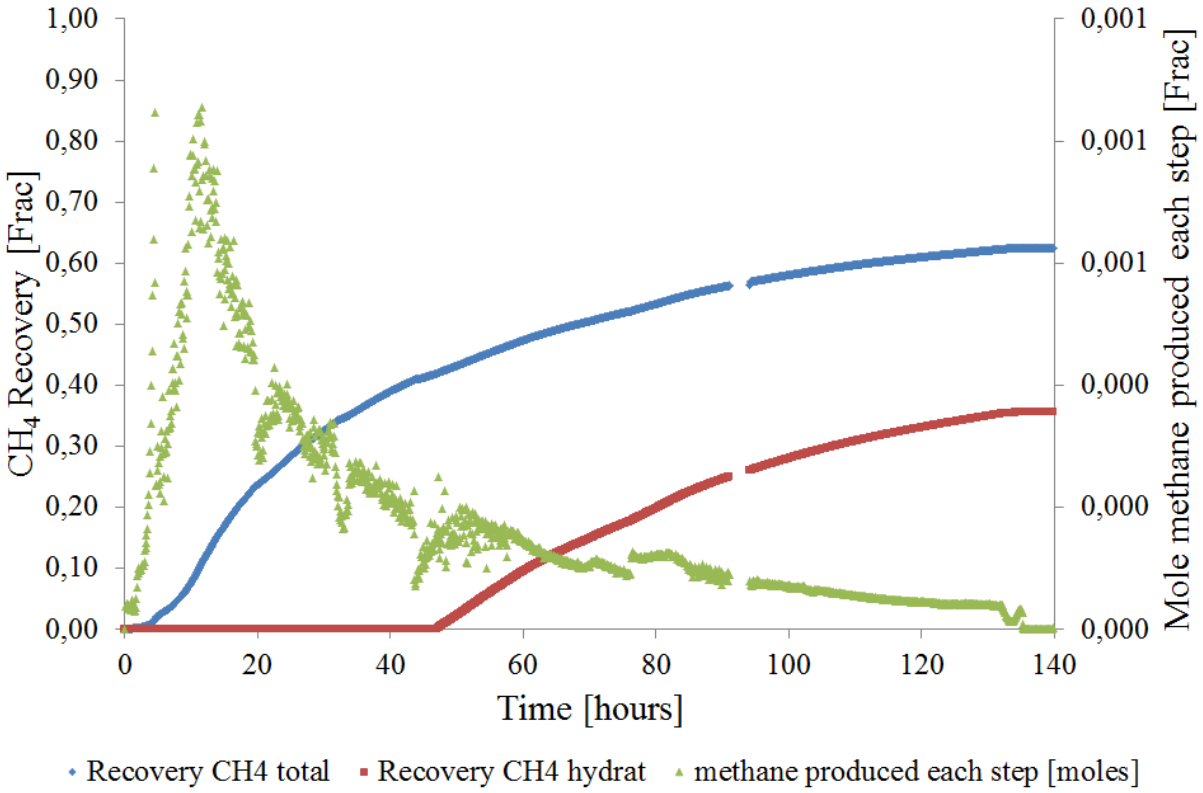

Figure 5-21 – Total methane recovery, recovery from hydrate and methane produced each step as a function of time are shown in the figure. Note the high methane production during an injection period of 80 hours. The latter has not been seen during exchange experiments conducted at 4ºC.

Results from CO_2 injection into experiment CO2_27 and injection of MEA from a separate pump

The experimental setup was modified in order to allow for injection of MEA and CO_2 separately. The end-piece on the inlet side of the core sample allowed for two inlets, one for injection and one for temperature measurements. In order to directly inject MEA into the core, one had to compromise the possibility of taking temperature measurements at the inlet side of the core. Detection of the generated heat from the reaction between MEA and CO_2 was implicated due to lack of the *in situ* temperature measurements. However, temperature measurements could be taken both at the outlet side of the core sample and also in confinement oil above the inlet side of the core sample. Prior to CO_2 injection, MEA was filled into a separate injection pump and pressurized up to 83bar. 1.5ml MEA was injected from the inlet side of the core before CO_2 was introduced to the system. MEA was at room temperature inside the pump. However, a temperature gradient existed within the injection line prior to injection that may have cooled MEA to a lower temperature prior to it being introduced to the hydrate saturated core. When production pressure reached pressure limit on back pressure valve, injection rate of both MEA and CO_2 was reduced to 1.2 [ml/h]. A total volume of 21ml MEA was injected into the core over 17 hours. Fluid fraction in effluent and temperature during injection as function of time are shown in Figure 5-22. Temperature measurements were taken at the outlet side of the core sample as well as the in confinement liquid. Both temperatures fluctuated between 4 ºC and 9 ºC in 24 hours intervals. This indicates that the temperature during the experiment has been under great impact from fluctuations in the room temperature.

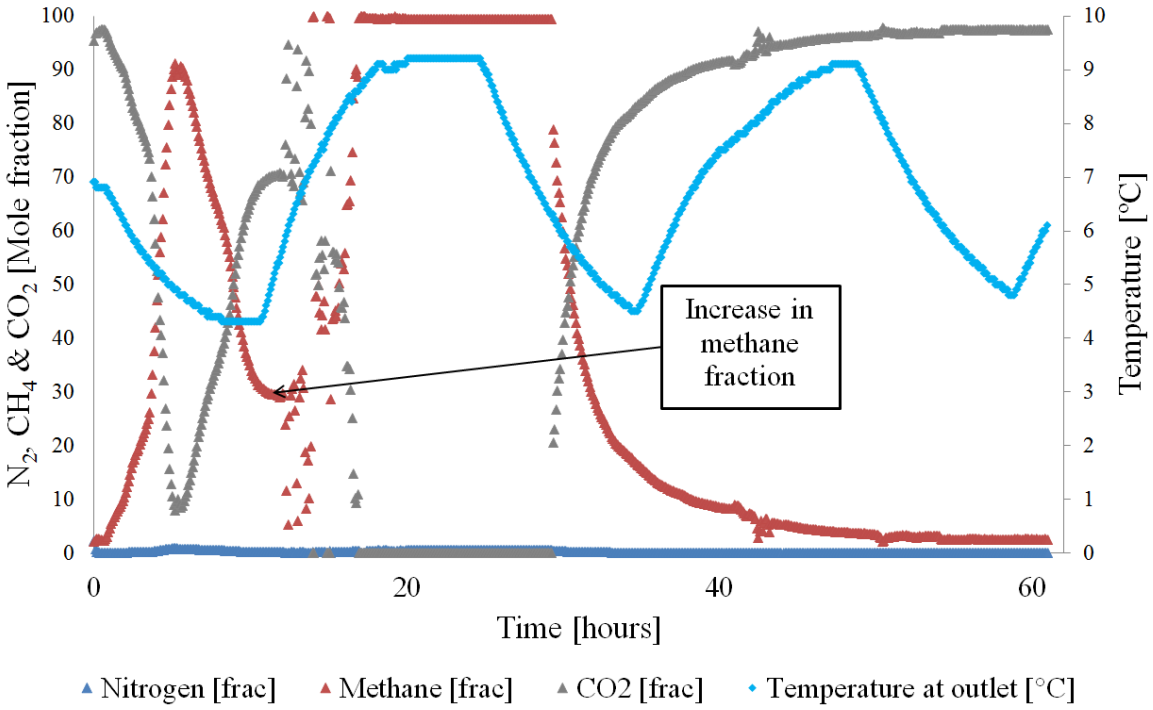

Figure 5-22 - Fluid fraction in effluent and temperature as function of time for experiment CO2_27 are shown in the figure. Note the increase in methane fraction at 12 hour. MEA was pre-injected to the core before CO_2 was introduced during this experiment. High methane fraction was observed in period 13 – 29 hours. A total of 1.11 pore volumes of CO_2 and 0.30 of MEA were injected during this experiment.

As shown in Figure 5-22, methane fraction increases up to 90% during the first 5 hours of injection before it gradually drops. An increase in methane fraction can be observed at 13 hour. This may be due to a possible reaction between MEA and CO_2 since such behavior has not been seen during earlier experiments. Observations from earlier experiments (CO2_21, CO2_23 and CO2_24) indicate that the methane fraction increased during the initial 5-25 hours of injection before it decreased gradually throughout the experiment. Earlier studies have also confirmed decrease in methane production (Birkedal, 2009; Graue et al., 2008). As for experiment CO2_27, methane fraction in effluent seems to be passing a turning point at 12 hour. The increase in methane fraction is marked in Figure 5-22. Interestingly, water drops were observed at the downstream side of the GC at this time. The heat generated from the reaction between CO_2 and MEA has the potential of triggering hydrate dissociation. Heat of reaction between MEA and CO_2 is 1900 KJ mol^{-1} (Prakash et al., 2006) and the heat adsorbed during the dissociation of a mole CH_4 hydrate is 52.7-55.4 KJ mol^{-1} (Jung et al., 2010). The colossal amount of heat generated during mentioned reaction could potentially lead to massive hydrate dissociation. Liquid production and increased methane fraction observed at this point can strengthen the possibility of assisted production due to generated heat from reaction between MEA and CO_2. Looking at Figure 5-22, an increase in temperature is seen during time period (10-18 hour). It is unknown to which extent temperature increase could be related to the reaction between MEA and CO_2, as temperature fluctuated between 4-9 ºC during the whole experiment. Temperature measurements were taken at the outlet side of the core and also in confinement oil. At 14 hour, pressure dropped from 86bar to 77bar due to cylinder change in pump injecting MEA. The pressure drop is marked in Figure 5-23. The pressure drop itself is not enough to cause hydrate dissociation, but pressure drop in combination with increased temperature may have contributed to increased hydrate dissociation. CSMGem (Sloan et al., 2008) calculations show that the dissociation pressure for methane hydrate at 7.5ºC and 0.1wt% brine salinity is 55.7bar. The dissociation pressure at this

temperature is even lower for a system containing both methane- carbon dioxide hydrates. It is important to note that MEA could have acted as a thermodynamic hydrate inhibitor and caused a higher dissociation pressure. If so, the pressure drop may have caused hydrate dissociation. But if not, the generated heat from reaction between CO_2 and MEA could have caused hydrate dissociation and methane production.

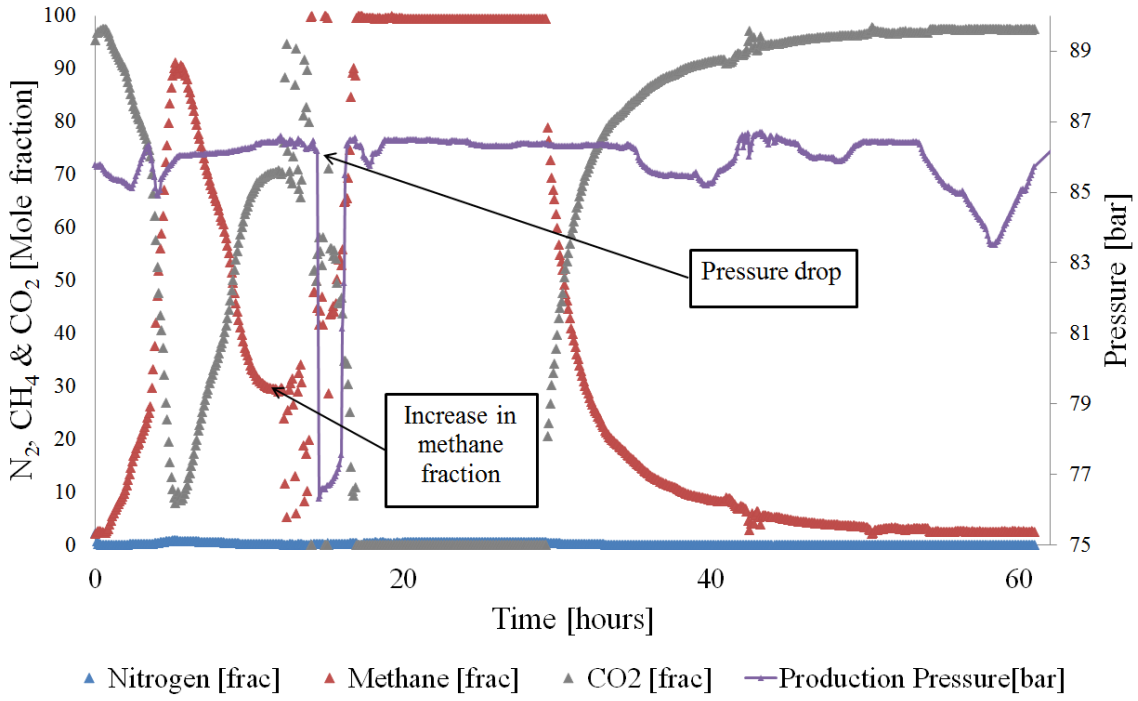

Figure 5-23 - Fluid fraction in effluent as a function of time for experiment CO2_27. Production pressure is also shown as a function time. Note increase of the methane fraction in effluent and the pressure drop at 14 hour which may have contributed to methane production at this point.

Times of substantial liquid production may be seen as a sudden increase in mass production rate in Figure 5-24. Since MEA was pre-injected into the core prior to CO_2, it could be assumed that advancement of CO_2 within the core resulted in more MEA reacting with the injected CO_2. This in turn may have led to temperature advancement in the core which led to hydrate dissociation. 0.3 pore-volume of MEA was injected over 17 hours; however the amount of injected MEA can be adjusted in order to get the desired effect. As stated earlier, the colossal amount of heat generated is able to effectively dissociate methane hydrate in a reservoir. Such massive hydrate dissociation may alter the formation integrity and lead to less stability of the formation. This is especially risky for regions closed to injection and production site, where a subsidence is hazardous. Mass flow rate increased in period where high methane fraction in effluent was observed. The produced liquid could be both water and MEA as MEA is highly soluble in water. The chemical composition of the produced liquid could not be analyzed due to limitations on apparatus used.

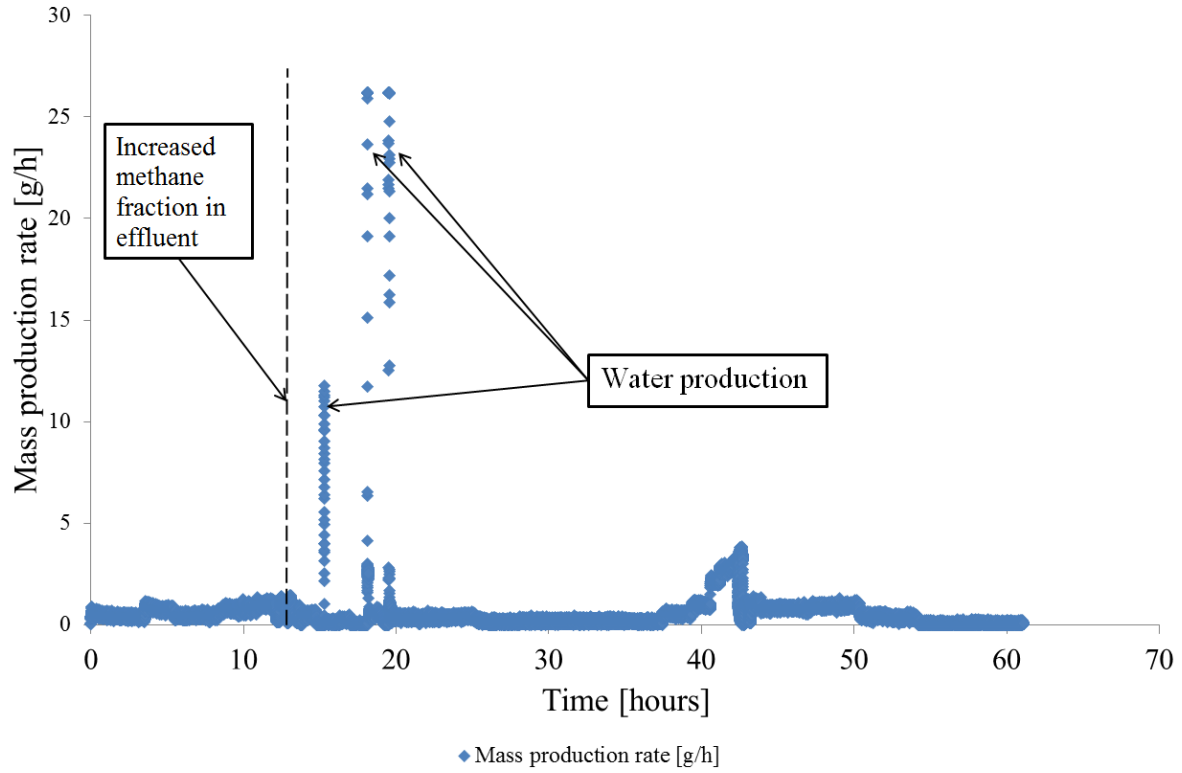

Figure 5-24 - Rate of mass production during experiment CO2_27. Note the increase in mass flow rate in period after methane fraction in effluent started increasing again.

The recovery from the experiment was calculated based on data measured by mass flow meter in conjunction with gas fraction data taken by GC, where methane fraction in effluent was multiplied by the mass of the produced effluent during each time step. Mass production rate during time steps where water production occurred was accounted for by eliminating rates higher than 3 [g/h]. Methane recovery as a function of time and pore volume CO_2 and MEA injected are shown in Figure 5-25. About 1.10 pore volumes of CO_2 and 0.30 pore volumes of MEA were injected during the experiment and a recovery of 0.90 was achieved after 60 hours of injection. The results show great recovery improvement compared to earlier experiments conducted during this study. Interestingly, more methane was produced during the first 20 hours than any other experiments conducted during this study. A comparison of recoveries is reviewed in section 5.5.4.

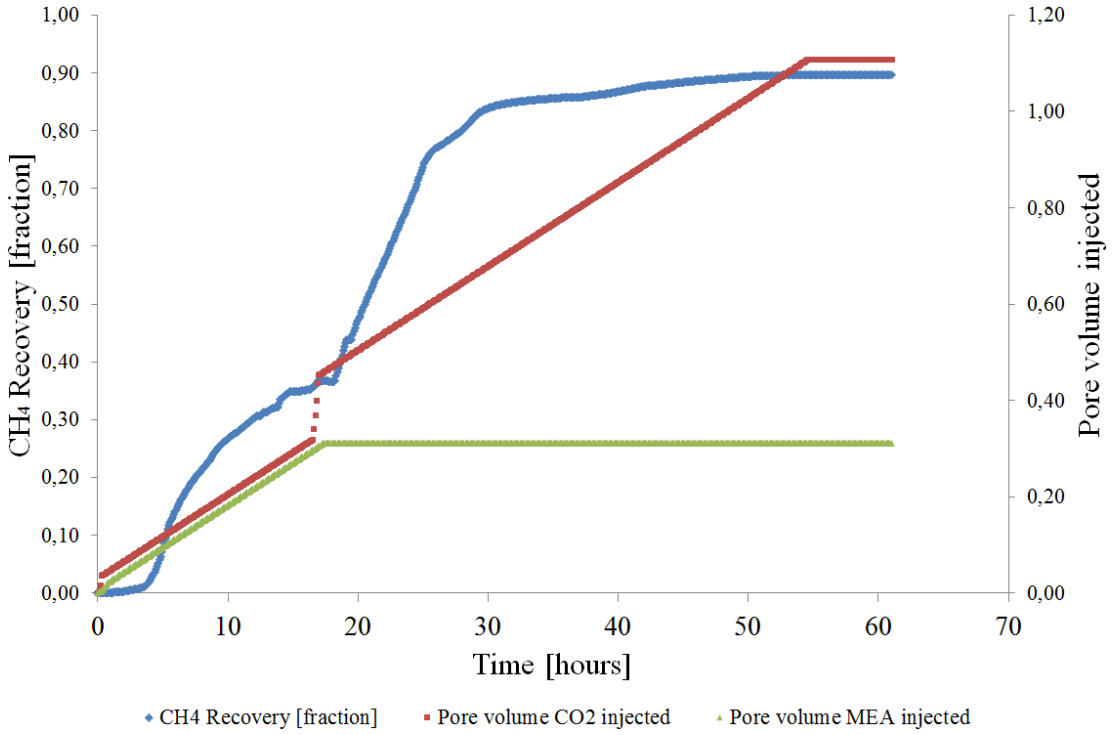

Figure 5-25 - Methane recovery during production from core CO2_27 is shown in the figure. Pore volume CO_2 and MEA injected as function of time are also shown in figure. A total of 1.11 pore volume of CO_2 and 0.30 pore volume of MEA were injected during the experiment. MEA injection was stopped at 17 hour. Note the increase in recovery rate after 17 hour. The generated heat from reaction between CO_2 and MEA may have improved the production from methane hydrate.

5.5.3 Recovery calculations

Recovery for earlier CH_4 – CO_2 exchange experiments were estimated based on the volume of the produced gas during the experiment. This estimate is highly uncertain and is the motivation of implementing a mass flow meter. When a pump was used during the production, the pump was filled with CO_2 and set to keep a constant pressure during the production. As the experiment continued, the produced methane would flow from the core and into to the cylinder of the production pump which led to a volume change in the production pump. The density of the mixture of produced CH_4 and CO_2 in the pump was changed. When calculating recovery, one assumed that there was no change in density of the gas mixture inside the production pump. Density of mixtures of CH_4 and CO_2 fractions as a function of mole fraction of CH_4 is shown in Figure 5-26. Looking at the graph in Figure 5-26, the change in the density of a gas mixture of CH_4 and CO_2 is significant as the fraction of methane in the gas mixture increases. This would result in smaller changes inside the receiving pump which could lead to less methane produced being measured. A consequence of this would be an underestimated recovery. Assumption of volume injected equals to volume produced was also used when calculation recovery for earlier studies. The assumption would result in incorrect volume being measured, as the injected CO_2 may form hydrate with the remaining water. The error is even bigger when injecting CO_2 into the core with higher initial water saturations as more CO_2 could form hydrate with the remaining water.

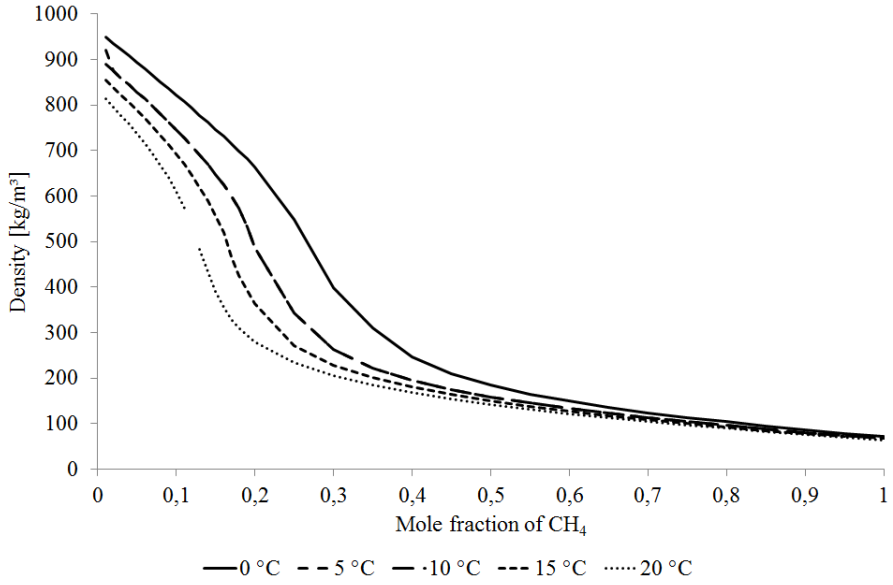

Figure 5-26 - Density of mixtures of CH_4 and CO_2 fractions at 83bar and different temperatures is shown in the figure. Note the change in the density of the gas mixture as the number of moles of methane in the mixture increases.

For the experiments conducted during this study, produced mass and gas fraction in effluent during the production were used to calculate the recovery. A mass flow meter and gas chromatograph were successfully used to quantify the production. The produced mass at each time step was multiplied by the molar mass mix composition in order to calculate number of moles produced. Molar mass mix composition is the sum of the molar masses of the gases, CH_4, CO_2 and N_2 multiplied by their fraction in the effluent. Number of moles produced was then multiplied with the methane fraction in effluent to calculate methane produced at each step. The cumulative amount of methane produced was used to estimate the total recovery for each experiment. When all free methane was assumed produced, recovery from hydrate could be estimated. Recovery measurements during this study were more accurate compared to earlier studies. This is explained by the fact that the recovery was calculated based on the mass of the produced effluent. Drawback with the mentioned method is during the time periods with liquid production. Mass of the produced water could be registered as mass of the produced gas. Recovery would be overestimated for such a system if the measurements are not accounted for the water production. During CH_4 – CO_2 experiments studied during this thesis, the limitation of the apparatus did not allow for separation of the liquid from the produced effluent. This was particularly the case for the experiment CO2_27, when use of MEA resulted in hydrate dissociation. When estimating recovery for experiment CO2_27, mass flow rates over 3 [g/h] were eliminated at the time where water production was observed.

5.5.4 Comparison of recovery

A total of six CH_4 – CO_2 experiments were conducted where recovery could be calculated. A comparison of the recovery from CH_4 – CO_2 experiments investigated in this study is presented in Figure 5-27. Experiment CO2_21 was conducted as a base line experiment where no slugs of chemical additives where added during the experiment. A total of 2.06 pore volumes of CO_2 injected resulted in a recovery of 0.42 at the exchange temperature of 9.6ºC. Experiment CO2_23 was done in order to investigate the potential of MDEA to enhance the methane production. Slugs of MDEA were injected at different times during the exchange experiment with a total volume of 4ml. A total of 4.51 pore volumes of CO_2 were injected resulting in a recovery of 0.54. Slugs of MDEA had no impact on the

recovery during the production from the core CO2_23. This may be due to low heat generation as a result of the reaction between MDEA and the injected CO_2, and that the generated heat may have been lost along the injection line. Experiment CO2_24 studied the possibility of enhancement the production using MEA slugs. As stated under section 2.3.4, reaction between MEA and CO_2 has an exothermic nature. The generated heat from such reaction is several orders of magnitude greater than for the reaction between MDEA and CO_2 (Kierzkowska, 2007; Prakash et al., 2006). The injected slugs had no impact on the recovery due to reaction happening at a distance away from the core. This again resulted in loss of the generated heat along the production line. Injection of 2.95 pore volumes of CO_2 and 2ml of MEA resulted in a recovery of 0.42. Recovery results for the various experiments are shown in Table 5-4.

Table 5-4 – Achieved total recovery after CO_2 injection, pore volume CO_2 and temperature during the exchange process for the conducted experiments.

Core	Temperature during exchange [°C]	Pore volume injected	CH_4 recovery
CO2_21	9.6	2.06	0.41
CO2_23	4.0	4.51	0.54
CO2_24	4.3	2.95	0.42
CO2_25	4.3	2.76	0.50
CO2_26	9.6	2.33	0.62
CO2_27	4.0	1.10	0.90

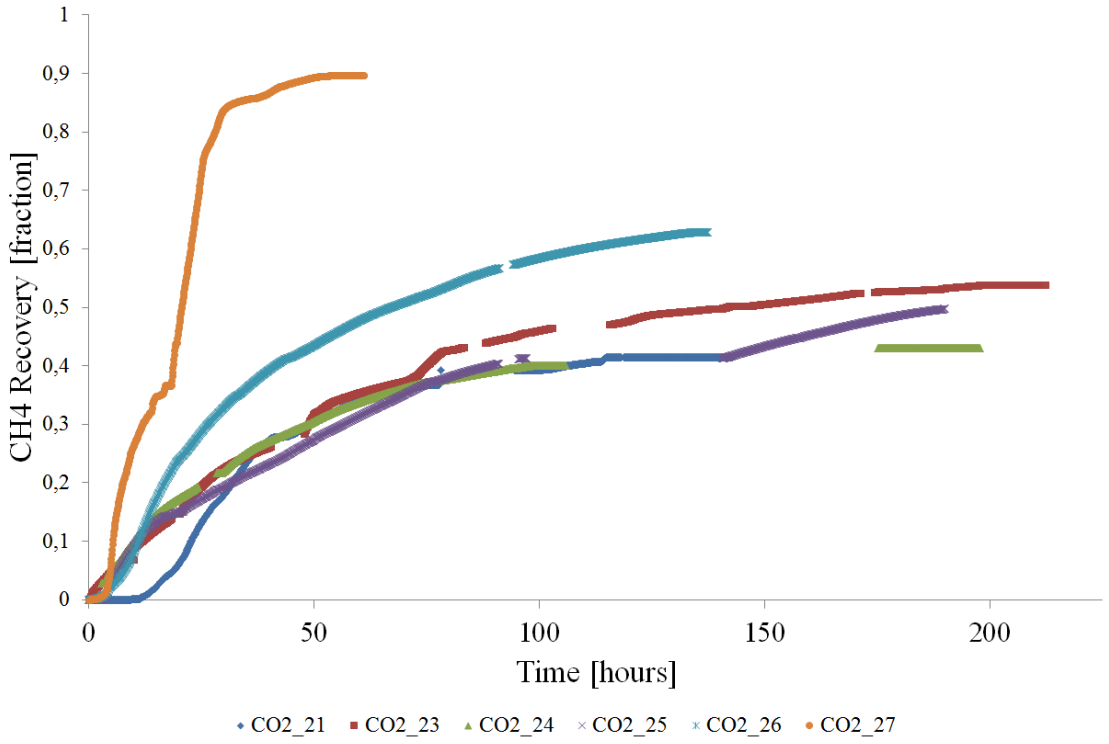

Figure 5-27 – A Comparison of the total methane recovery for CH_4 – CO_2 experiments is shown in the figure. Note the high methane recovery gained during experiment CO2_27. Use of MEA as a catalyst was tested during this experiment. As shown in figure, the recovery accelerates after 17 hours for this experiment. The second highest recovery was achieved from CO2_26 where the exchange process was conducted at 9.6°C. The exchange experiments conducted at 4°C show the same trend for recovery; however experiments with most pore CO_2 injected achieved higher recover.

Experiment CO2_25 was conducted at 83bar and 4ºC to investigate how lower temperature affects the exchange rate. Injection of 2.76 pore-volume of CO_2 resulted in a recovery of 0.5. Experiment CO2_26 was conducted at 9.6ºC. A total of 2.33 pore volumes of CO_2 injected resulted in a recovery of 0.62. The high recovery ratio achieved during experiment CO2_26 can be explained by the experimental condition under which CH_4 – CO_2 replacement occurred. Experimental conditions for exchange experiments both at 4ºC and 9.6ºC are shown in Figure 5-28. Experiment CO2_26 was conducted at 83bar and 9.6ºC. At such condition, methane hydrate is closer to its equilibrium curve, which makes the hydrate less stable compared to experiments conducted at 4ºC.

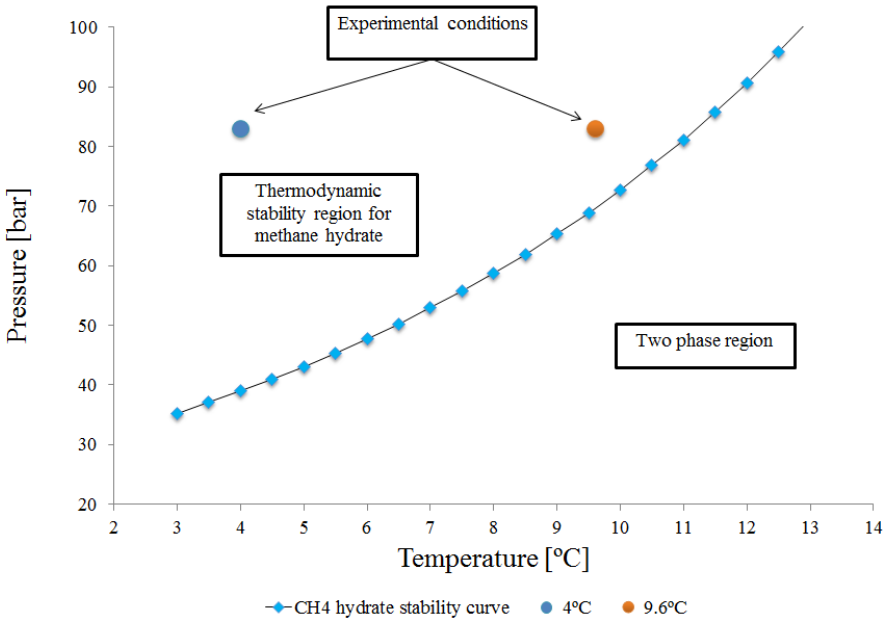

Figure 5-28 - CH_4 hydrate stability curve at brine salinity of 0.1wt% is shown in the figure. The experimental conditions during exchange studies both at 4 and 9.6ºC are also marked in the figure. Note that experimental conditions at 83bar and 4ºC is far inside the methane hydrate stability zone. At 83bar and 9.6ºC, experimental condition is closer to the methane hydrate equilibrium line. The exchange experiment conducted at this condition achieved a higher recovery compared to other experiments conducted at 4ºC.

Experiment CO2_27 achieved a recovery of 0.9 after injection of 1.1 pore volumes of CO_2 and 0.3 pore volume of MEA. Achieving such high recovery after 50 hours of injection is significant compared to results from other experiments. However, in order to confirm the effect from the injected MEA several results are needed. The generated heat from the reaction between MEA and CO_2 was able to dissociate methane hydrate and resulted in high methane production for a period of 11 hours during the experiment. This should be noted when comparing recovery values from different experiments. The achieved recovery results indicate that for the experiments conducted at the exchange temperature of 4ºC where injection of chemical additives had no impact on the recovery, the recovery increased with pore volume CO_2 injected. A higher recovery was achieved for the experiment at higher exchange temperature (9.6ºC) where a recovery of 0.62 was reached after injection of 2.33 pore volumes of CO_2. Effect of brine salinity on the rate of exchange has not been studied during this study, but earlier hydrate study at the university of Bergen (Birkedal, 2009) demonstrated increasing recovery values for experiments with higher salinities. Birkedal (2009) used CO_2 flushes within single and double fractured cores. Birkedal (2009) indicated that higher brine salinities resulted in higher post hydrate water saturation. This could be beneficial as CO_2 diffusion into the aqueous solution may result in easier CO_2 advancement within the core. The latter has been limited in experiments conducted in this thesis due to low post hydrate formation water saturation. However, it could be

argued that CO_2 advances easier in an excess gas system due to CO_2's high solubility in methane, a process which occurs much faster than diffusion (Jung et al., 2010). The experiments studied by Graue *et al.* (2008) achieved a recovery of 0.5 – 0.85. These experiments were conducted at 83bar and 4ºC using fractured cores where initial water saturation of 0.5 and a brine salinity of 0.1 wt% were used. In addition, unlike experiments conducted during present study, flushes of CO_2 were injected through the core during experiments conducted by Graue et, al. (2008) and Husebø (2008). Three CO_2 flushes were injected into the core with a total duration of 900 hours. For CH_4 - CO_2 replacement experiments conducted during present study, a continuous CO_2 injection at a rate of 1.2 ml/h was used. In addition, during experiment conducted by Graue et, al (2008) a spacer was used that acted as fracture and an accumulation volume for the released methane. The higher recovery from the experiments by Graue *et al.* (2008) and Husebø (2008) could be explained by the longer CO_2 exposure time as well as greater surface area between the injected CO_2 and methane hydrate due to use of spacer and fractured cores. The use of fractured core and spacer has been absent for experiments studied during this study. Birkedal (2009) studied CH_4 – CO_2 exchange experiments both in single fractured and double fractured cores. Birkedal (2009) indicated that when CO_2 flushes were used, chemical potential of the CO_2 decreased as a result of decreasing CO_2 concentration and increasing CH_4 concentration within the spacer volume. During experiments conducted in this thesis, a continuous CO_2 injection was used. The advantage of use of continuous CO_2 injection is, firstly, both free and released methane can be displaced by the injected CO_2 and secondly, decrease in chemical potential of CO_2 is less as fresh CO_2 is being injected continuously.

5.6 Uncertainties

Several uncertainties have to be considered studying the achieved results from experiments in this thesis. Uncertainties and errors may differ by several orders of magnitude eliminating the insignificant errors while the others have to be considered. Many measuring devices have been used during the experimental work where the uncertainty is given by manufacture. However, the given uncertainty by manufacture is in many cases much smaller than operational errors. One example is the given uncertainty for the slide caliper used for cutting core samples (0.005mm). But the non-uniformity of the stone results in far higher errors during the cutting process. The digital weight was used during the core preparation. The cores were weighted before they were packed. Water from the water saturated cores may have been evaporated while they were being packed resulting in insignificancy of the uncertainty of the instrument. Table 5-5 lists some of the instruments used during experiment and their given uncertainties. It is important to consider the magnitude of uncertainties as the given uncertainty given by manufacture is sometimes insignificant when compared to experimental uncertainties.

Table 5-5 – Equipment used during experiments and their uncertainties given by manufacture.

Equipment	**Measurement**	**Uncertainty (±)**
Slide caliper	Length & diameter	0.005 [cm]
AND GF-3000 Digital Balance	Weight	0.02[g]
ST Stigma 500	Flow	0.10 %
ST Stigma 500	Pressure	0.10 %
Thermocouple	Temperature	0.1
Druck PMP	Pressure	0.08%

5.6.1 Leakage rate

Leakage is unavoidable during experimental work using high pressure systems and low viscosity fluids. Despite frequent controls of the valves and lines connected to the system, small gas leakage have always existed during the experiments investigated during this master thesis. Prior to every experiment, the system was pressurized and monitored for a period of time (about 24 hours) and checked for possible leaks along the connected lines. The method used for estimating the leakage rate was the same method used during previous hydrate studies (Birkedal, 2009; Bringedal, 2011; Hauge, 2011). Since mass conservation was assumed during all experiments, establishing leakage estimates were crucial in order to rectify the amount of injected gas into the system. The generated PVT data were acquired from pumps and digital thermometers. When hydrate formation came to end, the system was monitored for 3-4 days and a leak rate was estimated based on the volume changes of the gas inside the pump. At stable pressure and temperature conditions, no methane consumption was supposed to occur when hydrate formation was over. However, leakage along the lines and fluctuations in room temperature resulted in pump injecting gas in order to keep the pressure constant. Observed pump logs that the leakage rate was under impact of the temperature fluctuations, see Figure 5-29.

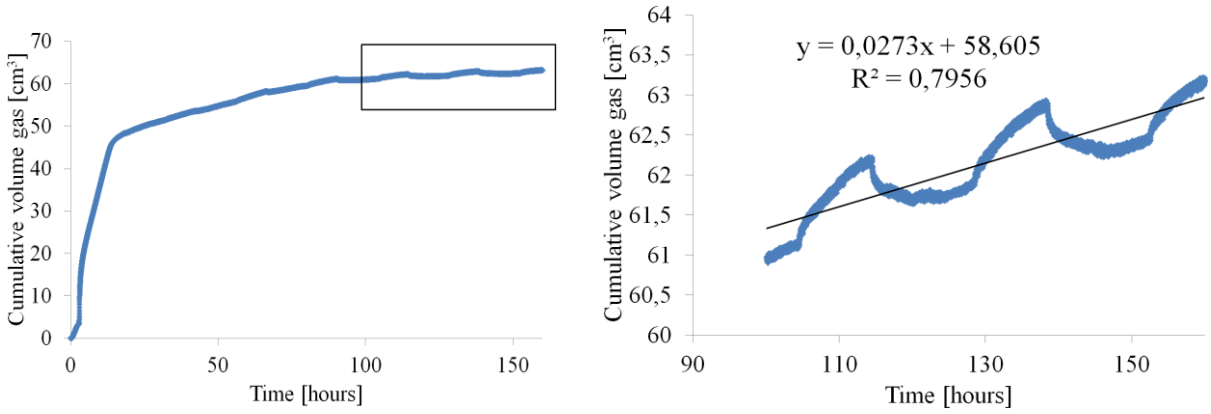

Figure 5-29 – The figure shows how leakage rate was estimated during hydrate formation experiments. When hydrate formation was assumed ceased, the system was monitored for 2-3 days and the leakage rate was for the 50-60 hours. The black rectangle shows the time period the leakage rate was estimated from. It was assumed no more methane hydrate was formed during this time period. Note 24 hours interval of leak rate fluctuations. The leak rate was under great of room temperature fluctuations.

In Figure 5-29, the leakage rate was estimated to be 0.027 ml/h, which was under the approved rate of 0.05 ml/h (Ersland, 2013). The leakage rate found using the method mention above was assumed to be constant during the whole experiment. The leakage rates for experiments investigated during present study varied from 0.01 ml/h to 0.05 ml/h having an avarage of 0.026 ml/h. Birkedal (2009) reported leakage rates ranging from 0.0001 ml/h to 0.05 ml/h being generally good as confirmed by compliance of PVT data with *in situ* MRI images.

Difference between core samples

Although Bentheim sandstone is considered a homogenous rock (Klein et al., 2003), differences in pore structures and pore throats in the core sample make them unique. Water imbibes differently in core samples with different pore structures resulting in varied initial water saturation prior to hydrate formation. Gas distribution will also be affected by the pore structure and pore throats. This in turn results in different hydrate growth patterns for different cores. To reduce the number of variables, one

and the same core sample should have been used for all experiments. This would have been unfavorable considering time consuming process of the cleaning the core samples.

5.6.2 Hydration number

The theoretical hydration number for structure I hydrate is given by 46 water molecules per 8 gas molecules resulting in a hydration number of 5.75. For hydrate formation experiments conducted during this study the amount of hydrate bound methane has been calculated assuming a hydration number of 5.99. A hydration stoichiometry $n_w = 5.81 – 6.10$, with an average of 5.99 ± 0.07, has been measured for a range of hydrate formation experiments along the equilibrium boundary (Circone et al., 2005). Circone *et al.* (2005) indicated that a slight systematic decrease have been observed for a hydrate system away from the equilibrium boundary. Hydrate formation experiments in this study have been conducted at 83bar and 4ºC. Such experimental condition is well within the methane hydrate equilibrium boundary and a hydrate system formed at such conditions may have a lower hydration number according to Circon *et al.* (2005). A lower hydration number means more CH_4 per H_2O in hydrate. The latter results in a higher post hydrate formation water saturation as less water consumed during hydrate formation. Variation in hydration number will compromise the estimations in data analysis, where a lower value than hydration number assumed here would result in less water consumed during the formation process; less final hydrate saturation and consequently higher post hydrate formation water saturation.

Free methane post to hydrate formation

A correct estimation of the amount of free methane after hydrate formation is crucial when it comes to estimating recovery from the hydrate. The amount of free methane in the core sample was estimated using equation (5.1):

$$\text{Free } CH_4 \text{ [ml]} = (1 - S_h - S_w) \,.\, (PV) \tag{5.1}$$

Where S_h is final hydrate saturation, S_w is post hydrate formation water saturation and PV is the pore volume [ml]. As shown in equation (5.1), amount of free methane in the core is also affected by estimation of hydration number as established in previous section.

5.6.3 Uncertainties during CO_2 injection experiments

During exchange experiments, CO_2 was injected using a STIGMA 3000 pump from Sanchez Technologies. This is a high precision pump where rate of delivery and the delivered volume are considered as exact values. However, variety and number of uncontrolled leakage along the injection and production line as well as CO_2 seepage through the sleeve[9] and into the confining oil makes it difficult to estimate the amount of escaped CO_2. However, the amount of produced CO_2 is known as it has been measured using GC and mass flow meter. The difference between injected CO_2 and produced CO_2 varies between several pore volumes. The difference in amount of injected and produced CO_2 cannot be explained by CO_2 being sequestrated within the core sample alone. The latter indicates that CO_2 has escaped from the system during the experiment. Future experiments should implement better isolating sleeve as well as gas detectors in order to reduce leakage.

[9] The confining sleeve has wettability preference for CO_2 in presence of other phases during the $CH_4 – CO_2$ experiments (Ersland, 2013).

5.6.4 Uncertainties during injection of chemical additives

Injection of chemical additive using a separate pump

During experiment CO2_27, both MEA and CO_2 were injected into the core using separate pumps. CO_2 was injected using a STIGMA 3000 pump from Sanchez Technologies and MEA was injected using a Quizix SP-5200. Both pumps are high precision pumps, where injected volume is an exact value. As established under section 2.3.4, reaction between MEA and CO_2 generates a colossal amount of heat. The generated heat from the reaction resulted in hydrate dissociation and production of associated water. As methane production is estimated based on the produced mass and methane fraction in effluent, liquid production may have compromised methane recovery calculations. Due to limitations on apparatus used, produced liquid could not be separated from the gaseous effluent. Liquid production may have resulted in an overestimated mass measurement which in turn may have resulted in an overestimated methane production from the system. Mass production rates over 3 [g/h] were eliminated during time periods with liquid production. Since mass of the produced liquid could not be measured specifically, it is impossible to exclude mass of the produced water from the mass of the produced gas. Therefore, no uncertainty estimate could be made on water production.

Temperature of the system during injection of MEA was under great impact of temperature fluctuation in the laboratory. The temperature fluctuated between 4.5ºC and 9ºC during the production. This may have compromised the energy balance of the system as heat was added to system when room temperature increased and was taken from the system when room temperature decreased. Further work should include better temperature stability during MEA injection.

6 Conclusions and future works

6.1 Conclusions

Based on the results acquired from the experimental work done in this thesis the following conclusions have been drawn:

MEA and liquid CO_2 were separately injected into partly hydrate-saturated Bentheim sandstone resulting in an exothermic reaction. The heat generated from the reaction led to dissociation of the methane hydrate in the core. A total recovery of 0.9 was achieved when 1.1 pore-volume of CO_2 and 0.3 pore-volume of MEA were injected.

Due to heat loss along the injection line, the injection of the chemical additives, MEA and MDEA, into liquid CO_2 prior to it being introduced the hydrate saturated core did not have any observable impact on the production.

A total of six CH_4 – CO_2 exchange experiments were conducted where the total methane recovery increased with increasing exchange temperature and pore-volume CO_2 injected.

Implementing of a mass flow meter resulted in better recovery estimations than previous hydrate studies. However, the accuracy of the method used could be poor when liquid is produced from the system.

Methane hydrate was dissociated through depressurization within Bentheim sandstone. Dissociation occurred at 32.5bar and 4ºC resulting in full recovery after 34hrs.

Methane hydrate was dissociated through thermal stimulation within Bentheim sandstone. A stepwise temperature increase was used where the hydrate dissociated at 83bar and 10.6ºC. Comparison with computer simulations, CSMGem, showed a higher dissociation threshold temperature of 11.2ºC.

The hypothesis about the water structure's memory effect was investigated during four hydrate formation and hydrate decomposition experiments. Methane hydrate was formed and dissociated several times with different time intervals. Measured data showed a tendency for shorter induction time for a hydrate system with a previous hydrate formation history.

Methane hydrate was successfully formed within Bentheim sandstone core samples in all experiments where processes involved in hydrate formation were studied. The generated PVT-data were used to estimate the amount of methane stored in hydrate, amount of free methane in the pores as well as post hydrate formation water saturation. A comparison of experimental data acquired in this study and in house data showed a trend towards higher post hydrate formation water saturation with increased initial water saturation and brine salinity.

6.2 Future work

Future experiments should study recovery improvements using more moderated amounts of MEA than used here.

Several experiments with the same initial conditions should be conducted in order to confirm the reproducibility of the result attained here.

A better temperature monitoring system should be implemented in order to detect heat from the reaction between MEA and CO_2. Several thermocouples should be implemented in order to better monitor the heat advancement within the core.

The experiments discussed in this thesis were conducted within consolidated sandstone core samples. Impacts of use of MEA should also be studied in unconsolidated porous medium.

Future experiments should study injection of MEA into a fractured core with a spacer.

Future experiments should implement more stable cooling system during experiments.

Produced water should be separated from the effluent on order to achieve more accurate recovery estimations.

Gas detector as well as better valves should be implemented into the setup in order to detect and reduce leak.

References

Alan, Sharon, & Jacek. (1994). *The Current Distribution And Thermal Stability of Natural Gas Hydrates In the Canadian Polar Regions*. http://www.onepetro.org/mslib/app/Preview.do?paperNumber=ISOPE-I-94-043&societyCode=ISOPE

Atkins, & De Paula. (2006). *Atkins' Physical chemistry* (8th ed.). Oxford ; New York: Oxford University Press.

Bernal, & Fowler. (1933). A Theory of Water and Ionic Solution, with Particular Reference to Hydrogen and Hydroxyl Ions. *Journal of Chemical Physics, 1*(8), 515-548. doi: citeulike-article-id:8441181

Birkedal. (2009). *Hydrate Formation and CH4 Production from Natural Gas Hydrates - Emphesis on Boundary Conditions And Production Methods.* (Master Thesis), University of Bergen, Bergen.

Birkedal, Ersland, Huseb, Kvamme, & Graue. (2010). *Geomechanical Stability During CH4 Production From Hydrates - Depressurization Or CO2 Sequestration With CO2-CH4 Exchange*. http://www.onepetro.org/mslib/app/Preview.do?paperNumber=ARMA-10-321&societyCode=ARMA

Birkedal, Freeman, Moridis, & Graue. (2013). Numerical Reproduction of Empirical Methane Hydrate Dissociation and Reformation in Sandstone. *In Prep.*

Boswell. (2006). The Gas Hydrate Resource Pyramid. *Fire in the ice, NETL Fall Newsletter, 5-7.(2006)*, 5-7.

Bringedal. (2011). *Impacts of Temperature on Methane Production from Hydrates by CO2 injection.* (Master thesis), University of Bergen, Bergen.

Buchanan, Soper, Thompson, Westacott, Creek, Hobson, & Koh. (2005). Search for memory effects in methane hydrate: Structure of water before hydrate formation and after hydrate decomposition. *The Journal of Chemical Physics, 123*(16), 164507-164507.

Carroll. (2009). *Natural Gas Hydrates: A Guide for Engineers*: Gulf Professional Pub./Elsevier.

Castaldi, Zhou, Yegulalp, & Aiche. (2006). *Down-hole combustion method for gas production from methane hydrate*. Paper presented at the AIChE Spring National Meeting, Orlando, FL, United States, Apr. 23-27, 2006; AIChE, Ed.; pp 1-12., New York, N.Y.

Chaplin. (2008). Water structure and science. http://www.lsbu.ac.uk/water/index2.html

Chuvilin, Istomin, & Safonov. (2011). Residual nonclathrated water in sediments in equilibrium with gas hydrate: Comparison with unfrozen water. *Cold Regions Science and Technology, 68*(1–2), 68-73. doi: http://dx.doi.org/10.1016/j.coldregions.2011.05.006

Circone, Kirby, & Stern. (2005). Direct Measurement of Methane Hydrate Composition along the Hydrate Equilibrium Boundary. *The Journal of Physical Chemistry B, 109*(19), 9468-9475. doi: 10.1021/jp0504874

Clennell, Hovland, Booth, Henry, & Winters. (1999). Formation of natural gas hydrates in marine sediments: 1. Conceptual model of gas hydrate growth conditioned by host sediment properties. *Journal of Geophysical Research: Solid Earth, 104*(B10), 22985-23003. doi: 10.1029/1999JB900175

Daintith, & Martin. (2010). *Dictionary Of Science 6 Ed :Opr*: Oxford University Press.

Derks. (2006). *Carbon dioxide absorption in piperazine activated N- methyldiethanolamine.* University of Twente, Enschede. Retrieved from http://doc.utwente.nl/57600/

Ebinuma. (1993). *Method for dumping and disposing of carbon dioxide gas and apparatus therefor*.

Ersland. (2008). *Studies of Flow Mechanisms and Hydrate Phase Transitions in Fractured Rocks*: University of Bergen.

Ersland. (2013). Personal communication.

Ersland, Husebo, Graue, & Kvamme. (2008). *MEASUREMENTS OF GAS PERMEABILITY AND NON-DARCY FLOW IN GAS-WATER-HYDRATE SYSTEMS.* Paper presented at the 6th International Conference on Gas Hydrates (ICGH 2008), Vancouver, British Columbia, Canada.

Ersland, Husebø, Graue, & Kvamme. (2009). Transport and storage of CO2 in natural gas hydrate reservoirs. *Energy Procedia, 1*(1), 3477-3484. doi: http://dx.doi.org/10.1016/j.egypro.2009.02.139

Farmahini, Kvamme, & Kuznetsova. (2011). Molecular dynamics simulation studies of absorption in piperazine activated MDEA solution. *Physical Chemistry Chemical Physics, 13*(28), 13070-13081. doi: 10.1039/C0CP02238A

Fitzgerald, & Castaldi. (2013). Thermal Stimulation Based Methane Production from Hydrate Bearing Quartz Sediment. *Industrial & Engineering Chemistry Research, 52*(19), 6571-6581. doi: 10.1021/ie400025f

Goel. (2006). In situ methane hydrate dissociation with carbon dioxide sequestration: Current knowledge and issues. *Journal of Petroleum Science and Engineering, 51*(3–4), 169-184. doi: http://dx.doi.org/10.1016/j.petrol.2006.01.005

Graue, Bjorn, Bernard, James, James, Geir, Jarle, & David. (2006). *Magnetic Resonance Imaging of Methane - Carbon Dioxide Hydrate Reactions in Sandstone Pores*. Paper presented at the SPE Annual Technical Conference and Exhibition, San Antonio, Texas, USA. http://www.onepetro.org/mslib/app/Preview.do?paperNumber=SPE-102915-MS&societyCode=SPE

Graue, Kvamme, Baldwin, Stevens, Howard, Aspenes, Ersland, Husebo, & Zornes. (2008). MRI Visualization of Spontaneous Methane Production From Hydrates in Sandstone Core Plugs When Exposed to CO2. *SPE Journal, 13*(2), 146-152. doi: 10.2118/118851-pa

Hammerschmidt. (1934). Formation of Gas Hydrates in Natural Gas Transmission Lines. *Industrial & Engineering Chemistry, 26*(8), 851-855. doi: 10.1021/ie50296a010

Hauge. (2011). *Resistivity Measurements during Gas Hydrate Formation and Subsequent CO2 Exchange in Porous Sandstone.* (Master thesis), Bergen.

Hauge. (2013). In house data-base program, University of Bergen (Version 1.6) [MATLAB].

Hester, & Brewer. (2009). Clathrate Hydrates in Nature. *Annual Review of Marine Science, 1*(1), 303-327. doi: doi:10.1146/annurev.marine.010908.163824

Hirohama, Shimoyama, Wakabayashi, Tatsuta, & Nishida. (1996). Conversion of CH4 Hydrate to CO2 Hydrate in Liquid CO2. *JOURNAL OF CHEMICAL ENGINEERING OF JAPAN, 29*(6), 1014-1020.

Husebø. (2008). *Monitoring Depressurization and CO2-CH4 Exchange Production Scenarios for Natural Gas Hydrates*: University of Bergen.

Husebø, Ersland, Graue, & Kvamme. (2009). Effects of salinity on hydrate stability and implications for storage of CO2 in natural gas hydrate reservoirs. *Energy Procedia, 1*(1), 3731-3738. doi: http://dx.doi.org/10.1016/j.egypro.2009.02.172

Jeffrey. (1984). Hydrate inclusion compounds. *Journal of inclusion phenomena, 1*(3), 211-222. doi: 10.1007/bf00656757

Jung, Espinoza, & Santamarina. (2010). Properties and phenomena relevant to CH4-CO2 replacement in hydrate-bearing sediments. *Journal of Geophysical Research: Solid Earth, 115*(B10), B10102. doi: 10.1029/2009JB000812

Kashchiev, & Firoozabadi. (2003). Induction time in crystallization of gas hydrates. *Journal of Crystal Growth, 250*(3–4), 499-515. doi: http://dx.doi.org/10.1016/S0022-0248(02)02461-2

Kierzkowska. (2007). Enthalpies of Absorption and Solubility of CO2 in Aqueous Solutions of Methyldiethanolamine. *Separation Science and Technology, 42*(12), 2723-2737. doi: 10.1080/01496390701513032

Klein, & Reuschlé. (2003). A Model for the Mechanical Behaviour of Bentheim Sandstone in the Brittle Regime. In H.-J. Kümpel (Ed.), *Thermo-Hydro-Mechanical Coupling in Fractured Rock* (pp. 833-849): Birkhäuser Basel.

Kleinberg, Flaum, Griffin, Brewer, Malby, Peltzer, & Yesinowski. (2003). Deep sea NMR: Methane hydrate growth habit in porous media and its relationship to hydraulic permeability, deposit accumulation, and submarine slope stability. *Journal of Geophysical Research: Solid Earth, 108*(B10), n/a-n/a. doi: 10.1029/2003jb002389

Kvamme. (2012). Hydrate. Lecture ed. Bergen.

Kvamme. (2013). Personal communication.
Kvenvolden. (1988). Methane hydrate — A major reservoir of carbon in the shallow geosphere? *Chemical Geology, 71*(1–3), 41-51. doi: http://dx.doi.org/10.1016/0009-2541(88)90104-0
Lee, Seo, Seo, Moudrakovski, & Ripmeester. (2003). Recovering Methane from Solid Methane Hydrate with Carbon Dioxide. *Angewandte Chemie, 115*(41), 5202-5205. doi: 10.1002/ange.200351489
Li, Henni, & Tontiwachwuthikul. (2007). Reaction Kinetics of CO2 in Aqueous Ethylenediamine, Ethyl Ethanolamine, and Diethyl Monoethanolamine Solutions in the Temperature Range of 298−313 K, Using the Stopped-Flow Technique. *Industrial & Engineering Chemistry Research, 46*(13), 4426-4434. doi: 10.1021/ie0614982
Makogon. (1997). *Hydrates of Hydrocarbons*: PennWell Books.
Makogon, Makogon, & Holditch. (1999). *Gas Hydrate Formation and Dissociation with Thermodynamic and Kinetic Inhibitors*. Paper presented at the SPE Annual Technical Conference and Exhibition, Houston, Texas. http://www.onepetro.org/mslib/app/Preview.do?paperNumber=00056568&societyCode=SPE
Mccann, Phan, Wang, Conway, Burns, Attalla, Puxty, & Maeder. (2009). Kinetics and Mechanism of Carbamate Formation from CO2(aq), Carbonate Species, and Monoethanolamine in Aqueous Solution. *The Journal of Physical Chemistry A, 113*(17), 5022-5029. doi: 10.1021/jp810564z
Mcgrail, Schaef, White, Zhu, Kulkarni, Hunter, Patil, Owen, & Martin. (2007). Using Carbon Dioxide to Enhance Recovery of Methane from Gas Hydrate Reservoirs: Final Summary Report (pp. Medium: ED; Size: PDFN).
Milkov. (2004). Global estimates of hydrate-bound gas in marine sediments: how much is really out there? *Earth-Science Reviews, 66*(3–4), 183-197. doi: http://dx.doi.org/10.1016/j.earscirev.2003.11.002
Moridis, Collett, Boswell, Kurihara, Reagan, Koh, & Sloan. (2009). Toward Production From Gas Hydrates: Current Status, Assessment of Resources, and Simulation-Based Evaluation of Technology and Potential. *Spe Reservoir Evaluation & Engineering, 12*(5), 745-771.
Mullin. (2001). Crystallization, 4rd Edition, Butterworth-Heinmann, Oxford, U.K.
Nist. (2013). NIST Chemistry WebBook. http://webbook.nist.gov/chemistry/
Ohgaki, Takano, Sangawa, Matsubara, & Nakano. (1996). Methane Exploitation by Carbon Dioxide from Gas Hydrates—Phase Equilibria for CO2/CH4 Mixed Hydrate System. *JOURNAL OF CHEMICAL ENGINEERING OF JAPAN, 29*(3), 478-483.
Opec. (2011). World Proven Natural Gas Reserves by Country. Retrieved 22.01, 2013, from www.opec.org/library/Annual Statistical Bulletin/interactive/current/FileZ/Main-Dateien/SubSection3.html
Ota, Morohashi, Abe, Watanabe, Smith, & Inomata. (2005). Replacement of CH4 in the hydrate by use of liquid CO2. *Energy Conversion and Management, 46*(11–12), 1680-1691. doi: http://dx.doi.org/10.1016/j.enconman.2004.10.002
Park, Cha, Jong-Ho, & Lee. (2008). SWAPPING CARBON DIOXIDE FOR COMPLEX GAS HYDRATE STRUCTURES. *Proceedings of the 6th International Conference on Gas Hydrates*.
Prakash, & Vijaykumar. (2006). *Quickly design CO[2] - amine absorber* (Vol. 13). New Delhi, INDE: Indian National Science Academy.
Ripmeester, & Ratcliffe. (1990). Xenon-129 NMR studies of clathrate hydrates: new guests for structure II and structure H. *The Journal of Physical Chemistry, 94*(25), 8773-8776. doi: 10.1021/j100388a006
Roberts, Hardage, Shedd, Hunt, & Herron. (2006). Seafloor reflectivity; an important seismic property for interpreting fluid/gas expulsion geology and the presence of gas hydrate. *The Leading Edge, 25*(5), 620-628.
Schoderbek, Lloyd, Howard, Silpngarmlert, & Hester. (2012). *North Slope Hydrate Fieldtrial: CO2/CH4 Exchange*. Paper presented at the OTC Arctic Technology Conference, Houston, Texas, USA.

http://www.onepetro.org/mslib/app/Preview.do?paperNumber=OTC-23725-MS&societyCode=OTC
Sigma-Aldrich. (2013). Material Safety Data Sheet http://www.sigmaaldrich.com/norway.html
Sloan, & Koh. (2008). *Clathrate hydrates of natural gases, 3rd edition. Boca* CRC Press.
Stillinger, & Rahman. (1974). Improved Simulation of Liquid Water by Molecular-Dynamics. *Journal of Chemical Physics, 60*(4), 1545-1557. doi: Doi 10.1063/1.1681229
Tohidi, Burgass, Danesh, Østergaard, & Todd. (2000). Improving the Accuracy of Gas Hydrate Dissociation Point Measurements. *Annals of the New York Academy of Sciences, 912*(1), 924-931. doi: 10.1111/j.1749-6632.2000.tb06846.x
Travesset. (2008). The Many Phases of Ice.
Xie, Zhou, Zhang, & Johnson. (2010). Reaction Mechanism of Monoethanolamine with CO2 in Aqueous Solution from Molecular Modeling. *The Journal of Physical Chemistry A, 114*(43), 11844-11852. doi: 10.1021/jp107516k
Yoon, Kawamura, Yamamoto, & Komai. (2005). *Transformation of Methane Hydrate to Carbon Dioxide Hydrate: In Situ Raman Spectroscopic Observations*. http://www.onepetro.org/mslib/app/Preview.do?paperNumber=ISOPE-I-05-055&societyCode=ISOPE
Zhang, & Chen. (2010). Thermodynamic Modeling for CO2 Absorption in Aqueous MDEA Solution with Electrolyte NRTL Model. *Industrial & Engineering Chemistry Research, 50*(1), 163-175. doi: 10.1021/ie1006855
Zhou, Castaldi, & Yegulalp. (2009). Experimental Investigation of Methane Gas Production from Methane Hydrate. *Industrial & Engineering Chemistry Research, 48*(6), 3142-3149. doi: 10.1021/ie801004z
Zolotukhin, & Ursin. (2000). *Introduction to Petroleum Reservoir Engineering*: Høyskoleforlaget, Norwegian Academic Press.

Part III

Attachments

Nomenclature

N_H	=	Hydration number
ΔG	=	Gibbs free energy
r_c	=	Critical radius
Ø	=	Porosity
q	=	Total flow
μ	=	Viscosity
dp	=	Pressure difference
dx	=	Length
θ	=	Contact angle
P_a	=	Inlet pressure
P_b	=	Outlet pressure
K	=	Permeability
K_{eff}	=	Effective permeability
K_{abs}	=	Absolute permeability
K_r	=	Relative permeability
P_{nw}	=	Pressure in non-wetting phase
P_w	=	Pressure in wetting phase
σ	=	Interfacial tension

Appendix A: Supplementary tables and figures for part I

Appendix A 1: Summary of guest molecules and their molecular to cavity diameter ratio (Sloan et al., 2008).

		Molecular diameter / cavity diameter for cavity type			
Guest hydrate former		**Structure I**		**Structure II**	
Molecule	**Diameter (Å)**	**5^{12}**	**$5^{12}6^2$**	**5^{12}**	**$5^{12}6^4$**
He	2.28	0.447	0.389	0.454	0.342
H_2	2.72	0.533	0.464	0.542	0.408
Ne	2.97	0.582	0.507	0.592	0.446
Ar	3.8	0.745	0.648	0.757	0.571
Kr	4.0	0.784	0.683	0.797	0.601
N_2	4.1	0.804	0.700	0.817	0.616
O_2	4.2	0.824	0.717	0.837	0.631
CH_4	4.36	0.855	0.744	0.868	0.655
Xe	4.58	0.898	0.782	0.912	0.687
H_2S	4.58	0.898	0.782	0.912	0.687
CO_2	5.12	1.00	0.834	1.02	0.769
C_2H_6	5.5	1.08	0.939	1.10	0.826
c-C_3H_3	5.8	1.14	0.990	1.16	0.871
$(CH_2)_3O$	6.1	1.20	1.04	1.22	0.916
C_3H_8	6.28	1.23	1.07	1.25	0.943
i-C_4H_{10}	6.5	1.27	1.11	1.29	0.976
n-C_4H_{10}	7.1	1.39	1.21	1.41	1.07

Appendix B: Supplementary tables and figures for part II

Appendix B1: Summary of properties for core samples used during experiments in this study.

Sample ID	Weight dry [g]	Length [cm]	Diameter [cm]	Swi	Salinity [wt%]
CO2_20	572.02	13.98	5.05	0.416	0.1
CO2_21	579.58	14.17	5.06	0.412	0.1
CO2_22	595.39	14.24	5.10	0.379	0.1
CO2_23	587.50	14.52	5.06	0.412	0.1
CO2_24	567.18	14.17	5.04	0.41	0.1
CO2_25	579.80	14.55	5.06	0.40	0.1
CO2_26	572.84	14.12	5.05	0.40	0.1
CO2_27	573.10	14.17	5.06	0.40	0.1
CO2_28	575.10	14.18	5.06	0.40	0.1
DEP_5	571.99	14.19	5.06	0.43	0.1

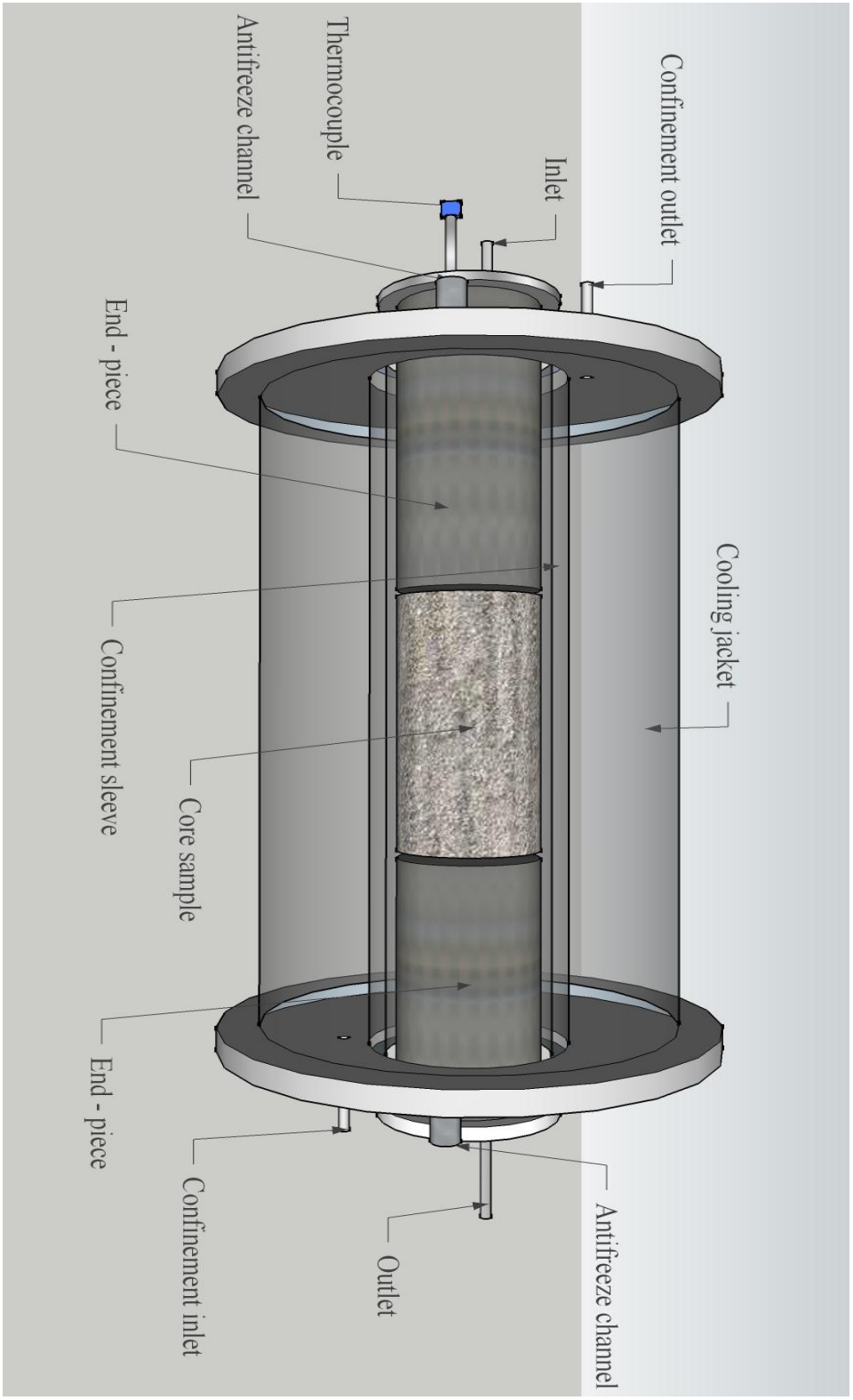

Appendix B 1 - Illustration of high pressure core holder, the cooling jacket and the way the core is placed inside the core holder. The two end-pieces hold the core steady inside the core holder. Inlet and outlet lines pass through the end-pieces and are in contact with the core sample. The illustration is made using GOOGLE SKETCHUP.